# Investigation of Polyhalides: Synthesis, Characterization, and Application Possibilities of Polybromides, Polychlorides, and Bromostannates

Inaugural-Dissertation

to obtain the academic degree

Doctor rerum naturalium (Dr. rer. nat.)

submitted to the Department of Biology, Chemistry and Pharmacy

of Freie Universität Berlin

by

KARSTEN SONNENBERG

2018

The work for the present dissertation has been conducted between May 2015 and October 2018 under the guidance of Prof. Dr. Sebastian Hasenstab-Riedel at the Institute of Chemistry and Biochemistry (Department Biology, Chemistry and Pharmacy) of Freie Universität Berlin.

| | |
|---|---|
| 1st referee: | Prof. Dr. Sebastian Hasenstab-Riedel |
| 2nd referee: | Prof. Dr. Christina Roth |
| Day of Disputation: | 07.12.2018 |

# Acknowledgement

My dissertation would not have been as successful without the help of others whom I want to thank at this point.

First, I want to express my sincere gratitude to my doctoral advisor Prof. Dr. Sebastian Hasenstab-Riedel for the possibility to work in his research group, for allowing me to work on this interesting topic and for the trust he placed in me.

I also want to thank Prof. Dr. Christina Roth for accepting the position as 2nd referee after having supervised me already during my master thesis. The skills I learned back then have greatly helped me during my doctoral studies.

The entire research group shall be thanked for their warm welcome, many helpful discussions and multiple first class coffee breaks. But also the second class shall never be forgotten and I will keep the second class in the fondest of memories!

Thanks to the workshops for their hard work, especially Mr Dirk Busold from the glass workshop who has quickly helped me in many instances.

Kudos to my students Rodrigue Sy, Steffen Frahm, Patrick Pröhm, Jonathan Schneider and Tyler Gully for their effort and motivation. It has been a great pleasure working with them.

Legends never die and neither will the Battery Boys! Many thanks to Benjamin Schmidt and Tyler Gully for mutual support and their loyalty. Together with Maximilian Stahnke they ensured that U406 had a fantastic atmosphere for which we are surely greatly envied. ;)

I am grateful to my work-wife Lisa Mann and my work-husband Benjamin Schmidt for several happy years of marriage, their support, the scientific exchange and most of all for brightening up my everyday life.

Moreover, I would like to acknowledge Benjamin Schmidt and Patrick Pröhm for proof-reading this dissertation.

Lastly but most importantly, I thank my friends and family for their moral support. In particular I am thankful to my family for “having my back” my entire life. My eternal gratitude goes to my grandmother Charlotte Gürnth, my parents Gerd and Loritta Sonnenberg, my siblings Stefan and Dr. Claudia Sonnenberg for their unconditional moral and financial support.

THANKS!

# Abstract

The increasing global energy demand requires the development of an infrastructure of renewable energies since fossil fuels are not disposable unlimitedly. Renewable energy sources such as solar panels and wind turbines deliver a fluctuating supply of energy. One way to store this harvested energy is in backup batteries, e.g. redox flow batteries (RFBs), which provide the energy to a given system when needed. Therefore, the present dissertation deals with the synthesis and characterization of ionic liquids based on bromostannates and polyhalides for a possible application in a new type of redox flow battery as well as expanding the spectrum of poly(inter)halides.

The preparation of bromostannate(II) ($[SnBr_3]^-$) and bromostannate(IV) ($[SnBr_5]^-$) was achieved by reaction of [OMIM]Br (OMIM = 1-octyl-3-methylimidazolium) with $SnBr_2$ and $SnBr_4$, respectively. The liquids were subject to Raman and NMR spectroscopic characterization. Additionally, solid [OMIM][$SnBr_5$] was analyzed by single crystal X-ray diffraction, making it the only second $[SnBr_5]^-$ containing compound in the Cambridge Crystallographic Data Centre (CCDC), and the first ionic liquid with this rare anion.

When employing the same cation, ionic liquids based on polybromides were obtained, namely [OMIM][$Br_3$] and [OMIM][$Br_9$], of which the electrical conductivity was determined. In addition, the field of polyhalides has been greatly expanded. In one project, the hexabromide dianion $[Br_6]^{2-}$ was stabilized by a cyclic Vilsmeier cation derivative in $[C_5H_{10}N_2Br]_2[Br_6]$. This L-shaped $[Br_6]^{2-}$ was the last gap to fill in the series of polybromides between $[Br_3]^-$ and $[Br_{11}]^-$. Moreover, the synthesis and characterization of other Vilsmeier salt derivatives $[BrC(NMe_2)_2][Br_3]$ and $[BrC(NMe_2)_2]_2[Br_8]$ showed the influence of the solvent and the cation on the resulting polybromides. A comparison to the corresponding polychlorides was drawn.

Lastly, the challenging synthesis of polychlorides was successfully accomplished and the hitherto unknown polychloride monoanions $[Cl_{11}]^-$ and $[Cl_{13}]^-$ were prepared in the compounds $[AsPh_4][Cl_{11}]$, $[PPh_4][Cl_{11}]$, $[PNP][Cl_{11}] \cdot Cl_2$, and $[PNP][Cl_{13}]$ (PNP = bis(triphenylphosphine)-iminium). The octahedral structure of $[Cl_{13}]^-$ is very uncommon in polyhalogen chemistry and represents the first and only isotridecahalide. On top of that, $[NMe_3Ph]_2[Cl_{12}]$ was prepared, consisting of the largest polychloride dianion known to date: $[Cl_{12}]^{2-}$. All compounds were thoroughly characterized by NMR and Raman spectroscopy, X-ray diffraction, and compared to molecular and periodic solid-state quantum-chemical calculations.

# Kurzzusammenfassung

Der steigende globale Energiebedarf verlangt die Entwicklung einer Infrastruktur erneuerbarer Energien, weil fossile Energien nicht unbegrenzt zur Verfügung stehen. Erneuerbare Energien beinhalten unter anderem Solaranlagen und Windkraftanlagen, welche eine fluktuierende Versorgung von Energie bieten. Eine Möglichkeit die Energie aus solchen Quellen zu speichern ist in sogenannten Pufferbatterien (z.B. Redox Flussbatterien (RFB)) gegeben, die diese Energie bei Bedarf freisetzen. Daher beschäftigt sich die vorliegende Dissertation mit der Synthese und Charakterisierung von ionischen Flüssigkeiten (IL) auf Basis von Bromostannaten und Polyhalogeniden mit dem Ziel einer mögliche Anwendung in neuen Redox Flussbatterien sowie mit der Erweiterung des stoffchemischen Spektrums von Poly- und Polyinterhalogeniden.

Die Herstellung von Bromostannaten(II) ($[SnBr_3]^-$) und Bromostannaten(IV) ($[SnBr_5]^-$) erfolgte durch die Reaktion von [OMIM]Br (OMIM = 1-octyl-3-methylimidazolium) mit $SnBr_2$ bzw. $SnBr_4$. Die erhaltenen Flüssigkeiten wurden Raman und NMR spektroskopisch untersucht. Zusätzlich wurde $[OMIM][SnBr_5]$ mittels Einkristallröntgendiffraktometrie näher charakterisiert und stellt somit die bisher zweite $[SnBr_5]^-$ enthaltende Verbindung im Cambridge Crystallographic Data Centre (CCDC) sowie die erste ionische Flüssigkeit mit diesem seltenen Anion dar.

Durch Verwendung des gleichen Kations wurden die ILs $[OMIM][Br_3]$ und $[OMIM][Br_9]$ synthetisiert und ihre elektrischen Leitfähigkeiten untersucht. Darüberhinaus wurde das Gebiet der Polyhalogenide merklich expandiert. In einem Projekt wurde das Hexabromid Dianion $[Br_6]^{2-}$ durch ein Derivat des Vilsmeier Kations stabilisiert ($[C_5H_{10}N_2Br]_2[Br_6]$). Dabei schließt das L-förmige $[Br_6]^{2-}$ die letzte Lücke in der Reihe der Polybromide zwischen $[Br_3]^-$ und $[Br_{11}]^-$. Des Weiteren zeigten die Synthese und Charakterisierung der Derivate des Vilsmeier Salzes $[BrC(NMe_2)_2][Br_3]$ und $[BrC(NMe_2)_2]_2[Br_8]$ den Einfluss des Lösungsmittel und des Kations auf die daraus resultierenden Polybromide. Diese wurden mit den entsprechenden Polychloriden verglichen.

Zuletzt wurde die herausfordernde Synthese von Polychloriden erfolgreich durchgeführt und die bis dato unbekannten Polychlorid-Monoanionen $[Cl_{11}]^-$ und $[Cl_{13}]^-$ in den Verbindungen $[AsPh_4][Cl_{11}]$, $[PPh_4][Cl_{11}]$, $[PNP][Cl_{11}] \cdot Cl_2$, und $[PNP][Cl_{13}]$ (PNP = bis(triphenylphosphin)-iminium) erhalten. Die oktaedrische Struktur von $[Cl_{13}]^-$ ist unter den Polyhalogenen zum einen sehr ungewöhnlich und stellt zum anderen das erste und einzige Isotridecahalogenid dar. Weiterhin ist die Darstellung von $[NMe_3Ph]_2[Cl_{12}]$ gelungen, welches das bisher größte Polychlorid Dianion enthält: $[Cl_{12}]^{2-}$. Alle Verbindungen wurden vollständig mittels NMR und Raman Spektroskopie sowie Röntgendiffraktometrie am Einkristall charakterisiert und mit molekularen und periodischen Festkörperrechnungen quantenchemisch verglichen.

# Abbreviations

| | |
|---|---|
| σ | conductivity |
| χ | mole fraction |
| AIM | atoms in molecules |
| AO | atomic orbital |
| aug-cc-PVTZ | augmented correlation-consistent polarized valence-only triple zeta |
| B3LYP | Becke, three-parameter, Lee-Yang-Parr |
| BCP | bond critical point |
| BMBF | Bundesministerium für Bildung und Forschung |
| BMP | 1-butyl-1-methylpyrrolidinium |
| BMPY | 1-butyl-4-methylpyridinium |
| $BrC(NMe_2)$ | tetramethylbromoamidinium |
| btmgn | 1,8-bis(tetramethylguanidinyl)naphthalene |
| Bu | butyl |
| Bz | benzyl |
| $C_4MPyr$ | 1-butyl-1-methylpyrrolidinium |
| $C_5H_{10}N_2Br$ | N,N'-dimethyl-2-bromoimidazolinium |
| $C_{10}Mpyr$ | 1-decyl-1-methylpyrrolidinium |
| Cat | cation |
| CCDC | Cambridge Crystallographic Data Center |
| CCSD(T) | Coupled Cluster with Single, Double and perturbative Triple excitations |
| $ClC(NMe_2)$ | tetramethylchloroamidinium |
| COSMO | conductor-like screening model |
| D | donor |
| D3 | dispersion correction |
| $d_3$-acetonitrile | perdeuterated acetonirile |
| $d_6$-acetone | perdeuterated acetone |
| def2-TZVPP | valence triple zeta with two sets of polarization functions |
| def2-TZVPD | valence triple zeta polarization with diffuse functions |
| DFT | density functional theory |

| | |
|---|---|
| DSC | differential scanning calorimetry |
| $E^+$ | electrophile |
| ESI | electrospray ionization |
| Et | ethyl |
| et al. | et alii |
| EU | European Union |
| FT | Fourier transformation |
| GOF | goodness of fit |
| HMIM | 1-hexyl-3-methylimidazolium |
| HOMO | highest occupied molecular orbital |
| $I_2b_{15}c_5$ | diiodobenzo-15-crown-5 |
| IL | ionic liquid |
| IR | infrared |
| LUMO | lowest unoccupied molecular orbital |
| m | mass |
| Me | methyl |
| MO | molecular orbital |
| n | amount of substance |
| $N_{0124}$ | butylethylmethylammonium |
| $N_{0133}$ | methyldiisopropylammonium |
| $N_{1111}$ | tetramethylammonium |
| $N_{1114}$ | butyltrimethylammonium |
| $N_{1123}$ | ethyldimethylpropylammonium |
| $N_{1134}$ | butyldimethylpropylammonium |
| $N_{1224}$ | butyldiethylmethylammonium |
| NASA | National Aeronautics and Space Administration |
| NHE | normal hydrogen electrode |
| NMR | nuclear magnetic resonance |
| $Nu^-$ | nucleophile |
| OMIM | 1-octyl-3-methylimidazolium |
| OTf | triflate |

| | |
|---|---|
| $P_{1111}$ | tetramethylphosphonium |
| PAW | projector augmented wave |
| PBDE | polybrominated diphenyl ether |
| Ph | phenyl |
| PNP | bis(triphenylphosphine)iminium |
| Pr | propyl |
| PTFE | poly(tetrafluoroethylene) |
| RFB | redox flow battery |
| RI | resolution of identity |
| RMIM | 1-alkyl-3-methylimidazolium |
| RT-IL | room temperature ionic liquid |
| SCS-MP2 | Spin-Component Scaled Second-Order Møller-Plesset Perturbation |
| T | temperature |
| $T_g$ | glass transition temperature |
| $T_{max}$ | maximum transmission factor |
| $T_{min}$ | minimum transmission factor |
| $T_{VFT}$ | Vogel temperature |
| tppz | tetra(2-pyridyl)pyrazine |
| ttmgn | 1,2,4,5-tetrakis(tetramethylguanidinyl)naphthalene |
| UV-Vis | ultraviolet-visible |
| VASP | Vienna Ab initio Simulation Package |
| VB | valence bond |
| VFT | Vogel-Fulcher-Tammann |
| VRFB | all vanadium redox flow battery |
| VSEPR | valence shell electron pair repulsion |
| XRD | X-ray diffraction |
| X, Y, Z | halogen atom |

# Table of Contents

# 1. Introduction

## 1.1 Motivation

The global energy consumption has drastically increased in the last century. So far, the world heavily relies on conventional energy supplies such as nuclear, coal, oil, and gas.[1] As a result, the $CO_2$ emission has increased exponentially which in turn leads to the climate change we are experiencing at the moment. In order to counteract this development and global warming, 195 signatories, including the European Union, have joined in the so-called "Paris Agreement"[2] aiming at reducing the global $CO_2$ emission and returning to a level of +2 °C in comparison to pre-industrial levels[3] and pursuing efforts to lower the level even further to +1.5 °C.[4] The Agreement entered into force on 4 November 2016, nearly a year after the 21st United Nations Climate Change Conference in Paris, France.[5] Unfortunately, on 1 June 2017 the U.S. have declared to withdraw from the Paris Agreement as soon as legally eligible,[6] which will be on 4 November 2019.[7] Since fossil fuels will not be available unlimitedly and because the global energy demand will continue to be high, the search for alternative and renewable energy sources is imperative. Renewable energies include solar, wind, and hydropower. It is important to recognize that these sources cannot offer a constant but rather fluctuating supply of energy because they mostly depend on the weather. Therefore, it is necessary to store the energy harvested from natural sources e.g. in backup batteries which provide energy to a given system when required. Commonly, these backup batteries are rechargeable (secondary battery) like the so-called redox flow battery (RFB) which was developed by NASA in the 1970s.[8] Particulary interesting are the all vanadium redox flow battery (VRFB), in which only one redox active metal is employed, and the zinc/bromine hybrid flow battery, which contains *in-situ* formed polybromide anions.[9] RFBs can be utilized as backup batteries in wind power plants.[8] As opposed to conventional battery systems such as the omnipresent lithium ion or the lead-acid battery, energy capacity (volume) and power density (surface) can be scaled independently in the RFB which limits the energy capacity only by the size of the electrolyte tank.[8] It is therefore a declared will of the German government and acedamic insitutions to work on solutions regarding energy storage and to reevaluate the infrastructure of energy supply.[10]

In this precise framework, we want to examine a new possible redox flow battery prototype consisting of neat, conductive ionic liquids as electrolytes. This would drastically increase the energy density of the battery since the redox active species would not need to be dissolved in a solvent, hence increasing their concentration.

## 1.2 References

[1] J. Krane, *MRS Energy & Sustainability* **2017**, *4*, 21.
[2] https://unfccc.int/process/the-paris-agreement/status-of-ratification (11/1/2018).
[3] D. Campbell, *Energy & Environment* **2016**, *27*, 883.
[4] J. Rogelj, A. Popp, K. V. Calvin, G. Luderer, J. Emmerling, D. Gernaat, S. Fujimori, J. Strefler, T. Hasegawa, G. Marangoni, *Nat. Clim. Change* **2018**, *8*, 325.
[5] S. I. Karlsson-Vinkhuyzen, M. Groff, P. A. Tamás, A. L. Dahl, M. Harder, G. Hassall, *Climate Policy* **2018**, *18*, 593.
[6] J. Tollefson, *Nature* **2017**, *546*, 198.
[7] *Treaty Handbook*, UNITED NATIONS, **2012**.
[8] M. L. Perry, A. Z. Weber, *J. Electrochem. Soc.* **2016**, *163*, A5064-A5067.
[9] A. Z. Weber, M. M. Mench, J. P. Meyers, P. N. Ross, J. T. Gostick, Q. Liu, *J. Appl. Electrochem.* **2011**, *41*, 1137.
[10] E. Gawel, P. Lehmann, K. Korte, S. Strunz, J. Bovet, W. Köck, P. Massier, A. Löschel, D. Schober, D. Ohlhorst et al., *Energ. Sustain. Soc.* **2014**, *4*, 73.

# 2. Theoretical and Historical Background

## 2.1 Redox Flow Batteries

First developed in the 1970s, redox flow batteries have become increasingly important as a new type of battery. Rechargeable batteries of this class typically offer features such as long life, flexible design, high reliability, and low operations and maintenance costs.[1] The all-vanadium redox flow battery is a commercial representative, often referred to for comparison as a standard redox flow battery.

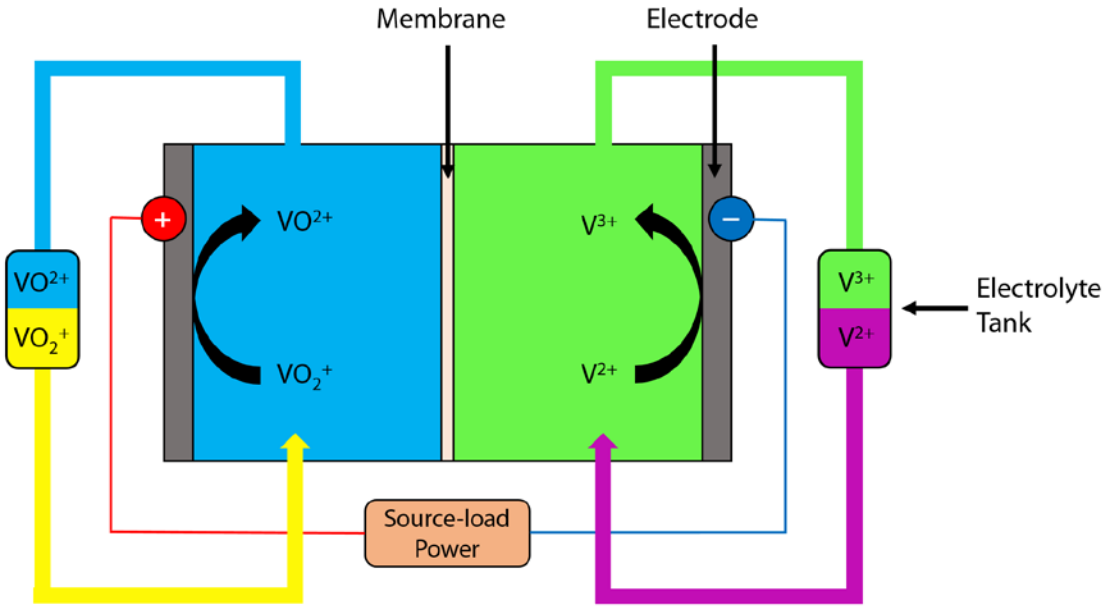


**Figure 2.1.** Schematic setup of the VRFB showing the reactions during discharge.

A RFB system comprises two electrolyte storage tanks (catholyte and anolyte), a pump, the electrodes, and the membrane. During charge and discharge, the electrolyte solutions are circulated through the electrodes where the electrochemical reactions take place. The two half cells are seperated by a membrane, completing the basic setup, see Figure 2.1. In the VRFB four stable oxidation states of vanadium are used (+II, +III, +IV, and +V). The usage of only one redox active metal prevents the possibility of cross contamination. The processes during charge (forward reaction) and discharge (backward reaction) occuring at the negative electrode and positive electrode are shown in reactions (2.1) and (2.2).[2]

$$\text{negative electrode:} \quad V^{3+} + e^- \rightleftharpoons V^{2+} \qquad (2.1)$$

$$\text{positive electrode:} \quad VO^{2+} + H_2O \rightleftharpoons VO_2^{+} + e^- + 2\,H^+ \qquad (2.2)$$

The electrolyte contains acidic solutions of vanadium salts. Even though the salts generally possess a low solubility in aqueous media, this is overcome by the high concentration of sulfuric acid. This in return causes another challenge because sulfuric acid limits the temperature range in which the battery can operate (+10 °C to +40 °C) since the electrolyte will crystallize below +10 °C, while pentavalent vanadium tends to undergo condensation reactions above +40 °C, or at basic pH-values.[3] Aqueous media are also limited by the electrochemical window of the solvent water. The exact position of this electrochemical window is pH-dependent but always amounts to 1.23 V. Outside this stable region the evolution of oxygen or hydrogen is observed.[4]

Not only the stability of the electrolyte is essential, but also the choice of a suitable electrode material is crucial. In VRFBs carbon based electrodes are employed, which can be modified chemically or by heat treatment, to obtain higher currents.[5] One possibility is the usage of carbon felts, which have the advantage of a high surface area, acidic resistance, and a large limiting overpotential towards the evolution of hydrogen in aqueous media.[5]

A major advantage of RFBs is the decoupling of energy and power density. The power is dependent on the number of cells in the block and on the surface of the electrodes, which can be drastically increased by the beforementioned carbon felts. The energy is a function of the concentration of the redox active species in the electrolyte and the volume of the electrolyte tanks, hence, given a certain concentration, the energy is only limited by the size of the electrolyte tanks.[6]

Clearly, conventional RFBs are limited by low concentrations of the redox active species as well as by the electrochemical window of the solvent, which is usually water. A promising alternative we pursue is the use of neat, conductive ionic liquids which are redox active themselves.

## 2.2 Ionic Liquids

The term ionic liquid (IL), or “molten salts” describes a fairly simple concept, which is generally defined as "an ionic material that is liquid below 100 °C".[7] The first ionic liquid, which is also the first room-temperature ionic liquid (RT-IL), dates back to Paul Walden and his synthesis of ethylammonium nitrate in 1914.[8] Very similar compounds such as methylammonium nitrate have been used as explosives.[9] However, nowadays ionic liquids are commonly used as solvents. Usually, ionic materials, or salts, have a melting point well above ambient temperatures. Similarly sized cations and anions can be densely packed and give rise to a high lattice energy due to strong electrostatic interaction. If the size of the anion and cation differs greatly, dense packing is no longer possible. Thus the strength of electrostatic interaction and the lattice energy decreases, which leads to a drastically lower melting point. Commonly ionic liquids contain a bulky

asymmetric cation, such as imidazolium, ammonium, phosphonium, piperidinium, and pyridinium. Typical anions are triflate (trifluoromethanesulfonate), hexafluorophosphate, triflimide (bis(trifluoromethylsulfonyl)imide), or simple halides like chloride, bromide, and iodide to mention only a few, see Fig. 2.2. In general, the melting points of ionic liquids increase with the number of charges per anion and with higher symmetry and decrease with increasing ion size. With respect to organic cations, which usually carry only one positive charge, the symmetry and the length of alkyl substituents are the most influencing factors of melting points.

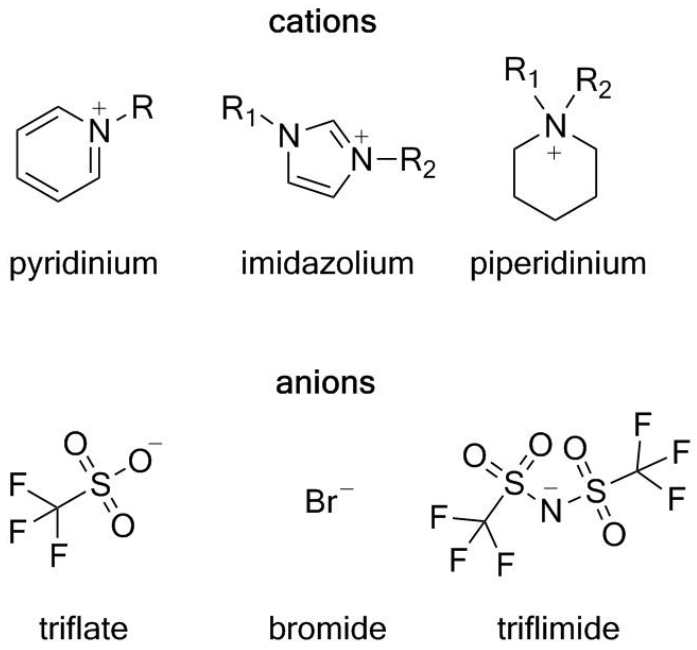


**Figure 2.2.** Selection of frequently used cations and anions in ILs.

The usage of asymmetric cations and anions also prevents dense packing. The imidazolium cation is considered to illustrate this. The 1-alkyl-3-methylimidazolium tetrafluoroborates ([RMIM][$BF_4$], R = methyl to R = octadecyl) have different melting points and glass transitions depending on the number of carbon atoms in the *n*-alkyl chain. The initial lengthening of the alkyl chain (from R = methyl to R = octyl) leads to a decrease of the melting point while additional lengthening (from R = octyl to R = octadecyl) leads to an increase of the melting point. The reduction in the melting points can be rationalized by destabilization of Coulomb packing, while the increase after R = octyl can be explained by increased attractive van der Waals forces between the alkyl chains and hence an increased structural ordering.[7]

Because of the theoretically infinite combination possibilites of cations and anions, and thus countless unique ionic liquids, they are also referred to as “designer solvents”.[10] In other words, ionic liquids can be tuned to fulfill desired physical properties such as viscosity, density, and melting point. Apart from a low melting point, ionic liquids have a very low vapor pressure, low flammability, and high thermal stability, which are the same properties possessed by other salts,

e.g. sodium chloride (NaCl). In addition, ionic liquids usually have a low toxicity and offer a large electrochemical window. Indeed, one of the limiting factors for the use of a solvent in an electrochemical cell is its potential window. For ionic liquids, this is usually defined by the potentials for the reduction and the oxidation of the cation and the anion. The potential window is usually measured by cyclic voltammetry and can be significantly influenced by impurities like water.

While the electrical conductivity of ionic liquids such as [HMIM]Br (HMIM=1-hexyl-3-methylimidazolium) (54.2 μS $cm^{-1}$) is rather low, polyhalide based ionic liquids exhibit an unusually high conductivity, e.g [HMIM][$Br_9$] shows a conductivity of 52.1 mS $cm^{-1}$ at 25.6 °C which is 1000 times higher than that of the simple bromide [HMIM]Br. So far, the best explanation for this is that a Grotthuss-type hopping mechanism may be involved, similar to that of water.[11]

## 2.3 Poly(inter)halides

Chapter 2.3 is based on the publication "Karsten Sonnenberg, Lisa Mann, Frenio Redeker, Benjamin Schmidt, and Sebastian Riedel, Poly- and Interhalogen Anions from Fluorine to Bromine, *manuscript in preparation*." Subchapters 2.3.6 Polyfluorides (Frenio Redeker), 2.3.7 Polychlorides (Benjamin Schmidt), and 2.3.9 Polyinterhalides (Lisa Mann) were rewritten by the author of this dissertation.

### 2.3.1 Introduction

The halogens fluorine, chlorine, bromine and iodine are versatile elements with various important applications including industrial use in e.g. halogenated compounds. Among these elements chlorine is most important (75 Mton per year) as it was estimated that more than 50% of all industrial chemicals including polymers, around 20% of molecular drugs, and ca. 30% of agrochemicals contain or are produced from chlorine (Figure 2.3).[12] The second most important halogen is still bromine (0.8 Mton per year) which is largely used in the manufacture of drilling fluids and flame retardants[13] such as PBDEs (polybrominated diphenyl ether), however, the EU has reduced the production of these flame ratardants based on problematic environmental effects.[14]

The demand of iodine and fluorine is estimated to be less than 0.04 Mton per year with an increasing importance of fluorinated products. The main consumption of elemental fluorine is still applied for the manufacture of $UF_6$ and $SF_6$ while many sophisticated materials and biological active compounds show unique properties based on fluorinated groups. That is why fluorine plays

a key role in drug design (medicinal chemistry) since crucial physicochemical properties can be tuned by the degree of fluorination.[15] Perfluorinated organic compounds are widely spread such as PTFE (polytetrafluoroethylene)[16] or Nafion (membrane in fuel cells).[17] Iodine is also widely used, e.g. in pharmaceuticals, as contrast agent in medical imaging,[18] as disinfectants based on iodated organic compounds like iodoform,[19] as well as catalysts.[20]

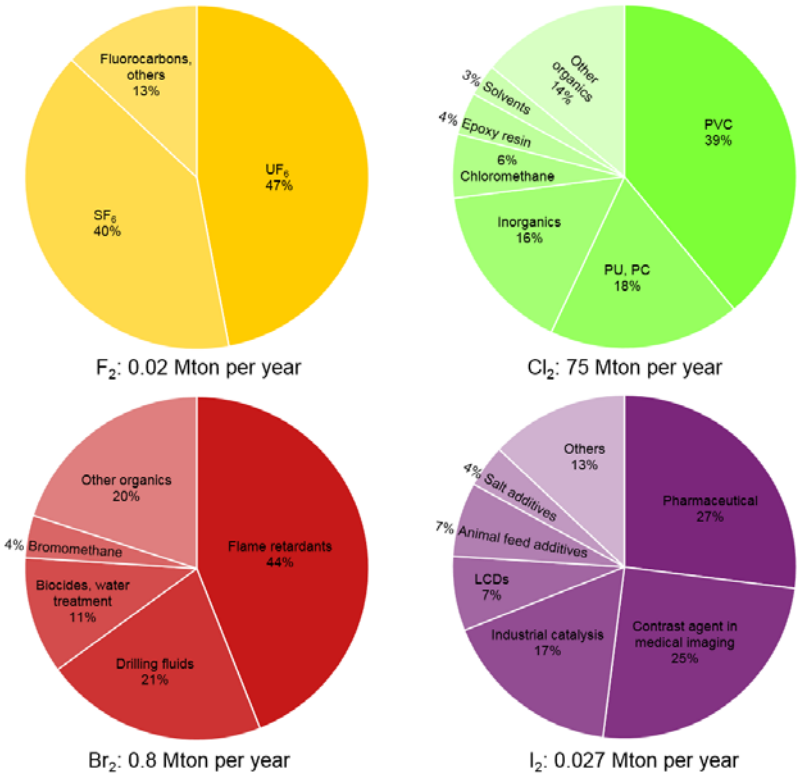


**Figure 2.3:** Yearly production and use of the halogens fluorine, chlorine, bromine, and iodine.[11]

Apart from their use in important halogenated compounds, as described above, halogens can also form e.g. interhalides or polyhalogen ions. Neutral interhalogen species (e.g. BrCl, $BrF_3$, $ClF_5$, $I_2Cl_6$, $IF_7$), cationic (e.g. $[I_3]^+$[21], $[Cl_3]^+$[22], $[Br_5]^+$[23], $[I_{15}]^{3+}$[24], $[Br_3F_8]^+$[25]) and anionic polyhalogens are known. In contrast to the yet underexplored polyhalogen cations, of which only few examples exist, the diversity of polyhalogen anions is vast. Obviously, polyhalides do not only exist as homoatomic $[X_m(X_2)_n]^{m-}$, but also multiple combinations of halogens of the type $[X_m(Y_2)_n]^{m-}$ or $[X_m(YZ)_n]^{m-}$ (X, Y, Z = halogen) are feasible and have been successfully synthesized and thoroughly characterized. Hereinafter, polyhalogen anions of the type $[X_m(X_2)_n]^{m-}$ are referred to as polyhalides while $[X_m(Y_2)_n]^{m-}$ and $[X_m(YZ)_n]^{m-}$ are called (poly)interhalides.

The first report on a trihalide was in 1819 when Pelletier and Caventou discovered strychnine triiodide.[26] Polyiodides have been extensively investigated since then, with a variety of mono, di-tri-, and even tetraanions and some extensive reviews already summarize their chemistry and structures in detail.[27,28] Therefore we focus in the present review on the lighter homologues

fluorine, chlorine, bromine and their interhalogens which are known, so far, to form mono- and dianions (Fig. 2.4).

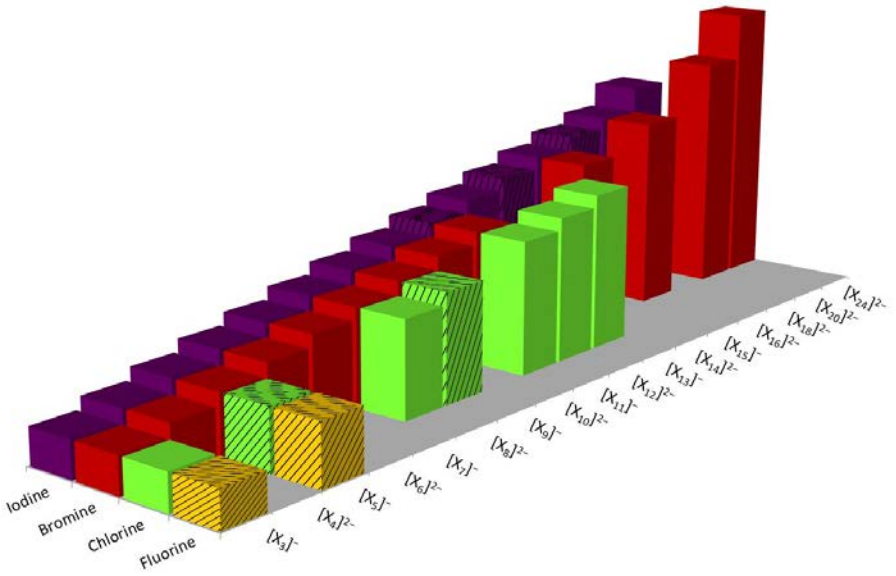


**Figure 2.4:** Overview of experimentally known polyhalogen mono- and dianions. These anions have been crystallographically characterized; except the shaded ones which are only observed spectroscopically.

The first systematic investigation of polychlorides and polybromides was done by Chattaway and Hoyle in 1923.[29] They dissolved tetraalkylammonium halides in acetic acid or alcohol and added the corresponding dihalogen. The products were analyzed by any means available at that time which includes their physical properties, gravimetric methods, color, and their melting point. Additionally, they observed that when bromine and a bromide salt were put in a desiccator large quantities of the bromine vapor were absorbed by the bromide salt, up to six equivalents. A similar observation was found for polychlorides. It was described that the absorption of chlorine occurs rapidly at first and then becomes significantly slower. In an open system, higher polyhalides release the corresponding dihalogen again until the trihalide remained.[29] The structure of the resulting higher polyhalides were not known at that time.

Some reviews describing polyhalogen anions have been published in the past and can be ordered according to the elements: general reviews about polyhalogen anions,[30,31] and polyiodide anions[27,28] as well as very encompassing articles on polyfluoride anions,[32] polychloride anions,[33] and polybromide anions.[34] Adonin *et al.* also recently published a review on polyhalide-bonded metal complexes.[35]

### 2.3.2 General Aspects of Polyhalides

Commonly, polyhalides are synthesized in organic solvents,[36] ionic liquids[37–39] or in the neat dihalogen[34] by addition of a dihalogen to the corresponding halide (eq. 2.3).

$$n\,X_2 + m\,X^- \xrightarrow[\text{or ionic liquid,}\\ \text{or neat halogen}]{\text{organic solvent,}} [X_{2n+m}]^{m-} \qquad (2.3)$$

The observed structures of monoanions are depicted in Fig. 2.5. Note, they often follow the VSEPR model in their general structures.

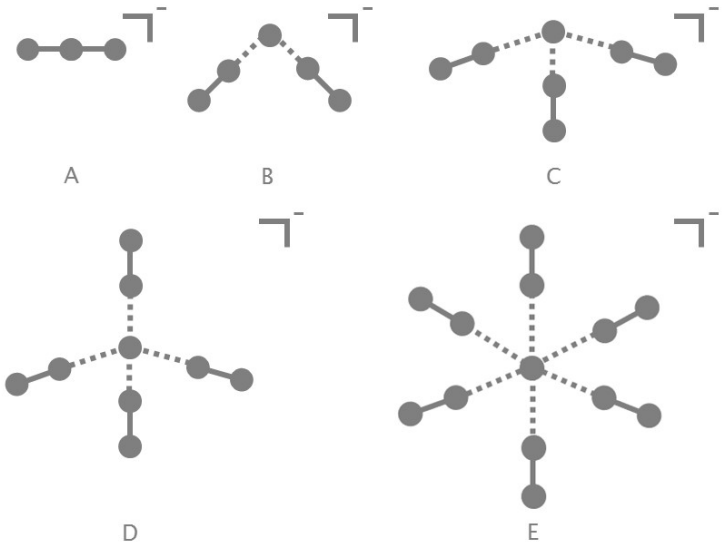


**Figure 2.5:** Typical structural motifs of polyhalogen monoanions: (A) linear $[X_3]^-$ ($D_{\infty h}$), (B) V-shaped $[X_5]^-$ ($C_{2v}$), (C) trigonal pyramidal $[X_7]^-$ ($C_{3v}$), (D) tetrahedral $[X_9]^-$ ($T_d$), (E) octahedral $[X_{13}]^-$ ($O_h$).

In general, all polyhalides have a tendency towards the loss of the coordinated dihalogen $X_2$. In order to minimize this tendency, the vapor pressure can be significantly lowered by the usage of

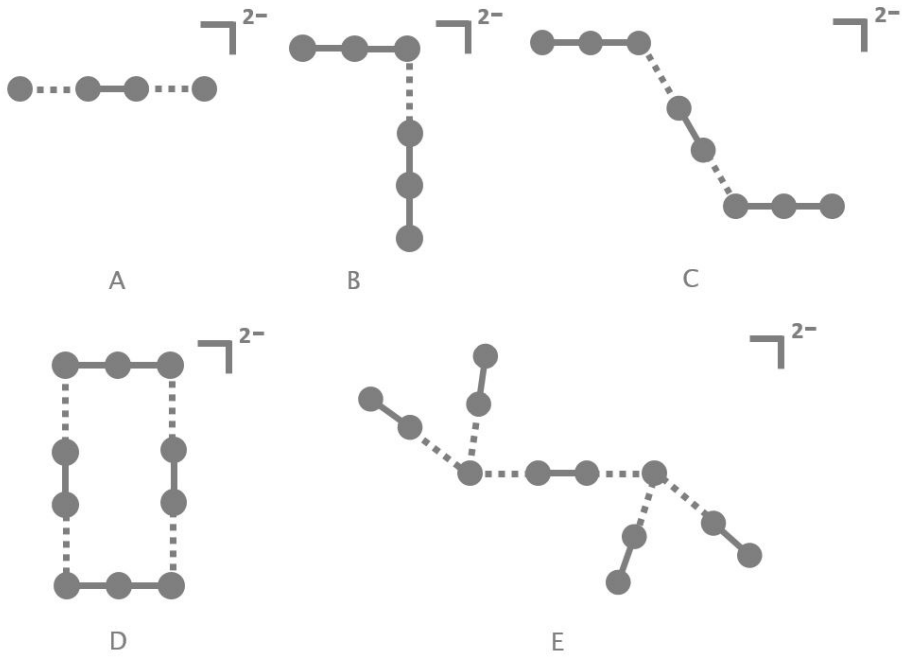


**Figure 2.6:** Typical structural motifs of polyhalogen dianions: (A) linear $[X_4]^{2-}$ ($D_{\infty h}$), (B) L-shaped $[X_6]^{2-}$ ($C_s$), (C) Z-shaped $[X_8]^{2-}$ ($C_{2h}$), (D) rectangular $[X_{10}]^{2-}$ ($D_{2h}$), (E) non-planar $[X_{12}]^{2-}$ ($C_{2h}$).

ionic liquids. It is known that gases show a high solubility in ionic liquids.[40] Consequently, the highest polybromides $[Br_{20}]^{2-}$[41] and $[Br_{24}]^{2-}$[42] have been synthesized in eutectic mixtures of ionic liquids. Possible structural motifs of such dianions are illustrated in Fig. 2.6.

### 2.3.3 Quantum-chemical description

In principle, higher polyhalides can be broken down to the building blocks $X^-$, $[X_3]^-$ and $X_2$. The Lewis bases $X^-$ or $[X_3]^-$ donate charge from the HOMO into the LUMO ($\sigma^*$) of the Lewis acid $X_2$ resulting in a weakening and elongation of the X–X bond of the coordinated $X_2$ molecule which is also experimentally observed. Specifically, the bonding situation in polyhalogen monoanions $[X_{2n+1}]^-$ has been extensively studied by the block-localized wave function (BLW) method with valence bond (VB) analysis.[43] Based on these investigations, the halogen bond between a central $X^-$ and the surrounding dihalogens $X_2$ indeed leads to a charge-transfer from the lone pair of $X^-$ into the anti-bonding orbital of the coordinated $X_2$ moiety ($n \rightarrow \sigma^*$). Consequently, the investigated halogen bonds are essentially dative covalent. In particular, the hypervalent $[X_3]^-$ ion is of great interest and its bonding situation has been subject of many publications.[44–46] One curiosity related to the bond distances in the $[X_3]^-$ anion is that both theoretical and experimental values for the distances between two halogen atoms X–X are always longer than the sum of the covalent radii.[44]

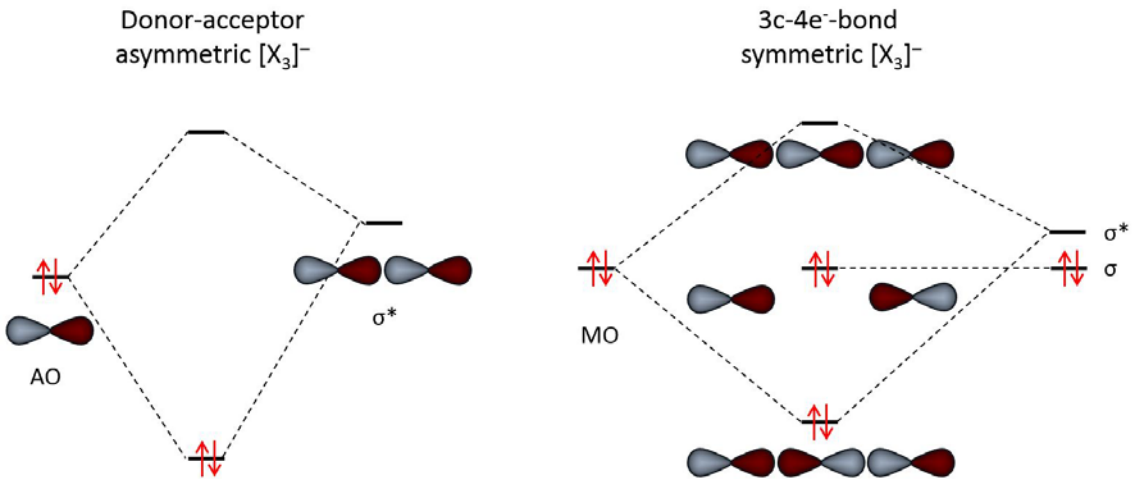


**Figure 2.7:** Molecular orbital scheme for the formation of $[X_3]^-$: Left as donor-acceptor complex for asymmetric trihalides ($[X\cdots X–X]^-$); Right as 3c-4e-bond in symmetric trihalides ($[X–X–X]^-$). AO are atomic orbitals, MO are molecular orbitals.

As mentioned above, asymmetrically bonded trihalides ($[X\cdots X–X]^-$) can be described as donor-acceptor complexes between $X^-$ (donor) and $X_2$ (acceptor). However, for symmetric trihalides ($[X–X–X]^-$) of $D_{\infty h}$ symmetry, a 3c-4e-bond can be formulated, which is analogues to the

isolelectronic and -structural description of e.g. $XeF_2$. The corresponding MO diagram of a trihalide system is shown in Figure 2.7.

Quantum-chemical calculations indicate that the negative charge of the trihalide is in principle split between the two peripheral atoms and the central atom shows a more positive charge than the peripheral ones. The natural population analysis (NPA) underlines that the central halogen atom X1 becomes increasingly neutral going from the trifluoride down to the triiodide which is in line with a more negative charge of the terminal halogen atom X2, see Table 2.1.[31]

**Table 2.1:** NPA charges of different trihalides calculated at CCSD(T)/aug-cc-pVTZ//B3LYP/aug-cc-pVTZ level.[31]

$X^2 - X^1 - X^2$

| X | $X^1$ | $X^2$ |
|---|---|---|
| F | –0.113 | –0.444 |
| Cl | –0.104 | –0.448 |
| Br | –0.098 | –0.451 |
| I | –0.092 | –0.454 |

Beyond that donor/acceptor or multiple center bonding description discussed above a third bonding concept, called halogen bonding, has been more and more proposed in the recent years, to describe the interactions between covalently bonded halogens with other elements like nitrogen, oxygen etc.[47] It is therefore logic to extend this to halogen-halogen bonding if we consider polyhalogen anions. Plotting the electrostatic potential surface of a dihalogen, one observes that it is anisotropic and not equally distributed among the entire dihalogen molecule. In contrast, a belt of charge accumulation perpendicular to the molecule's main axis is observed. Additionally, a region of a more positive electrostatic potential on the bonding axis is unfolded, the so called σ-hole, see Figure 2.8.

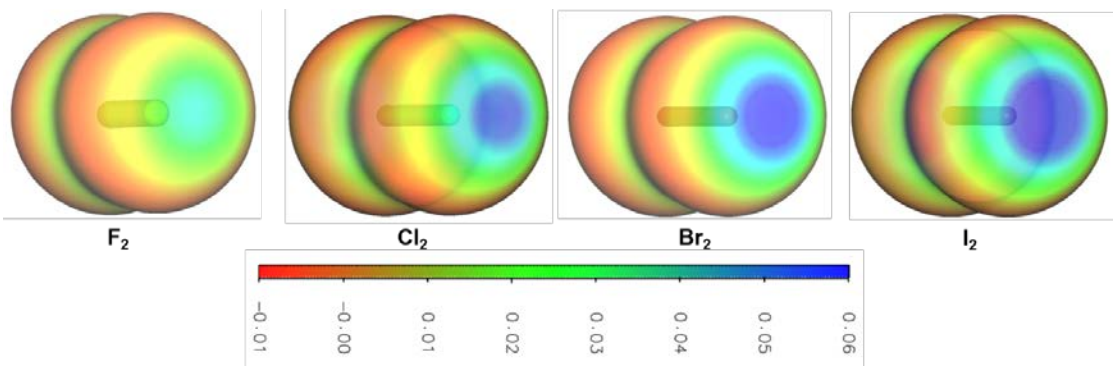


**Figure 2.8:** Electrostatic potential of the halogens $F_2$, $Cl_2$, $Br_2$ and $I_2$ in the range of –0.01 a.u. (red) to 0.06 a.u. (blue) is mapped (isosurface value 0.0035 a.u.); calculated at B3LYP-D3/def2-TZVPP level.

Based on this anisotropy of the electrostatic potential a trihalide $[X_3]^-$ can interact with a nucleophile ($Nu^-$) or electrophile ($E^+$), see Figure 2.9. The trihalide interacts with a nucleophile in a 180° angle using its σ-hole (blue region) and with an electrophile ($E^+$) by the belt of negative charge (red region) in a 90° angle.

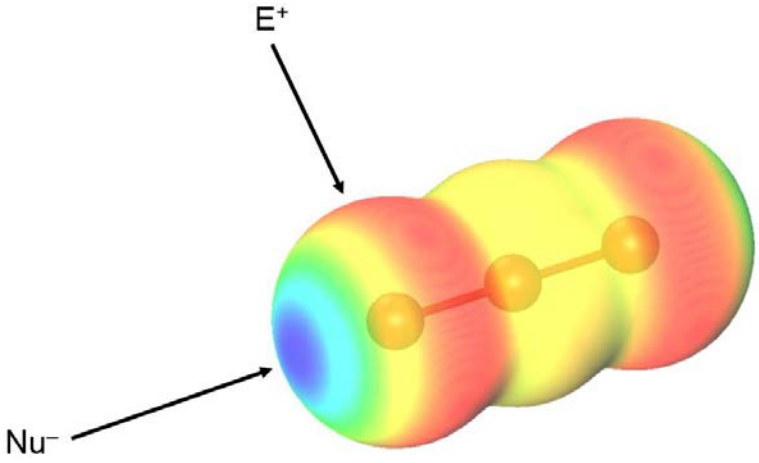


**Figure 2.9:** Electrostatic potential of a trihalide (here tribromide) in the range of –0.175 a.u. (red) to –0.15 a.u. (blue) is mapped (isosurface value 0.0035 a.u.); calculated at B3LYP-D3/def2-TZVPP level. The interaction of a nucleophile ($Nu^-$) and of an electrophile ($E^+$) with the trihalide is illustrated.

Clearly, the σ-hole becomes more pronounced in the order F << Cl < Br < I resulting in an enhanced stability of polyiodide anions by halogen bonding in contrast to polyfluorides. Based on many examples in the literature, Pennington *et al.* make the following generalizations:[48]

*1. Halogen bonding is largely an electrostatic phenomenon. Therefore, when the halogen is bound to a more electronegative element, it becomes a better electron acceptor. Conversely, base strength parallels (at least to the first order of approximation) the effectiveness of a given species as a halogen bond electron donor.*

*2. Halogen bond electron acceptor ability decreases in the order I > Br > Cl. Fluorine (acting as an electron acceptor) forms only very weak halogen bonds, if at all.*

*3. When a halogen is in close contact with another atom approximately 180° from the halogen-halogen sigma bond, it is acting as an electron acceptor. When the contact is approximately 90°, it is acting as an electron donor.*

*4. Formation of a halogen-halogen bond at one atom of a dihalogen does not preclude the second atom from acting as an electron acceptor. The stronger the electron donor, however, the less likely that a D···X–X···D complex will be formed.*

*5. Halogen bond formation results in partial occupation of a σ* antibonding orbital, weakening the bond. Depending on the electron donor strength and the environment, this can result in heterolytic fragmentation of the bond, leading to ionic products.*

In several publications[48-50] Resnati and Metrangolo have given new insights into halogen bonding and a comparison of halogen bonds with hydrogen bonds, where the latter ones can be very strong (>155 kJ mol$^{-1}$ in $[HF_2]^-$[51]). Halogen bonds cover a wide range from e.g. 5 kJ mol$^{-1}$ (Cl···Cl in chlorocarbons) all the way to 180 kJ mol$^{-1}$ ($I^-\cdots I_2$ in triiodide).[50] Note, that these halogen bonding interactions can be cumulative e.g. in larger molecules and can therefore increase the stability of compounds or adducts dramatically. These interactions can for example be used as a driving force in an attempt to crystallize various organic compounds in supramolecular chemistry.[52]

**Table 2.2:** Calculated dissociation enthalpies [kJ mol$^{-1}$] for polyhalides at the SCS-MP2/def2-TZVPP level of theory.

| Reaction | X=F | X=Cl | X=Br[a] | X=I[a] |
|---|---|---|---|---|
| a) $[X_3]^- \rightarrow X_2 + X^-$ | 110/*100*[53] (98±11)[46] | 110/*103*[54] (99±5)[55] | 127/*127* (127±7)[55] | 132/*131* (126±6)[56] |
| b) $[X_5]^- \rightarrow [X_3]^- + X_2$ | 12/*18*[53] | 36/*38*[54] | 56/*56* | 67 |
| c) $[X_7]^- \rightarrow [X_5]^- + X_2$ | 12 | 31 | 43/*44* | 60 |
| d) $[X_9]^- \rightarrow [X_7]^- + X_2$ | 6 | 28 | 37 | 41 |

[a] Values taken from Haller *et al.*[57]; Values in *italics* are calculated at CCSD(T) level; Values in parenthesis are experimental values.

While all trihalides are very stable, the formation of larger polyiodides is far more favorable than the equivalent polyfluorides, see Table 2.2. The calculated dissociation energies of the trihalides at SCS-MP2 level is close to the high-level CCSD(T) values, which agree excellently with the experimental values. This allows us to use SCS-MP2 calculations to predict the stability of large polyhalides instead of the costly CCSD(T) calculations. Based on these reaction enthalpies a clear trend is visible: Polyiodides are more stable than polybromides and polychlorides which in turn are far more stable than polyfluorides. Furthermore, with increasing size of the polyhalogen anions the bond energy decreases which is due to a larger charge distribution among the coordinated dihalogen molecules.

This represents precisely the current state of research: Polyiodides have been known for decades, polybromides have received attention in the past few years, polychlorides are currently under investigation and only few polyfluorides have been observed spectroscopically under cryogenic conditions in rare gas matrices so far.

### 2.3.4 Analytical Methods

The characterization of polyhalogen compounds has become more thorough as methods have improved over time as well. Even though Chattaway and Hoyle have laid the ground work in the field of polyhalogen chemistry in the 1920s. Their characterization methods were limited to visual

assessment, physical appearance, color, melting point and gravimetric analysis, see above. Nowadays, almost a century later, the methods are of course much more sophisticated.
Polychlorides, polybromides, and polyinterhalides are excellent Raman scatterers which makes Raman spectroscopy in conjunction with X-ray diffraction the methods of choice to precisely describe the polyhalogen anions at hand. In some cases infrared spectroscopy can also be of interest as a complimentary method to support experimental findings. Mass spectrometry as well as NMR spectroscopy are only used as supporting methods in order to fully characterize the synthesized compounds because often only the stability of the corresponding organic cation can be examined. Basic parameters such as viscosity and density of polyhalogen anions are easily obtained. In some instances, the electrochemical characterization of polyhalides can be quite insightful using methods such as conductivity measurement, cyclic voltammetry, and impedance spectroscopy in case of battery applications. State-of-the-art quantum chemical calculations complete the thorough characterization and understanding of polyhalogen compounds.

### 2.3.5 Classification of Polyhalogen Anions

Before we discuss the various polyhalogen anions found in the literature, it is important to make clear how these anions are classified. We want to show this based on the examples of $[Cl_{11}]^- \cdot Cl_2$ vs. $[Cl_{13}]^-$.

1) Spectroscopy: A fundamental characterization method for polyhalides is spectroscopy, especially Raman spectroscopy as mentioned above. The shift (or lack thereof) of the coordinated $X_2$ molecule corresponds to the bond weakening and is largest for a symmetric trihalide.
2) Crystallography: The most important method to distinguish polyhalides is X-ray diffraction which gives undeniable evidence of the atomic positions in relation to one another. This again gives information on angles and bond lengths, not only of the coordinated $X_2$ but also the distance of this $X_2$ to the halide $X^-$. These distances need to be within twice the van der Waals radii to be considered to be part of the polyhalogen anions. In accordance with Pennington's generalizations of halogen bonding,[48] 90° and 180° angles corresponds to strong halogen bonds.
3) Quantum-chemical calculations: The polyhalides can be computed and the differences between theory and experiment can be discussed.

Even though the stoichiometry of chlorine in $[PNP][Cl_{11}] \cdot Cl_2$ and $[PNP][Cl_{13}]$ is the same, the anions are completely different. $[Cl_{11}]^- \cdot Cl_2$ shows six dichlorine molecules of which five are in

direct contact to the central chloride. They show bond lengths between 201.5(1) and 203.6(1) pm. The sixth dichlorine molecule is embedded in the crystal and has a bond length of 198.8(4) pm which is not elongated in comparison to elemental dichlorine (198.5(2) pm). This is in agreement with the Raman spectrum where two bands (540 ($^{35}Cl_2$), 534 ($^{35/37}Cl_2$) $cm^{-1}$) belong to the sixth dichlorine molecule which shows no shift to elemental dichlorine. Additional bands at 494, 480, 465 and 452 $cm^{-1}$ belong to the five coordinated dichlorine moieties. Even though the distance between the sixth dichlorine molecule is as low as 336.6(0) pm, and therefore below the sum of the van der Waals radii, the compound is described as $[PNP][Cl_{11}] \cdot Cl_2$ for the reasons mentioned before. In contrast, in $[Cl_{13}]^-$ all six dichlorine molecules are in interaction with the central chloride in an octahedral arrangement. The elongation of these dichlorine moieties are not only seen by X-ray diffraction but also by the shift in the Raman spectrum (499, 484, 465 $cm^{-1}$).[33]

### 2.3.6 Polyfluorides

Due to the high reactivity of fluorine and the demanding experimental setup, only two polyfluorides have been reported so far: the trifluoride monoanion $[F_3]^-$ and the pentafluoride monoanion $[F_5]^-$.

The first time the trifluoride monoanion $[F_3]^-$ was believed to be synthesized was by Klesper *et al.* in 1952.[58] They treated alkali metal chlorides with a stream of fluorine and insufficiently characterized the product by gravimetric analysis, X-ray powder diffraction, and density measurements. Nine years later, in 1961, it was shown that the reported synthesis actually lead to the formation of fluorochlorates instead of the desired $[F_3]^-$.[59]

The first spectroscopic proof of $[F_3]^-$ was given by Andrews *et al.* in 1977. $MF_3$ (M = K, Rb, Cs) ion pairs were formed after codeposition of thermally evaporated alkali metal fluorides with a fluorine/argon gas mixture under cryogenic conditions. The Raman spectrum showed two bands at 460 $cm^{-1}$ ($\nu_s(CsF_3)$), and 389 $cm^{-1}$ which was assigned to a higher salt complex of CsF and $F_2$. The IR bands at about 550 $cm^{-1}$ were assigned to the antisymmetric stretch of $MF_3$.[60] Free trifluoride was first observed in mass spectrometry experiments by Compton *et al.* in 1999.[61] The first spectroscopic validation was found after co-deposition of laser ablated transition metals with fluorine under cryogenic conditions. The isolated trifluoride anion showed metal independent IR absorption bands at 525 and 511 $cm^{-1}$ in neon and argon, respectively, which were assigned to the anti-symmetric stretching vibration of the free trifluoride monoanion $[F_3]^-$. [61]

The pentafluoride monoanion $[F_5]^-$ was first predicted to be thermodynamically stable in 2010 with an energy barrier of 18 kJ $mol^{-1}$ towards elimination of fluorine (CCSD(T)/aug-cc-pVTZ). As opposed to the all other pentahalide monoanions, the ground state structure of $[F_5]^-$ was computed to show a “hockey stick” like motif which was calculated to be favoured over the

"V-shape" $C_{2v}$ structure by 6.2 kJ mol$^{-1}$ at CCSD(T)/aug-cc-pVTZ level.[53] IR-spectroscopic evidence for the free $[F_5]^-$ anion was first found in 2015 after co-deposition of laser ablated transition metals with fluorine in solid neon under cryogenic conditions with a metal independent band at 850 cm$^{-1}$ ($\nu_{as}([F_5]^-)$.[32,62] Because of the lack of a second band, which would be necessary for the "hockey stick" motif, it seems most logic that the structure is in fact the "V-shaped" one. The contradiction between experiment and calculations is still subject to further high-level quantum-chemical investigations. Polyfluoride dianions or monoanions beyond $[F_5]^-$ have not been reported so far. Moreover, attempts to stabilize polyfluorides in bulk material have not yet been successful.

### 2.3.7 Polychlorides

As expected by the larger σ-hole and stronger halogen bond, a few more polychlorides than polyfluorides are known. The two monoanions $[Cl_3]^-$[63] and $[Cl_5]^-$,[64] the dianion $[Cl_8]^{2-}$[39] and a two dimensional network[65] have been crystallographically characterized, while the monoanion $[Cl_9]^-$[66] has only been observed spectroscopically.

In 1923 Chattaway and Hoyle laid the groundwork for polybromides and polychlorides. They observed that the reaction of tetraethylammonium chloride $[NEt_4]Cl$ with chlorine $Cl_2$ was exothermic and that the reaction with one equivalent of chlorine was more exothermic than the subsequent addition of chlorine,[29] which is congruent with current quantum-chemical calculations, see Table 2.2.

The first structural proof of a trichloride $[Cl_3]^-$ was given by Bogaard *et al.* in 1981.[63] They obtained tetraphenylarsonium trichloride $[AsPh_4][Cl_3]$ after diffusion of chlorine through an aqueous solution of the chloride salt. The resulting trichloride is almost linear (177.5°) and asymmetric with bond lengths of 222.7 and 230.6 pm. In the solid state the trichlorides exist as discrete anions and are arranged in zigzag chains.[64]

Even though 37 years have passed since then, only a few more structures of trichlorides in the solid state have been reported. None of these trichlorides are symmetric with the most symmetric showing a difference in bond lengths of 3.9 pm in $[C_5H_{10}N_2Cl][Cl_3]$.[66] This can be explained by effects in the solid such as halogen-halogen bond or hydrogen bonds with the cation. A plot of the bond lengths of all reported trichlorides in the CCDC is shown in Figure 2.10. Dots on the bisector line would represent symmetric trichlorides, therefore the most symmetric anions are located close to the line.

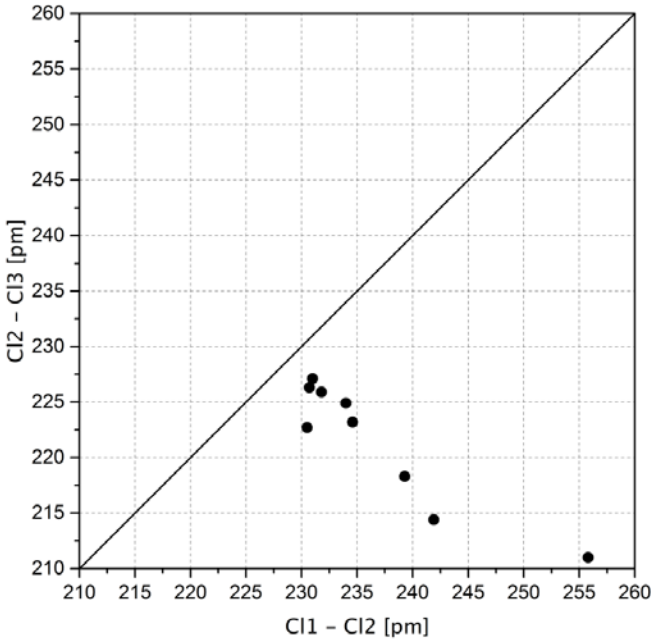


**Figure 2.10:** Plot of Cl-Cl distances of the nine known $[Cl_3]^-$ crystal structures, the bond lengths of the $[Cl_3]^-$ units of the hockey-stick like structure as well as the 2D-polychloride network are included.

The first spectroscopic indication of a pentachloride was presented by Evans and Lo in 1966.[67] They added chlorine to a solution of tetraalkylammonium chlorides in acetonitrile and observed a broad Raman band at 482 $cm^{-1}$, which could neither be assigned to elemental chlorine nor to a trichloride anion. With an excess of chlorine in a 2:1 ratio the trichloride anion band (275 $cm^{-1}$) was still observed in the spectra. However, in a 3:1 ratio the trichloride anion band in the Raman spectra disappeared and only the bands at 482 $cm^{-1}$ and 538 $cm^{-1}$ ($\nu(Cl_2)$) remained. They assumed that the polychloride might be the L-shaped pentachloride anion, which they compared with the already known pentaiodide monoanion $[I_5]^-$.[68] However, it is problematic to characterize a compound based on only one method as has been shown recently. It was also proposed that the pentachloride monoanion is formed when a large excess of chlorine is condensed on tetramethylammonium chloride and subsequently released.[66] The Raman spectrum shows two bands at 341 $cm^{-1}$ and 315 $cm^{-1}$ which are in good agreement with quantum chemical calculations at the CCSD(T)/aug-cc-pVTZ level (371 $cm^{-1}$, 321 $cm^{-1}$), assuming the calculated ground state structure of $C_{2v}$ symmetry with a central chloride coordinating two $Cl_2$ moieties at a distance of 254.3 pm. [66] Nevertheless, the compound was very recently crystallized, measured by single-crystal X-ray diffraction and found to be an extremely asymmetric trichloride which explains the misinterpretation. The bond lengths of this unusual trichloride are 212.7 pm and 249.4 pm. This strong asymmetry can be explained by multiple hydrogen bonds in the solid, disrupting the favored 3c-4e-bond (Fig. 2.11).

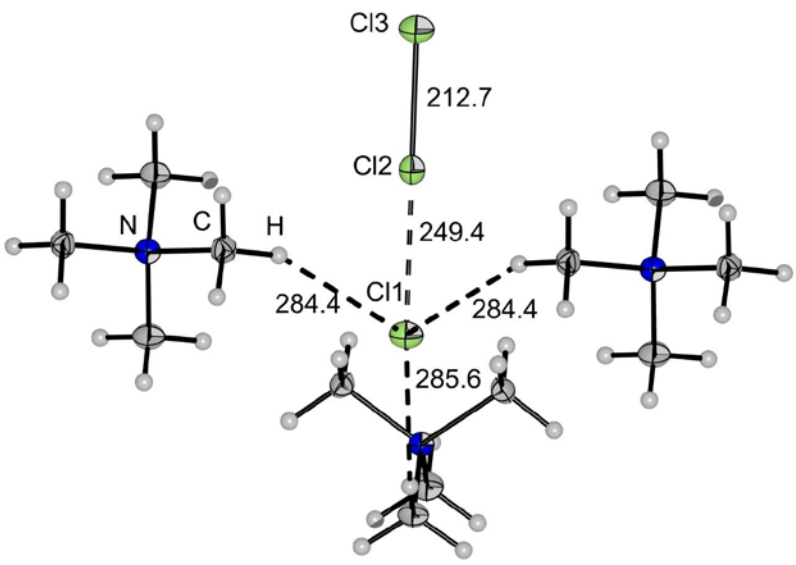


**Figure 2.11:** Structure of $[NMe_4][Cl_3]$ in the solid illustrating an extremely asymmetric trichloride. Bond lengths given in [pm].

Depending on the amount of $Cl_2$ coordination, the vibrational bands are shifted between the lowest frequencies in the case of $[Cl_3]^-$ at 279 $cm^{-1}$[54] and free $Cl_2$ at 539 $cm^{-1}$.[69] In 2003 Taraba and Zak treated $[PPh_2Cl_2][Cl_3]$ with an excess of $Cl_2$ and observed two Raman bands (286 $cm^{-1}$ and 466 $cm^{-1}$), similar to those of Evans and Lo (275 and 482 $cm^{-1}$), when they proposed the pentachloride anion.[64] As opposed to Evans and Lo, Taraba and Zak were able to characterize their compound by single crystal X-ray diffraction and gave the first structural proof of a pentachloride monoanion $[Cl_5]^-$, while it can also be described as an interaction between a trichloride and a chlorine moiety as the original authors have done (Fig. 2.12). The hockey-stick structure consists of an asymmetric trichloride anion with bond length of 241.9(3) and 214.4(3) pm and a coordinated $Cl_2$ molecule at a distance of 317.1(3) pm, which is shorter than the sum of the van-der Waals radii of chlorine (350 pm).[70] Furthermore, the bond length of the coordinated $Cl_2$ is 202.5(3) pm and therefore elongated by 4.1 pm in comparison to elemental chlorine.[64]

Similarly, it has been suggested that the nonachloride has been synthesized while the only characterization for the nonachloride monoanion $[Cl_9]^-$ is Raman spectroscopy. At the RI-MP2/def2-TZVPP level of theory the Raman spectrum of an isolated $[Cl_9]^-$ with $T_d$-symmetry is calculated to show two Raman active bands at 473 $cm^{-1}$ and 436 $cm^{-1}$. Brückner has proposed the synthesis of five nonachloride salts including $[C_5H_{10}N_2Cl][Cl_9]$ (491, 458 $cm^{-1}$), $[NMe_3Ph][Cl_9]$ (475, 448 $cm^{-1}$) and $[NEt_4][Cl_9]$ (460, 430 $cm^{-1}$).[66] Considering the broad range of bands, one can certainly agree that polychlorides have been obtained but that the exact nature of them cannot unambiguously be declared as nonachlorides.

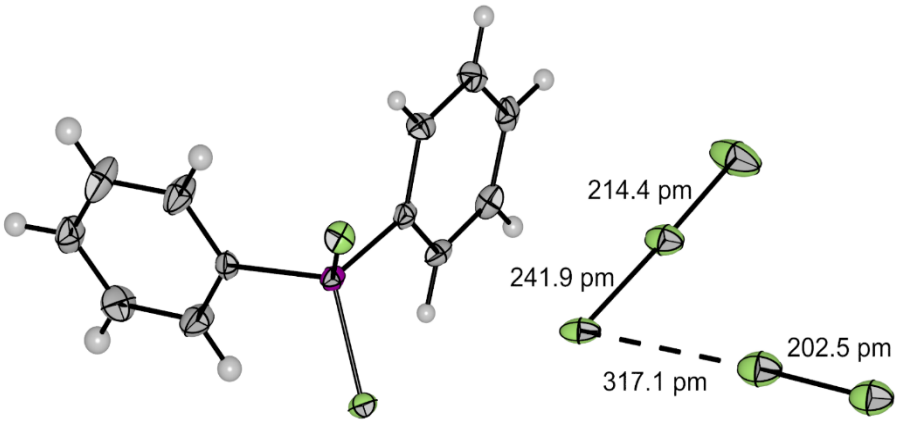


**Figure 2.12:** Hockey stick like structural motif of the polychloride monoanion in $[PPh_2Cl_2][Cl_3^-\cdots Cl_2]$.[64]

Apart from these monoanions, one report mentions the first and hitherto only polychloride dianion.[39] $[CCl(NMe_2)_2]_2[Cl_8]$ (tetramethylchloroamidinium octachloride) was synthesized in an eutectic mixture of ionic liquids ([BMP]Cl/[BMP][OTf]) based on the success of this technique in the synthesis of polybromides. The octachloride is structurally similar to the heavier homologues $[Br_8]^{2-}$ and $[I_8]^{2-}$.[38,71,72] The Z-shape structure can be described twofold: either as two distorted $[Cl_3]^-$ units bridged by a $Cl_2$ molecule or as a more chloride centered bonding in $[Cl_2\text{-}Cl^-\text{-}Cl_2\text{-}Cl^-\text{-}Cl_2]$. Interestingly the $[Cl_8]^{2-}$ and $[Br_8]^{2-}$ dianions present a more linear structure in comparison to the more Z-like shape of its iodine counterpart, see Figure 2.13.

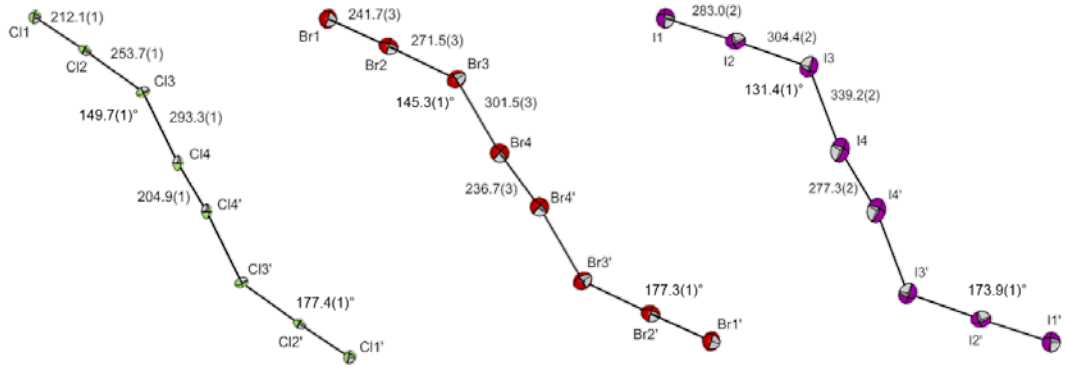


**Figure 2.13:** Comparison of the polyhalogen dianion structures of $[Cl_8]^{2-}$[39], $[Br_8]^{2-}$[38] and $[I_8]^{2-}$[72]. Bond lengths given in [pm].

On the one hand the bonding situation in the $[Cl_8]^{2-}$ can be explained by weaker σ-hole interactions, since the angle of 149.7(1)° differs from the ideal 90° expected for strong σ-hole interactions. On the other hand quantum-chemical calculations revealed that the deviation from the Z-like structure of the dianions arises due to packing effects in the crystal.[39] This assumption is supported by the polybromide dianion $[Br_8]^{2-}$ in $[BrC(NMe_2)_2][Br_8]$, which shows almost the same crystal packing.[38]

### 2.3.8 Polybromides

A relatively large variety of polybromide anions is known. These range from small monoanions and dianions to large networks consisting of thirteen known mono- and dianions. As metioned above, the first systematic investigation of polybromides dates back to Chattaway and Hoyle and their report in 1923.[29] In the following decades, some spectroscopic and electrochemical investigations of polybromides were published. However, it wasn't until the last decade that polybromides have once again become a center of attention resulting in a variety of new structurally proven anions. So far, five polybromide monoanions beyond the $[Br_2]^-$ have been structurally characterized: $[Br_3]^-$,[29,73,74] $[Br_5]^-$,[73,75] $[Br_7]^-$,[76,77] $[Br_9]^-$[11,34,57] and $[Br_{11}]^-$.[78] The typically observed and calculated Raman bands are listed in Table 2.3.

**Table 2.3:** Raman bands in [$cm^{-1}$] of polybromide monoanions in comparison to calculations.

| Monoanion | Compound | Exp. | Calc. |
|---|---|---|---|
| $[Br_3]^-$ | $[NEt_4][Br_3]$[73] | 163 | 171[a] |
| | | 198 | 218[a] |
| $[Br_5]^-$ | $[NEt_4][Br_5]$ [73] | 253 | 252[a] |
| | | | 147[a] |
| | | 210 | 217[a] |
| | | | 136[a] |
| $[Br_7]^-$ | $[NEt_4][Br_7]$ [73] | 270 | 282[a] |
| | | | 135[a] |
| | | | 250[a] |
| | | | 109[a] |
| $[Br_9]^-$ | $[NPr_4][Br_9]$[34] | 274 | 277[b] |
| | | 259 | 255[b] |
| | | | 116[b] |
| $[Br_{11}]^-$ | $[PNP][Br_{11}] \cdot Br_2$[78] | 297 | 334[c]/310[d] |
| | | 286 | 295[c]/277[d] |
| | | 269 | 278[c]/259[d] |
| | | 264 | 271[c]/255[d] |

Calculated at [a] MP2/6-31G(d) [b] RI-MP2/def2-TZVPP [c] SCS-MP2/ def2-TZVPP (square payramidal) [d] SCS-MP2/def-SV(P) (trigonal bipyramidal)

**Dibromide Monoanion $[Br_2]^-$:** The dibromide anion $[Br_2]^-$ was first observed by Andrews *et al.* who performed matrix-isolation experiments of alkali metals such as Li, Na, K, Rb and Cs in an $Ar/Br_2$ environment at cryogenic conditions. The observed Raman bands for the alkali metal salts were around 149-160 $cm^{-1}$ except for sodium where the band was observed at 115 $cm^{-1}$. In addition, they found that the dibromide anion has a strong $\sigma \rightarrow \sigma^*$ absorption near 365 nm and a weak $\pi^* \rightarrow \sigma^*$ band at 660 nm.[79] Also in bulk material, a band in the UV/Vis-spectrum can be assigned at $\lambda_{max} = 360$ nm.[80]

Mainly in marine chemistry such radical anions $[Br_2]^-$ can be observed. Bromide is a scavenger for OH· radicals resulting in a bromide radical which easily reacts with another bromide to form these $[Br_2]^-$ radicals.[81] In return, dibromide radicals, which can further react with dissolved organic matter, are consequently brominating agents in nature. The electrochemical potential of $E([Br_2]^-/2\ Br^-)$ is at 1.63 V vs. NHE.[82]

**Tribromide Monoanion $[Br_3]^-$:** Among all polybromides, the tribromide has been studied to the largest extent. The linear ion can be symmetric or asymmetric depending on the counter ion used. In 2011, Pichierri closely examined all tribromides in high resolution crystal structures ($R1 \leq 0.05$) and found approximately one fourth to be symmetric (Fig. 2.14).[83] Asymmetric tribromides most often rise from interactions with the cation. Indeed, the two most asymmetric tribromides both show strong interactions either by hydrogen bond[84] or halogen-halogen bonding[85] (Fig. 2.15).

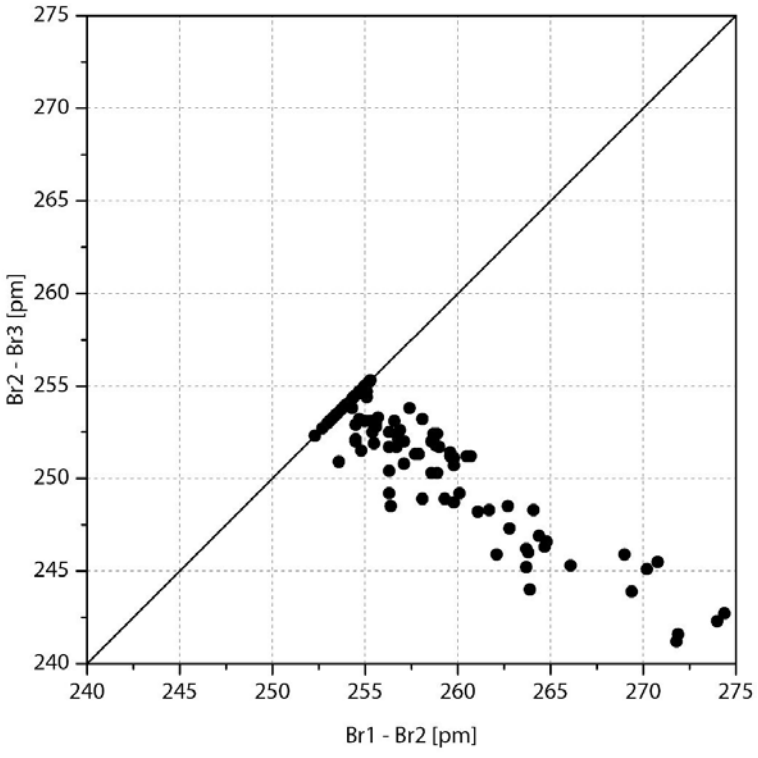


**Figure 2.14:** Plot of Br-Br distances of the 101 known $[Br_3]^-$ crystal structures (CCDC, $R1 \leq 0.05$).

Polybromide anions are formed in zinc-bromine redox-flow-batteries which substantially enhance the conductivity in such system.[86] In 1958 Popov and Geske examined the voltammetric behavior of tetra-*n*-butylammonium tribromide and various interhalides.[87] They observed three waves using a setup with a rotating platinum electrode and a silver-silver nitrate reference electrode. Two waves were assigned as:

$$6\ Br^- \rightleftharpoons 2\ [Br_3]^- + 4\ e^- \qquad (2.4)$$

$$2\ [Br_3]^- \rightleftharpoons 3\ Br_2 + 2\ e^- \qquad (2.5)$$

However, it was noted that the reactions are not reversible as seen by the voltammograms and the altered surface of the platinum electrode. The authors could not rationalize their observation of a third wave. Based on the previous work by Popov and Geske, Iwasita and Giordano analyzed the electrochemical behavior of the tribromide anions in more depths.[88] They used the same setup but with lithium bromide in acetonitrile instead. Again, the two waves were observed and the cathodic and anodic waves were assigned to the same reactions as done by Popov and Geske. Additionally, kinetic parameters as well as diffusion coefficients were determined.

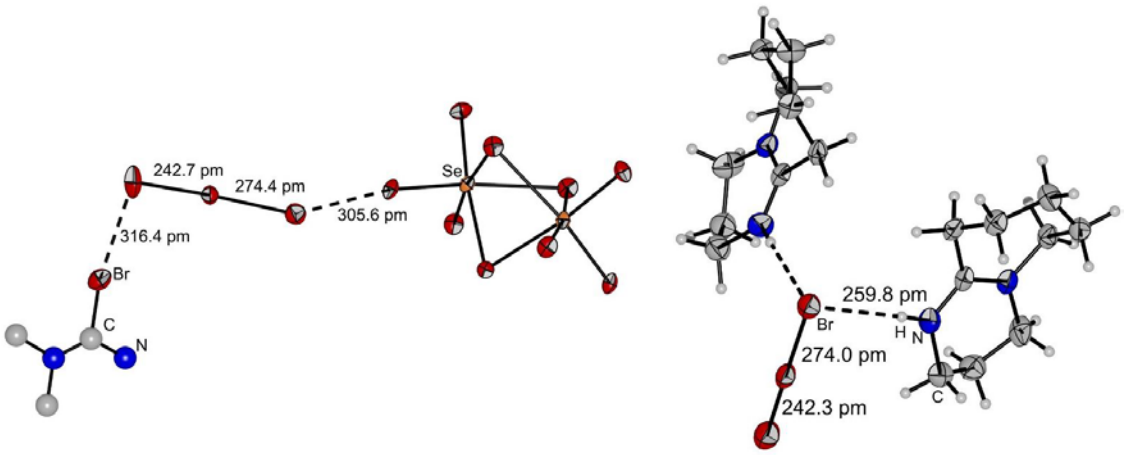


**Figure 2.15:** The two most asymmetric tribromides: Halogen bond[85] (left) and hydrogen bond[84] (right).

**Pentabromide Monoanions $[Br_5]^-$:** Bellucci *et al.* proposed that the tribromide and the pentabromide play a role in the formation of the intermediate bromonium ion.[89] They investigated the equilibrium between the two polybromides by UV-spectroscopy and observed a new band when bromide and bromine were dissolved in an aprotic solvent. This band is bathochromically shifted to that of the tribromide but hypsochromically to that of elemental bromine and was assigned to the formation of a pentabromide anion. The first evidence of the formation of a pentabromide monoanion was shown by vibrational spectroscopy by Evans and Lo in 1967.[90] They investigated the Raman bands of a potassium bromide solution upon addition of one and two equivalents of bromine. While the 1:1 ratio gave the expected Raman band of the

tribromide, the solution with a 1:2 ratio had a new band at 250 $cm^{-1}$. This band could neither be assigned to the known tribromide anions nor to free bromine. Their conclusion was that a symmetric $[Br_2–Br–Br_2]^-$ species was formed. They suggested that it had a V-shaped structure with the two outer Br-Br bonds being stronger than the inner ones. Similarly, Chen *et al.* observed a Raman band at 245 $cm^{-1}$ for $[NEt_4]Br$ upon addition of two equivalents of $Br_2$ forming $[NEt_4][Br_5]$.[73]

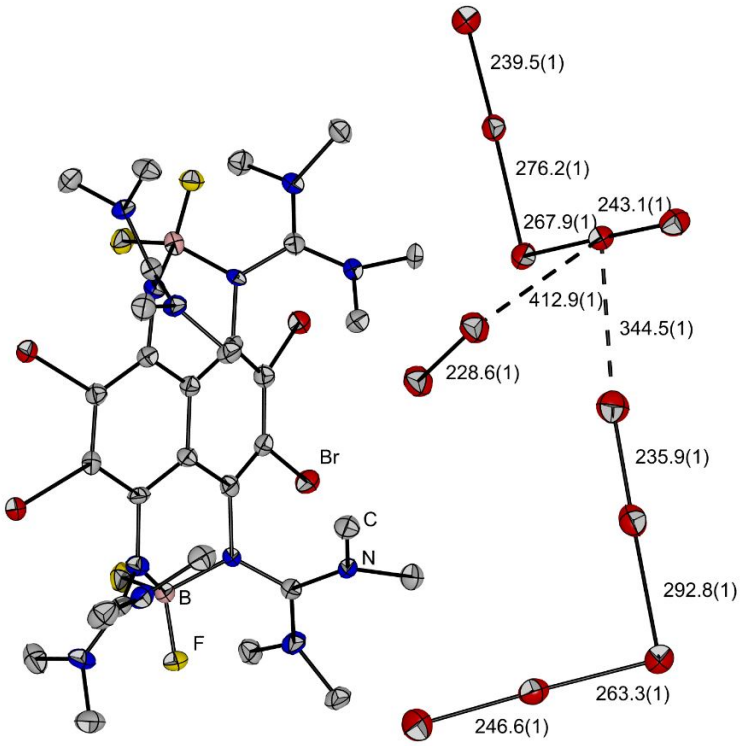


**Figure 2.16:** Structure of $[(ttmgn\text{-}Br_4)(BF_2)_2](Br_5)_2(Br_2)_{0.65}$ in the solid state. Bond lengths given in [pm].[75]

The first structural evidence was provided more than fifty years later by Himmel *et al.* in 2012.[75] They synthesized and crystallized $[(ttmgn\text{-}Br_4)(BF_2)_2][Br_5]_2$ ttmgn = [1,2,4,5-tetrakis(tetramethylguanidinyl)naphthalene] by adding an excess of bromine to ttmgn in acetonitrile (Fig. 2.16). In the same work, they also reported another $[Br_5]^-$ in $[(btmgn\text{-}Br_4)(BF_2)][Br_5]$ btmgn=1,8-bis(tetramethylguanidinyl)naphthalene]. The observed pentabromide monoanions consist of a central bromide coordinated by two bromine molecules. The bond lengths of the coordinated bromine molecules are significantly elongated in comparison to elemental bromine because electron density from the HOMO of the bromide is donated into the LUMO of the coordinated $Br_2$ resulting in a bond length elongation. In average, the outer Br-Br bond lengths are 241.3 pm and 240.6 pm (elemental $Br_2$: 227 pm[91]) while the inner Br-Br bond lengths are 275.1 pm and 276.2 pm for ttmgn and btmg, respectively.

**Heptabromide Monoanion $[Br_7]^-$:** The next higher polybromide monoanion is the heptabromide $[Br_7]^-$ which shows a trigonal pyramidal structure with $C_{3v}$ symmetry as expected by VSEPR theory. In 2010, Chen *et al.* characterized tetraethylammonium heptabromide by Raman spectroscopy and compared their experimentally observed results to quantum-chemical calculations at MP2/6-31G(d) level of theory.[73] The theoretically possible linear $[Br_7]^-$ structure was dismissed as unlikely by Pichierri in 2011 and a $C_{3v}$ symmetric isomer was predicted to be the most stable isomer.[83] Indeed, a few weeks later, Feldmann *et al.* successfully synthesized $[PPh_3Br][Br_7]$ and obtained the first structure of this polybromide monoanion in the solid state (Fig. 2.17). As expected the $[Br_7]^-$ structure shows a trigonal pyramidal motif.[77] As already discussed above for the polychlorides, they used an eutectic mixture of two ionic liquids ($[C_{10}MPyr]Br$ and $[C_4MPyr][OTf]$) as solvent in the reaction of triphenylphosphine and elemental bromine in a 1:5 ratio.

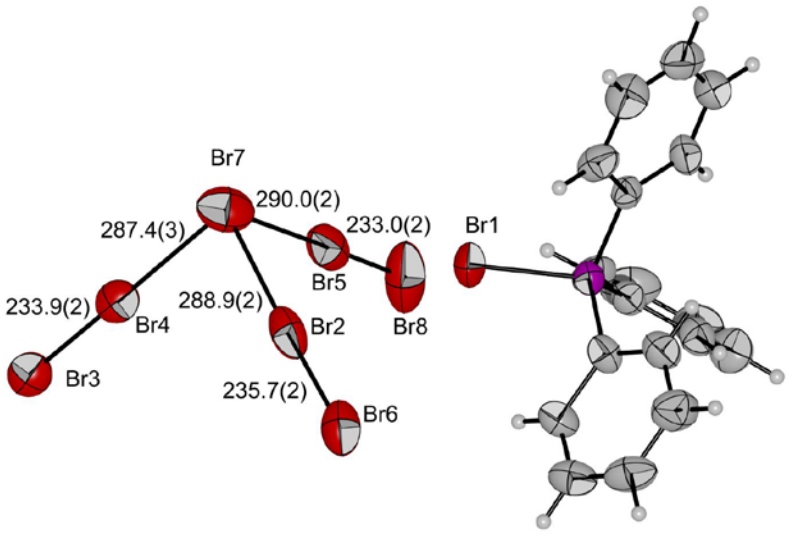


**Figure 2.17:** Structure of $[PPh_3Br][Br_7]$ showing the trigonal pyramidal $[Br_7]^-$ anion. Bond lengths given in [pm].[77]

The heptabromide units are more or less connected to four neighboring heptabromides. The distance between the heptabromides are much longer than the intramolecular distances within a heptabromide. Based on these observations they can be regarded as discrete anions. Alhanash *et al.* prepared another example of such a $[Br_7]^-$ anion in $[o\text{-}SCH_3C_6H_4)_3PBr][Br_7]$.[76] In both cases, a contact between the phosphonium cation and the heptabromide is observed due to halogen-halogen interactions between the bromine atom of the cation and one of the anion. So far, these two reported structures remain the only structurally observed heptabromide anions.[76,77]

**Nonabromide Monoanion $[Br_9]^-$:** Of all conceivable isomeric structures, the nonabromide anions ideally show a tetrahedral structure. Quantum-chemical calculations indicate that distortions of this structure are easily possible due to the flat hypersurface of the opening angle.[34] This distortion is to some extent dependent on the counter ion at hand. The first vibrational characterization of a nonabromide was again done by Chen *et al.* who examined the monoanions from $[Br_3]^-$ to $[Br_9]^-$ using the tetraethylammonium cation.[73] They observed two Raman bands at 257 and 276 $cm^{-1}$ which are in accordance with their *ab-initio* MP2/6-31G(d) calculations. A year later in 2011, the first structural proof of a nonabromide anion was found in the structure of $[N(n\text{-}Pr)_4][Br_9]$.[34] Haller *et al.* examined the structural motifs of the nonabromide in dependence of the ammonium counterions $[NMe_4]^+$, $[NEt_4]^+$, $[N(n\text{-}Pr)_4]^+$ and $[N(n\text{-}Bu)_4]^+$.[57] The nonabromide anions are linked to chains in the case of tetramethylammonium while the nonabromides form layers in the case of tetraethylammonium. By employing the tetrapropylammonium salt, the nonabromides are the most isolated but loosely form a three-dimensional network through much longer intermolecular Br-Br bond distances. In all three cases, the building blocks are $Br^-$ and $Br_2$. However, in the case of tetrabutylammonium three building blocks are observed: $Br^-$, $Br_2$ and $[Br_3]^-$. In the molecular structure of $[N(n\text{-}Bu)_4][Br_9]$ in the solid state, two structural motifs are observed. The first consists of a central bromide coordinated by six bromine molecules of which two are terminal and four are bridging. The other motif consists of a tribromide coordinated by three bridging bromine molecules on each terminal bromine atom of the tribromide. This is clearly shown in both determinations, the solid state structure and in the Raman spectra. All nonabromides show two bands at approximately 260 and 275 $cm^{-1}$. Only $[N(n\text{-}Bu)_4][Br_9]$ shows an additional third band which is assigned to the formed tribromide anion. Free tribromides are expected at about 160 $cm^{-1}$. However, the tribromide here is shifted to higher wavenumbers (219 $cm^{-1}$) due to its coordination (Fig. 2.18).

All nonabromides exhibit a surprisingly high conductivity, e. g. $[HMIM][Br_9]$ (HMIM=1-hexyl-3-methylimidazolium) shows a conductivity of 52.1 mS $cm^{-1}$ at 25.6 °C which is 1000 times higher than that of the simple bromide [HMIM]Br (54.2 µS $cm^{-1}$) and even higher than that of elemental bromine (isolator).[11] This conductivity is surpassed by ammonium based nonabromides that melt at higher temperatures. The mechanism of this conductivity is believed to follow a Grotthuss-type hopping mechanism as it is well-known from proton hopping in water. $[HMIM][Br_9]$ is a room temperature ionic liquid with a low viscosity, yet high viscosity and thermal stability, combined with a high electrochemical stability.

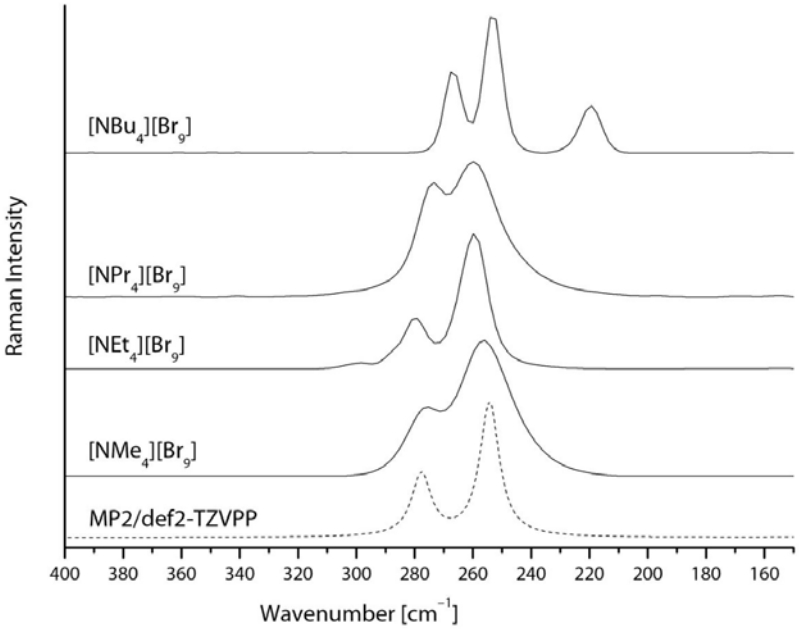


**Figure 2.18:** Raman spectra of tetraalkylammonium nonabromides.[57]

**Undecabromide Monoanion $[Br_{11}]^-$:** The first report on an undecahalide among the halogens was given by Groessl *et al.* in 2011. They observed a series of polyiodides such as $[I_{11}]^-$, $[I_{13}]^-$ and $[I_{15}]^-$ in a mass spectrometry investigation using the electro-spray-ionization technique.[92] Shortly after, the highest structurally known polybromide monoanion to date was found as $[PNP][Br_{11}] \cdot Br_2$ (Fig. 2.19).[78] PNP (PNP = bis(triphenylphosphine)iminium) is a very bulky cation which is stable against elemental chlorine and bromine. Therefore, it was used for the stabilization of bulky, high-order polybromides. The resulting undecabromide anion consists of a bromide which is coordinated by five bromine molecules. A sixth $Br_2$ is embedded in the crystal structure. But this $Br_2$ molecule is better described as an embedded crystal bromine based on structural and vibrational data. Using the τ-parameter proposed by Addison *et al.*[93] one can determine that the undecabromide ($\tau = 0.18$) has an almost square pyramidal structure. Haller *et al.* reported that the anions are loosely interconnected to form a three dimensional network. Quantum-chemical calculations at SCS-MP2 level show that the trigonal bipyramidal structure ($\tau = 1$) and the square pyramidal structure ($\tau = 0$) are almost equal in energy.

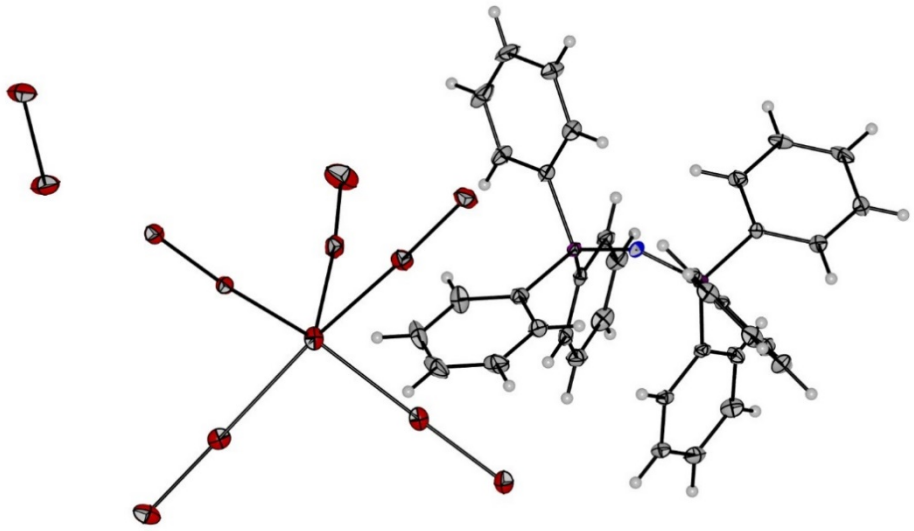

**Figure 2.19:** Structure of [PNP][$Br_{11}$] · $Br_2$ in the solid state.[78]

**Polybromide Monoanions beyond $[Br_{11}]^-$:** In 1923 Chattaway and Hoyle concluded to have [$NMe_4$][$Br_{13}$] and therefore the first $[Br_{13}]^-$ by exposing [$NMe_4$]Br to bromine vapor.[29] Their gravimetric methods showed that tetramethylammonium bromide absorbed 5.7 equivalents of bromine which is almost equal to the necessary ratio of 1:6 for the formation of the tridecabromide. However, they admittedly had no evidence for the formation of such a specific anion, especially the $[Br_{13}]^-$ and it sounds unrealistic, based on our current knowledge, that this anion is formed by such a small counter ion. Quantum-chemical calculations at RI-MP2/def2TZVPP level suggest that $[Br_{13}]^-$ indeed shows an octahedral structure with a central bromide coordinated by six bromine molecules. The calculated bond lengths of the $O_h$ symmetrical $[Br_{13}]^-$ are 297 and 233 pm for inner and outer Br-Br bonds, respectively.[31] The tridecabromide most likely represents the highest conceivable polybromide monoanion with a regular VSEPR structure of $O_h$ symmetry. But so far there has been no spectroscopical or structural proof for this species.

Even more polybromide dianions than monoanions are experimentally known, namely eight: $[Br_4]^{2-}$,[94–96] $[Br_6]^{2-}$,[97] $[Br_8]^{2-}$,[38,72,98] $[Br_{10}]^{2-}$,[99] $[Br_{14}]^{2-}$,[100] $[Br_{16}]^{2-}$,[100] $[Br_{20}]^{2-}$[37,41,100] and $[Br_{24}]^{2-}$.[42] The typically observed and calculated bands of the Raman spectra are listed in Table 2.4. The highest polybromides $[Br_{20}]^{2-}$ and $[Br_{24}]^{2-}$ show a broad band just below 300 $cm^{-1}$ which shows that high order polybromides are difficult to distinguish only by spectroscopical means.

**Table 2.4:** Raman bands in [$cm^{-1}$] of polybromide dianions in comparison to calculations.

| Dianion | Compound | Exp. | Calc. |
|---|---|---|---|
| $[Br_4]^{2-}$ | $(CH_3)_2SBr^+Br^-_{0.5}(Br_4^{2-})_{0.25}$[95] | 232 | |
| | $(H_4tppz^{4+})(Br^-)_2(Br_4^{2-})$[96] | 167 | 176[a] |
| | | 74 | 70[a] |
| $[Br_6]^{2-}$ | $[C_5H_{10}N_2Br]_2[Br_6]$[97] | 205 | 205[b] |
| | | 181 | 182[b] |
| | | 165 | 170[b] |
| | | 139 | 125[b] |
| $[Br_8]^{2-}$ | $[BrC(NMe_2)_2)]_2[Br_8]$[38] | 275 | |
| | | 252 | |
| | | 223 | |
| $[Br_{10}]^{2-}$ | $[C_{13}H_{11}N_4]_2[Br_{10}]$[99] | 193 | |
| | | 175 | |
| | | 144 | |

Calculated at [a] MP2/LanL2DZ [b] RI-MP2/aug-ccpVTZ, COSMO ε= 100

**Tetrabromide Dianion $[Br_4]^{2-}$:** The first in this series, the tetrabromide dianion, was also the first to be structurally proven by Strømme as early as 1959.[94] The dianion was easily prepared by adding a diluted bromine solution to dimethylammonium bromide in chloroform resulting in flat orange needles. The single crystal X-ray diffraction using Cuα radiation revealed that $[Br_4]^{2-}$ has an almost linear structure with a Br-Br-Br angle of 173°. The first Raman spectroscopic investigation of the tetrabromide dianion was done by Muir *et al.* in 1999.[95] They synthesized $[(CH_3)_2SBr^+][Br^-_{0.5}(Br_4^{2-})_{0.25}]$ and observed a band at 232 $cm^{-1}$ in the polybromide region which they assigned to the ν(Br-Br) in $Br_2$. In contrast, Ogilvie *et al.* also observed a $[Br_4]^{2-}$ in $[H_4tppz^{4+}][(Br^-)_2(Br_4^{2-})]$ (tppz = tetra(2-pyridyl)pyrazine) with inner and outer bond lengths of 241.7 pm and 296.8 pm, respectively.[96] However, they found two bands at 167 and 74 $cm^{-1}$ which they assigned to the inner and outer Br-Br stretching mode, respectively. This observation is in good agreement with quantum-chemical calculations at MP2/LanL2DZ level.[96]

**Hexabromide Dianion $[Br_6]^{2-}$:** The only known hexabromide was discovered very recently in $[C_5H_{10}N_2Br]_2[Br_6]$.[97] It consists of two tribromides connected end-on in an 87° angle. The formation of the anion is additionally stabilized by the cation in two ways. Firstly, the cation sterically hinders the thermodynamically more stable T-like structure and secondly, through

halogen bonding interactions between the anion and the bromine atom of the cation, the structural arrangement of the anion is stabilized even further (Fig. 2.20). This interaction of the two tribromides to form the hexabromide is also seen in the Raman spectrum with four bands in the region of polybromides at 205 (ν(Br2-Br8)), 181 ($\nu_{as}$(Br4-Br1-Br7)), 165 ($\nu_{s}$(Br4-Br1-Br7)) and 139(ν(Br2-Br6)) $cm^{-1}$.

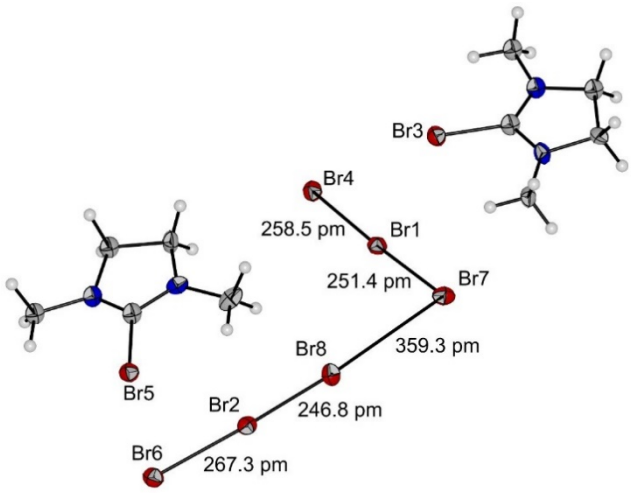


**Figure 2.20:** Structure of $[C_5H_{10}N_2Br]_2[Br_6]$ in the solid state.[97]

**Octabromide Dianion $[Br_8]^{2-}$:** Several octabromides $[Br_8]^{2-}$ are known which all consist of the building blocks $[Br_3]^-$ and $Br_2$ and have a planar Z-shaped structure. The first reported $[Br_8]^{2-}$ was found in diquinuclidinium octabromide by Knop *et al.* in 1997.[72] Later, Fromm *et al.* also reported on the polybromide dianion containing compound $[H_3O$(Br4-dibenzo-18-crown-6$][Br_3 \cdot Br_2]$.[98] Even though the stoichiometry is correct, the polybromide dianion present in the crystal structure is clearly a $[Br_8]^{2-}$. Also Feldmann *et al.* synthesized an octabromide in $[BzPh_3P]_2[Br_8]$, again in an eutectic mixture of ionic liquids.[77] Similar to the only known octachloride, the shape of the $[Br_8]^{2-}$ units can differ significantly from the ideal 90° angles between $Br_2$ and the two tribromides. In the case of $[BrC(NMe_2)_2]_2[Br_8]$ the angle can be widened to 145.2°.[38]

**Decabromide Dianion $[Br_{10}]^{2-}$:** The only known decabromide can be obtained by reaction of 1,5-diphenylformazan to yield the tetrazolium salt.[99] The rectangular $[Br_{10}]^{2-}$ consist of two $[Br_3]^-$ units interconnected by two $Br_2$ linkers. The $Br_2$ units have a bond length of 274 pm and are therefore elongated by 47 pm in comparison to solid $Br_2$ (227 pm). The Raman spectrum shows three significant bands at 144, 175 and 193 $cm^{-1}$. Cunningham *et al.* reasonably assigned the band at 193 $cm^{-1}$ to the elongated $Br_2$ unit. The bands at 175 and 144 $cm^{-1}$ are assigned to the anti-symmetric and symmetric stretching vibrations of the slightly anti-symmetric tribromide (291 and 294 pm).

**Tetradecabromide Dianion $[Br_{14}]^{2-}$:** Two examples of the tetradecabromide dianion $[Br_{14}]^{2-}$ are known. In $[(C_6H_5)_3PBr]_2[Br_{14}]$ the dianion consists of two very closely associated $[Br_7]^-$ subunits similar to the $[Br_7]^-$ by Feldmann *et al.*[77] The other example of $[Br_{14}]^{2-}$ shows a completely different structural motif. In $[(C_6H_4F)_3PBr]_2[Br_{14}]$ the anionic network is made up of planar $[Br_9]^-$ units which are interconnected by additional $Br_2$ units via the central bromide resulting in an octahedral arrangement which is a very rare motif in polyhalogen chemistry. These $[Br_9 \cdot Br_2]^-$ moieties are further connected by tribromides to form a complex three-dimensional network.[100]

**Sedecabromide Dianion $[Br_{16}]^{2-}$:** The compound $[PNP]_2[Br_{16}]\cdot Br_2$ was synthesized via the reaction of [PNP]I (PNP = bis(triphenylphosphine)iminium ) with seven equivalents of elemental bromine. As expected from the standard electrode potential, $Br_2$ most likely oxidizes $I^-$ to $I_2$ while $Br_2$ is reduced to $Br^-$. These bromide anions are then complexed by the excess of $Br_2$. The formed sedecabromide, which shows a broad Raman band at 283 $cm^{-1}$ is built of two T-shaped $[Br_7]^-$ anions interconnected by a dibromine moiety via the central $Br^-$.[101] Another example of a sedecabromide was recently reported using partly fluorinated cations: $[(C_6H_2F_3)_3PBr]_2[Br_{16}]$. Here, the dianion can also be broken down into two $[Br_7]^-$ anions which are connected by a dibromine molecule in a 89.6(1)° angle which is close to the typical 90° angle for halogen bonding. The cation $[(C_6H_2F_3)_3PBr]^+$ shows weak halogen bonding contacts to the dianion of 356.6(1) pm, see Figure 2.21.[100]

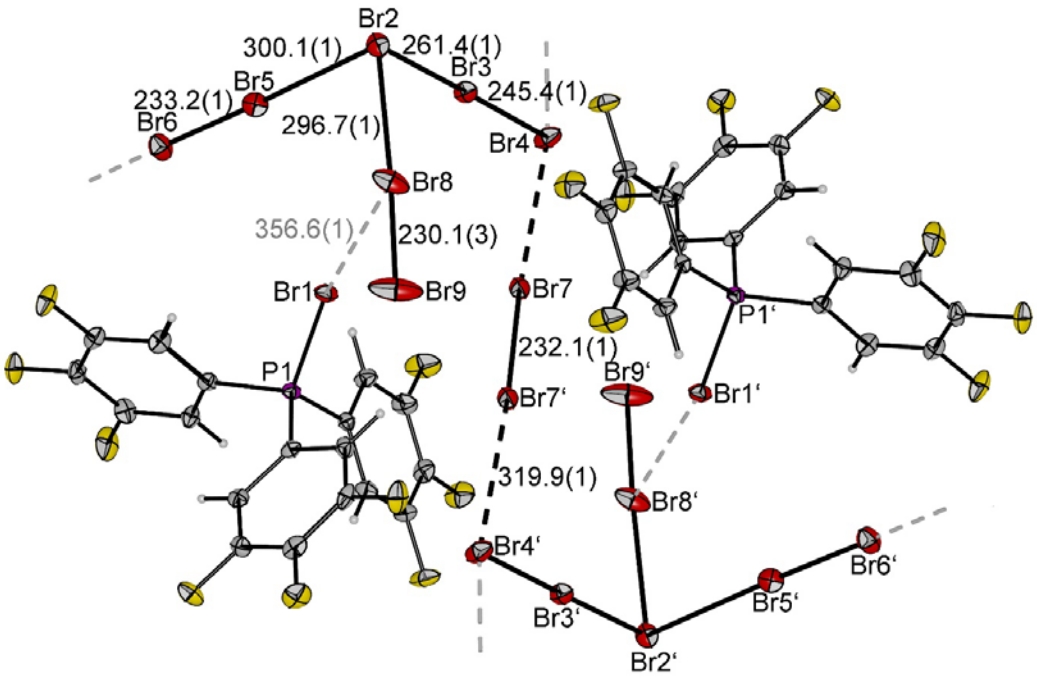


**Figure 2.21:** Structure of $[(C_6H_2F_3)_3PBr]_2[Br_{16}]$ in the solid state. Bond lengths given in [pm]. (Copyright Wiley-VCH Verlag GmbH & Co. KGaA.) [100]

**Eicosabromide $[Br_{20}]^{2-}$:** The next higher polybromide dianion is the eicosabromide $[Br_{20}]^{2-}$ found in $[C_4MPyr]_2[Br_{20}]$ and $[(n\text{-}Bu)_3MeN]_2[Br_{20}]$ by Feldmann *et al.*[41] This bromine rich compound was again synthesized and crystallized in an eutectic mixture of ionic liquids ($[C_4MPyr]Br$ and $[C_4MPyr][OTf]$). A central bromide is octahedrally coordinated by six bromine molecules which in turn have close contacts to the remaining bromine molecules (Fig. 2.22). This structurally results in a three dimensional network with distorted, corner-sharing octahedra with interlinked bromine molecules and embedded cations. Whereas the Raman spectra only show a broad signal between 100 and 300 $cm^{-1}$, the thermogravimetric measurements revealed that $[C_4MPyr]_2[Br_{20}]$ is slightly more stable than $[(n\text{-}Bu)_3MeN]_2[Br_{20}]$.

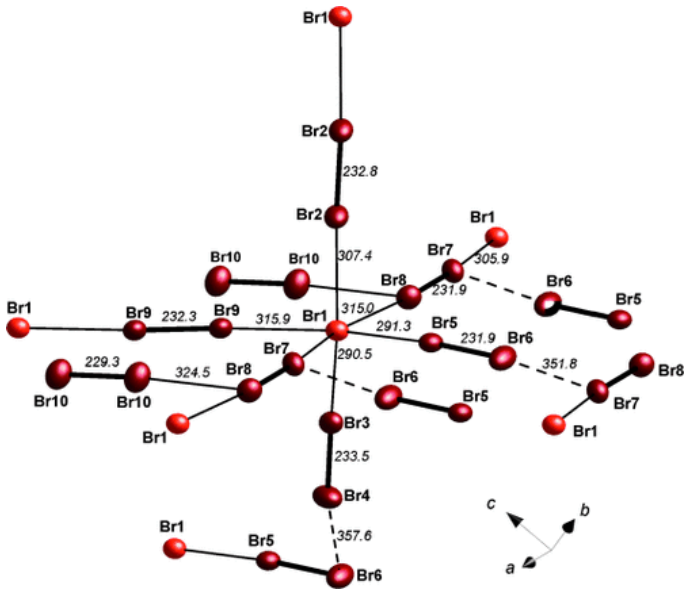


**Figure 2.22**: Structure of $[Br_{20}]^{2-}$ in $[C_4Mpyr]_2[Br_{20}]$. Bond lengths are given in [pm]. Light red atoms represent bromide, and dark red atoms represent dibromine. (Copyright Wiley-VCH Verlag GmbH & Co. KGaA.)[41]

**Tetracosabromide Dianion $[Br_{24}]^{2-}$:** The highest polybromide dianion network known to date is the tetracosabromide $[Br_{24}]^{2-}$.[42] Maschmeyer *et al.* synthesized $[(n\text{-}Bu)_4P]_2[Br_{24}]$ by volumetric addition of bromine to an eutectic mixture of $[(n\text{-}Bu)_4]Br$ and $[P_{6,6,6,14}]Br$. The resulting dianion (Fig. 2.23) shows similarities to the $[Br_{11}]^- \cdot Br_2$ by Haller.[78] The central bromide is five-fold coordinated by $Br_2$ units and a further bromine molecule is end-on coordinated. The latter bromine is elongated (230.4 pm) in contrast to the embedded bromine in $[PNP][Br_{11}] \cdot Br_2$ [78] which shows a Br-Br distance of 227.3 pm and therefore no elongation. This "embedded" bromine molecule in $[(n\text{-}Bu)_4P]_2[Br_{24}]$ is therefore considered to be part of the dianion, resulting in a three-dimensional network stabilized by twelve H···Br contacts per formula unit.

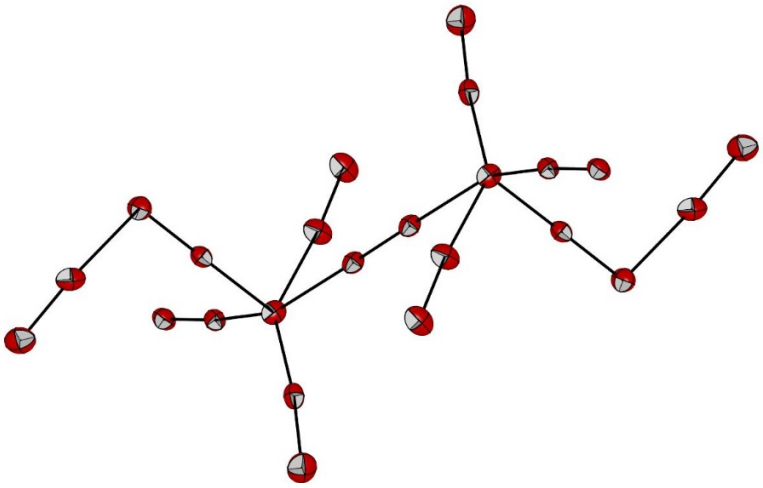

**Figure 2.23:** The highest known polybromide: $[Br_{24}]^{2-}$ in $[(n\text{-}Bu)_4P]_2[Br_{24}]$. Ellipsoids are shown at the 50% probability level. Cations are omitted for clarity.[42]

### 2.3.9 Polyiodides

The diversity of polyiodides is vast and has been extensively explored since the first report on a triiodide by Pelletier in 1819.[26] Polyiodides range from simple monoanions such as $[I_3]^-$ to di-, tri-, and even tetraanions (e.g. $[I_{26}]^{4-}$[102]) and complex three dimensional networks. Iodine also possesses a larger σ-hole in comparison to the lighter halogens (Fig. 2.8), leading to an enhanced stability of polyiodides. Arguably, polyiodides are far more easily synthesized than all the lighter homologues because iodine is a solid and easier to handle than the toxic lighter halogens: liquid bromine, and gaseous chlorine and fluorine. For this reason polyiodides were of great interest at the beginning but the focus has shifted to polybromides, polychlorides and polyfluorides. The rich world of polyiodides is subject to detailed reviews which we refer to for more information.[27,28]

### 2.3.10 Polyinterhalides

Polyinterhalides can be roughly divided into two parts: "classical" and "non-classical". Classical polyinterhalides consist of a positive central halide surrounded by more electronegative halogen atoms, such as $[BrF_4]^-$[103] or $[ICl_2]^-$.[104] Less common is the category of non-classical polyinterhalides which describes a central halide $X^-$ coordinating more electropositive halogen molecules $Y_2$ or XY, such as $[Cl(I_2)_4]^-$[105] or $[Cl(BrCl)_6]^-$,[106] respectively. Reviews on classical[107] and non-classical[31] contain all in-depth information on the subject. Here, we want to illustrate polyinterhalides on a few selected examples.

The Seppelt group has excelled at the synthesis and characterization of numerous compounds of high interest such as $[AuXe_4][Sb_2F_{11}]_2$ containing the first report on a bond between a noble gas and a noble metal.[108] Another appealing compound is $Cs[BrF_6]$ containing the classical interhalide $[BrF_6]^-$ monoanion.[109] As opposed to most poly- and interhalides, this anion does not

follow the valence shell electron pair repulsion (VSEPR) model and is found to be octahedral, both in solution[110] and in the crystal.[109] Therefore, packing effects cannot be the reason for the octahedral structure and also steric effects of the ligands were excluded. The most probable explanation is that the s-electrons on bromine are strongly bound to the nucleus due to incomplete shielding of the same.[109] The isovalence electronic anion $[IF_6]^-$, which in turn is isoelectronic to the non-octahedral $XeF_6$[111], was found to be a strongly distorted octahedron of near $C_{3v}$ symmetry, thus supporting the previous explanation, see Fig. 2.24.[112]

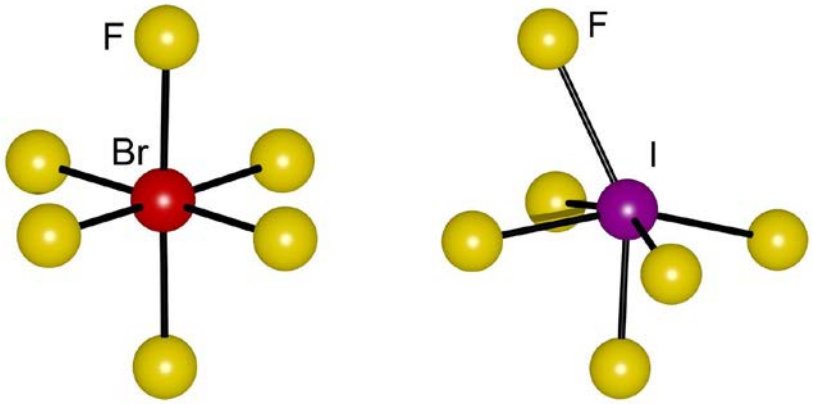


**Figure 2.24:** Comparison of $O_h$ symmetric $[BrF_6]^-$ (left) [109] and $C_{3v}$ symmetric $[IF_6]^-$ (right).[112] Ellipsoids cannot be shown since the displacement factors are not provided via the CCDC database.

While classical polyinterhalides have dominated in the past, non-classical polyinterhalides have moved into the centre of attention in the past decade. This has lead to very interesting compounds such as $[(H_5O_2)(I2b15c5)_2][Cl(I_2)_4]$. As expected from the standard reduction potentials of $Cl^-/Cl_2$ ($E^0$ = 1.36 V) and $I^-/I_2$ ($E^0$ = 0.54 V)[113] $Cl^-$ and $I_2$ should not undergo redox reactions with one another. The monoanion $[Cl(I_2)_4]^-$ consists of a central chloride $Cl^-$ coordinating four iodine $I_2$ molecules. Remarkably, this nonahalide, which is the first structurally characterized nonainterhalide, is square planar in contrast to the known nonahalides of $[Br_9]^-$ and $[I_9]^-$. Even quantum-chemical calculations of the isolated anion $[Cl(I_2)_4]^-$ in the gas phase at 0 K result in the tetrahedral geometry which was expected based on experimental and theoretical investigations of $[Br_9]^-$ and $[I_9]^-$. While the tetrahedron is the ground state structure of the isolated ion in the gas phase, the square-planar arrangement was computed to be a saddle point, which is 8 kJ $mol^{-1}$ higher in energy (SCS-MPS/def2TZVPP). However, the discussed compound is a solid, and therefore this small energy difference can be compensated by other effects, such as lattice energy, and hydrogen or halogen bonding.

Considering the arrangement of the $[Cl(I_2)_4]^-$ anions to one another, one observes that halogen-halogen bonding plays a key role here, see Fig. 2.25. The peripheral region of the $I_2$ molecule of $[Cl(I_2)_4]^-$ has a higher potential than the lateral side (σ-hole). When the σ-hole (blue region) of the peripheral iodine atome interacts with the belt of electron density (red region) of the lateral iodine atom, then additional stability is achieved. This lowers the energy of the system and is just enough to overcome the energy difference needed to obtain the square-planar structure.[105]

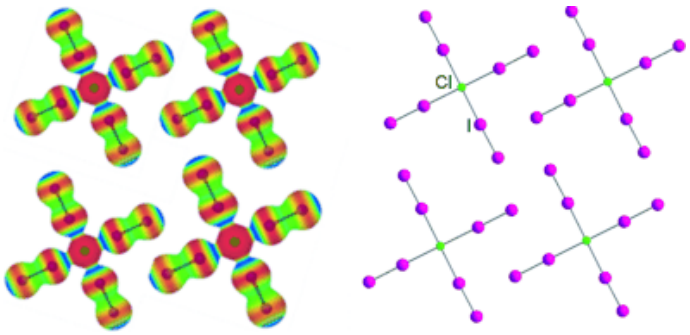


**Figure 2.25:** Interactions between $[Cl(I_2)_4]^-$ anions based on the electrostatic potential (red – blue: decreasing potential) and in the crystal structure. (Copyright Wiley-VCH Verlag GmbH & Co. KGaA.)[105]

Another noteworthy example of non-classical polyinterhalides is the compound $[NMe_4][I_4Br_5]$.[36] The anion can be synthesized in two modifications. In both cases the nonainterhalide consists of a central bromide coordinating two IBr units in a V-shape fashion, typical for pentahalides. This $[I_2Br_3]^-$ then coordinates two further IBr molecules via the terminal iodine atoms of $[I_2Br_3]^-$ and the bromine atom of IBr. When IBr is added to $[NMe_4]Br$ in the ionic liquid [HMIM]Br, the *syn*-modification is obtained with the two IBr molecules being on the same side of the $[I_2Br_3]^-$. Surprisisingly, $[HMIM]^+$ does not co-crystallize. This in turn can be explained by the higher symmetry of $[NMe_4]^+$ and hence favorable Coulomb packing. In contrast, the synthesis in dichloromethane as solvent instead of the ionic liquid results in the formation of the *anti*-product with the two IBr molecules being coordinated on opposite sides of the central $[I_2Br_3]^-$ ion, again via the terminal iodine atoms of $[I_2Br_3]^-$.[36]

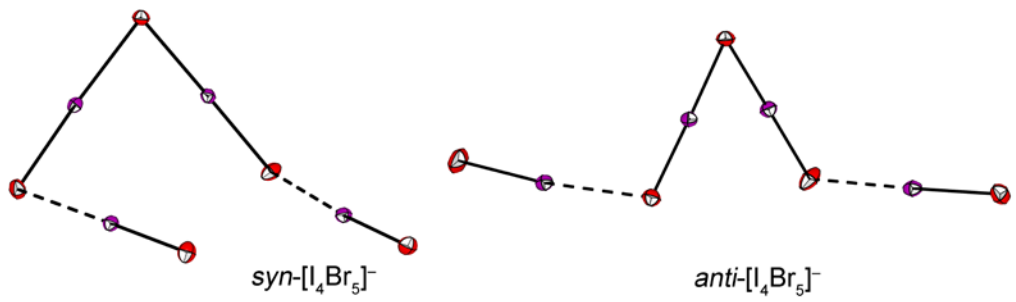


**Figure 2.26:** *Syn*- and *anti*-$[I_4Br_5]^-$ in the solid state structures of $[NMe_4][I_4Br_5]$ crystallized from [HMIM]Br and $CH_2Cl_2$, respectively.[36]

### 2.3.11 Applications of Polyhalogen Anions

*Halogenation Reactions*

In order to avoid the handling of elemental halogens which are either gaseous (fluorine, chlorine) or have a high vapor pressure (bromine), polyhalides can be employed as an alternative to perform halogenation reactions. Polybromide anions exist as stable solid bulk materials allowing for short handling on air and therefore also at the balance. Furthermore, a few polyhalogen anions exist as room temperature ionic liquids which likewise allow for an even more convenient handling and control of halogenating reactions.

Tribromides can be used as mild bromination reagents. They can be synthesized as liquids with no measurable vapor pressure[114] or as solids, depending on the cation. It has been shown that the bromination of various substrates occurs with high efficiency and regioselectivity.[115] Nonabromides have also been investigated as an alternative to bromine in organic chemistry. $[NPr_4][Br_9]$ has proven to be easier to handle and to show a higher chemo- and stereoselectivity than elemental bromine.[116]

Similar to tribromides, the use of trichlorides as an alternative to chlorine has been reported.[117,118] Chlorination of several substrates, such as ketones,[118] alkenes[119] and alkynes,[118] using tetraethylammonium trichloride, a substance which is stable at room temperature for months.[118] Moreover, tetrabutylammonium trichloride has been used as as a convenient chlorination source in total synthesis[120] and the chlorination of alkynes.[121]

*Electrochemistry: high conductivity of polyhalogen anions*

A prominent example of halogens in electrochemistry is the redox couple $I^-/[I_3]^-$ in for example dye-sensitized solar cells.[122] This redox couple stands out from most redox mediators because of the very slow recombination kinetics between electrons in $TiO_2$ and $[I_3]^-$. The analogous $Br^-/[Br_3]^-$ redox couple is chemically more promising since it shows a higher open-circuit photovoltage and a higher overall conversion efficiency in comparison to the control experiment with the redox couple $I^-/[I_3]^-$.[123] However, problems arise that stem from the corrosive nature of bromine.[124] Polybromides are also present in the zinc-bromine (redox flow) battery. It was found that polybromide compounds can be semi-conductors such as $[HMIM][Br_9]$. In general, polybromides possess a surprisingly high conductivity which can be explained by a hopping-like mechanism comparable to that of water.[11]

*Reactive ionic liquids*

Polyhalides can be obtained as room temperature ionic liquids with very low viscosities. As such, they have all the advantages of this class of chemicals but in addition they can be strong oxidizers as well, depending on the halogens applied. Binnemans *et al.* recently reported on the use of ionic

liquid trichlorides as reactive media to dissolve metals and alloys.[125,126] This could have further applications in the recycling or urban mining of metals because even elements such as gold dissolve in the liquid trichlorides examined.[125] Another publication reports on the safe, solvometallurgical method for oxidative dissolution of metals such as Fe, Cu, Sb, Co, Zn, In, Ga, Bi, Ge, Sn, Pd, and Au, using not only trichlorides but various tri(inter)halides.[126]

## 2.4 References

[1] M.Skyllas-Kazacos, M. Rychick, R. Robins, U.S. Patent 4786567, **1988**.
[2] A. Z. Weber, M. M. Mench, J. P. Meyers, P. N. Ross, J. T. Gostick, Q. Liu, *J. Appl. Electrochem.* **2011**, *41*, 1137.
[3] A. S. Tracey, D. C. Crans, *Vanadium compounds. Chemistry, biochemistry, and therapeutic applications : [developed from the symposium entitled "Chemistry, Biochemistry, and Therapeutic Applications of Vanadium Compounds", held at the 5th North America Chemical Congress, Cancun, November 10 - 14, 1997*, Distributed by Oxford University Press; American Chemical Society, Cary, NC, Washington, DC, **1998**.
[4] V. S. Bagotski, *Fundamentals of electrochemistry*, Wiley-Interscience, Hoboken, N.J, **2006**.
[5] I. Rubinstein, *Monographs in electroanalytical chemistry and electrochemistry*, Dekker, New York, NY, **1995**.
[6] a) C. Ponce de León, A. Frías-Ferrer, J. González-García, D. A. Szánto, F. C. Walsh, *J. Power Sources* **2006**, *160*, 716; b) M. Skyllas-Kazacos, M. H. Chakrabarti, S. A. Hajimolana, F. S. Mjalli, M. Saleem, *J. Electrochem. Soc.* **2011**, *158*, R55.
[7] F. Endres, D. MacFarlane, A. Abbott, *Electrodeposition from ionic liquids*, Wiley-VCH, Weinheim, **2008**.
[8] Paul Walden, *Bull. Acad. Imper. Sci. St. Petersbourg* **1914**, *8*, 405.
[9] W. Kurniadi, K. R. Brower, *J. Org. Chem.* **1994**, *59*, 5502.
[10] Patrick S. Bäuerlein, *Dissertation*, Eindhoven University of Technology, Eindhoven, **2009**.
[11] H. Haller, M. Hog, F. Scholz, H. Scherer, I. Krossing, S. Riedel, *Z. Naturforsch.* **2013**, *68b*, 1103.
[12] R. Lin, A. P. Amrute, J. Pérez-Ramírez, *Chem. Rev.* **2017**, *117*, 4182.
[13] M. Bertau, *Industrielle Anorganische Chemie*, Wiley-VCH, Verlag GmbH & Co. KGaA, Weinheim, **2013**.
[14] a) *Directive 2003/11/EC*; b) *Directive 2002/95/EC*.
[15] E. P. Gillis, K. J. Eastman, M. D. Hill, D. J. Donnelly, N. A. Meanwell, *J. Med. Chem.* **2015**, *58*, 8315.
[16] K. Hintzer, T. Zipplies, D. P. Carlson, W. Schmiegel in *Ullmann's encyclopedia of industrial chemistry // Ullmann's Encyclopedia of Industrial Chemistry* (Ed.: Barbara Elvers), Wiley; Wiley-VCH Verlag GmbH & Co. KGaA, Chichester, **2010**.
[17] C. Heitner-Wirguin, *J. Membr. Sci.* **1996**, *120*, 1.
[18] M. Urhan, S. Dadparvar, A. Mavi, M. Houseni, W. Chamroonrat, A. Alavi, S. J. Mandel, *Eur. J. Nucl. Med. Mol.* **2007**, *34*, 1012.
[19] S. S. Block, *Disinfection, sterilization and preservation*, Lippincott Williams & Wilkins, Philadelphia, **2001**.
[20] B. Maji, M. Breugst, H. Mayr, *Angew. Chem. Int. Ed.* **2011**, *50*, 6915.
[21] I. Masson, *J. Chem. Soc.* **1938**, 1708.

[22] T. Drews, W. Koch, K. Seppelt, *J. Am. Chem. Soc.* **1999**, *121*, 4379.
[23] H. Hartl, J. Nowicki, R. Minkwitz, *Angew. Chem.* **1991**, *103*, 311.
[24] J. Passmore, P. Taylor, T. Whidden, P. S. White, *Can. J. Chem.* **1979**, *57*, 968.
[25] S. I. Ivlev, A. J. Karttunen, M. R. Buchner, M. Conrad, F. Kraus, *Angew. Chem. Int. Ed.* **2018**, *57*,14640.
[26] J. Pelletier, J. B. Caventou, *Ann. Chim. Phys.* **1819**, 142.
[27] P. H. Svensson, L. Kloo, *Chem. Rev.* **2003**, *103*, 1649.
[28] L. Kloo, *in Comprehensive Inorganic Chemistry II, Vol. 1. Catenated Compounds - Group 17 - Polyhalides*. (Eds.: J. Reedijk, K. Poeppelmeier), Elsevier, **2013**.
[29] F. D. Chattaway, G. Hoyle, *J. Chem. Soc. Trans.* **1923**, *123*, 654.
[30] H. Haller, S. Riedel, *Nachr. Chem.* **2012**, *60*, 865.
[31] H. Haller, S. Riedel, *Z. Anorg. Allg. Chem.* **2014**, *640*, 1281.
[32] T. Vent-Schmidt, F. Brosi, J. Metzger, T. Schlöder, X. Wang, L. Andrews, C. Müller, H. Beckers, S. Riedel, *Angew. Chem. Int. Ed.* **2015**, *54*, 8279.
[33] K. Sonnenberg, P. Pröhm, N. Schwarze, C. Müller, H. Beckers, S. Riedel, *Angew. Chem. Int. Ed.* **2018**, *57*, 9136.
[34] H. Haller, M. Ellwanger, A. Higelin, S. Riedel, *Angew. Chem. Int. Ed.* **2011**, *50*, 11528.
[35] S. A. Adonin, M. N. Sokolov, V. P. Fedin, *Coord. Chem. Rev.* **2018**, *367*, 1.
[36] L. Mann, P. Voßnacker, C. Müller, S. Riedel, *Chem. Eur. J.* **2017**, *23*, 244.
[37] C. Feldmann, M. Wolff, *Z. Anorg. Allg. Chem.* **2010**, *636*, 2055.
[38] K. Sonnenberg, P. Pröhm, S. Steinhauer, A. Wiesner, C. Müller, S. Riedel, *Z. Anorg. Allg. Chem.* **2017**, *643*, 101.
[39] R. Brückner, P. Pröhm, A. Wiesner, S. Steinhauer, C. Müller, S. Riedel, *Angew. Chem. Int. Ed.* **2016**, *55*, 10904.
[40] D. Freudenmann, S. Wolf, M. Wolff, C. Feldmann, *Angew. Chem. Int. Ed.* **2011**, *50*, 11050.
[41] M. Wolff, J. Meyer, C. Feldmann, *Angew. Chem. Int. Ed.* **2011**, *50*, 4970.
[42] M. E. Easton, A. J. Ward, T. Hudson, P. Turner, A. F. Masters, T. Maschmeyer, *Chem. Eur. J.* **2015**, *21*, 2961.
[43] C. Wang, D. Danovich, S. Shaik, Y. Mo, *Chem. Eur. J.* **2017**, *23*, 8719.
[44] M. C. Aragoni, M. Arca, F. A. Devillanova, A. Garau, F. Isaia, V. Lippolis, A. Mancini, *Bioinorg. Chem. Appl.* **2007**, 17416.
[45] G. A. Landrum, N. Goldberg, R. Hoffmann, *J. Chem. Soc., Dalton Trans.* **1997**, 3605.
[46] A. Artau, K. E. Nizzi, B. T. Hill, L. S. Sunderlin, P. G. Wenthold, *J. Am. Chem. Soc.* **2000**, *122*, 10667.
[47] G. R. Desiraju, P. S. Ho, L. Kloo, A. C. Legon, R. Marquardt, P. Metrangolo, P. Politzer, G. Resnati, K. Rissanen, *Pure Appl. Chem.* **2013**, *85*, 1711.
[48] P. Metrangolo, G. Resnati, *Halogen bonding*, Springer, Cham, **2008**.
[49] a) P. Metrangolo, G. Resnati, *Halogen Bonding I*, Springer, Cham, **2015**; b) P. Metrangolo, J. S. Murray, T. Pilati, P. Politzer, G. Resnati, G. Terraneo, *Cryst. Growth Des.* **2011**, *11*, 4238; c) P. Metrangolo, J. S. Murray, T. Pilati, P. Politzer, G. Resnati, G. Terraneo, *CrystEngComm* **2011**, *13*, 6593; d) G. Cavallo, P. Metrangolo, R. Milani, T. Pilati, A. Priimägi, G. Resnati, G. Terraneo, *Chem. Rev.* **2016**, *116*, 2478; e) P. Metrangolo, F. Meyer, T. Pilati, G. Resnati, G. Terraneo, *Angew. Chem. Int. Ed.* **2008**, *47*, 6114.
[50] P. Metrangolo, H. Neukirch, T. Pilati, G. Resnati, *Acc. Chem. Res.* **2005**, *38*, 386.
[51] J. Emsley, *Chem. Soc. Rev.* **1980**, *9*, 91.

[52] a) M. Fourmigué, *Curr. Opin. Solid State Mater. Sci.* **2009**, *13*, 36; b) J. Halli, G. Manolikakes, *Nachr. Chem.* **2016**, *64*, 131.
[53] S. Riedel, T. Köchner, X. Wang, L. Andrews, *Inorg. Chem.* **2010**, *49*, 7156.
[54] R. Brückner, H. Haller, M. Ellwanger, S. Riedel, *Chem. Eur. J.* **2012**, *18*, 5741.
[55] K. E. Nizzi, C. A. Pommerening, L. S. Sunderlin, *J. Phys. Chem. A* **1998**, *102*, 7674.
[56] K. Do, T. P. Klein, C. A. Pommerening, L. S. Sunderlin, *J. Am. Soc. Mass Spectrom.* **1997**, *8*, 688.
[57] H. Haller, M. Ellwanger, A. Higelin, S. Riedel, *Z. Anorg. Allg. Chem.* **2012**, *638*, 553.
[58] H. Bode, E. Klesper, *Z. Anorg. Allg. Chem.* **1952**, *267*, 97.
[59] H. Bode, E. Klesper, *Z. Anorg. Allg. Chem.* **1961**, *313*, 161.
[60] a) B. S. Ault, L. Andrews, *J. Am. Chem. Soc.* **1976**, *98*, 1591; b) B. S. Ault, L. Andrews, *Inorg. Chem.* **1977**, *16*, 2024.
[61] A. A. Tuinman, A. A. Gakh, R. J. Hinde, R. N. Compton, *J. Am. Chem. Soc.* **1999**, *121*, 8397.
[62] F. Brosi, T. Vent-Schmidt, S. Kieninger, T. Schlöder, H. Beckers, S. Riedel, *Chem. Eur. J.* **2015**, *21*, 16455.
[63] M. P. Bogaard, J. Peterson, A. D. Rae, *Acta Crystallogr. B* **1981**, *37*, 1357.
[64] J. Taraba, Z. Zak, *Inorg. Chem.* **2003**, *42*, 3591.
[65] R. Brückner, H. Haller, S. Steinhauer, C. Müller, S. Riedel, *Angew. Chem. Int. Ed.* **2015**, *54*, 15579.
[66] R. Brückner, *Dissertation*, Freie Universität Berlin, Berlin, **2016**.
[67] J. C. Evans, G. Y.-S. Lo, *J. Chem. Phys.* **1966**, *44*, 3638.
[68] J. Broekema *Acta Crystallogr.* **1957**, *10*, 596.
[69] A. Anderson, T. S. Sun, *Chem. Phys. Lett.* **1970**, *6*, 611.
[70] A. Bondi, *J. Phys. Chem.* **1964**, *68*, 441.
[71] a) E. E. Havinga, K. H. Boswijk, E. H. Wiebenga, *Acta Crystallogr. A* **1954**, *7*, 487; b) A. Gräfe-Kavoosian, S. Nafepour, K. Nagel, K.-F. Tebbe, *Z. Naturforsch., B: Chem. Sci.* **1998**, *53*.
[72] K. N. Robertson, P. K. Bakshi, T. S. Cameron, O. Knop, *Z. Anorg. Allg. Chem.* **1997**, *623*, 104.
[73] X. Chen, M. A. Rickard, J. W. Hull, C. Zheng, A. Leugers, P. Simoncic, *Inorg. Chem.* **2010**, *49*, 8684.
[74] a) M. Fournier, F. Fournier, J. Berthelot, *Bull. Soc. Chim. Belg.* **1984**, *93*, 157; b) W. Gabes, H. Gerding, *J. Mol. Struct.* **1972**, *14*, 267; c) L. R. Morss, *J. Chem. Thermodyn.* **1975**, *7*, 709; d) A. I. Popov, R. E. Buckles, *Inorg. Synth.* **1957**, *5*, 167.
[75] V. Vitske, H. Herrmann, M. Enders, E. Kaifer, H.-J. Himmel, *Chem. Eur. J.* **2012**, *18*, 14108.
[76] F. B. Alhanash, N. A. Barnes, S. M. Godfrey, R. Z. Khan, R. G. Pritchard, *Polyhedron* **2013**, *65*, 102.
[77] M. Wolff, A. Okrut, C. Feldmann, *Inorg. Chem.* **2011**, *50*, 11683.
[78] H. Haller, J. Schröder, S. Riedel, *Angew. Chem. Int. Ed.* **2013**, *52*, 4937.
[79] C. A. Wight, B. S. Ault, L. Andrews, *Inorg. Chem.* **1976**, *15*, 2147.
[80] G. L. Hug, *Optical spectra of nonmetallic inorganic transient species in aqueous solution*, National Bureau of Standards, Gaithersburg, MD, **1981**.
[81] E. de Laurentiis, M. Minella, V. Maurino, C. Minero, G. Mailhot, M. Sarakha, M. Brigante, D. Vione, *Sci. Total Environ.* **2012**, *439*, 299.
[82] H. A. Schwarz, R. W. Dodson, *J. Phys. Chem.* **1984**, *88*, 3643.
[83] F. Pichierri, *Chem. Phys. Lett.* **2011**, *515*, 116.
[84] M. Bakavoli, A. M. Kakhky, A. Shiri, M. Ghabdian, A. Davoodnia, H. Eshghi, M. Khatami, *Chin. Chem. Lett.* **2010**, *21*, 651.

[85] P. D. Boyle, W. I. Cross, S. M. Godfrey, C. A. McAuliffe, R. G. Pritchard, S. J. Teat, *J. Chem. Soc., Dalton Trans.* **1999**, 2845.
[86] G. Bauer, J. Drobits, C. Fabjan, H. Mikosch, P. Schuster, *J. Electroanal. Chem.* **1997**, *427*, 123.
[87] A. I. Popov, D. H. Geske, *J. Am. Chem. Soc.* **1958**, *80*, 5346.
[88] T. Iwasita, Giordano, M. C., *Electrochim. Acta* **1969**, *14*, 1045.
[89] G. Bellucci, R. Bianchini, C. Chiappe, R. Ambrosetti, *J. Am. Chem. Soc.* **1989**, *111*, 199.
[90] J. C. Evans, G. Y.-S. Lo, *Inorg. Chem.* **1967**, *6*, 1483.
[91] B. M. Powell, K. M. Heal, B. H. Torrie, *Mol. Phys.* **1984**, *53*, 929.
[92] M. Groessl, Z. Fei, P. J. Dyson, S. A. Katsyuba, K. L. Vikse, J. S. McIndoe, *Inorg. Chem.* **2011**, *50*, 9728.
[93] A. W. Addison, T. N. Rao, J. Reedijk, J. van Rijn, G. C. Verschoor, *J. Chem. Soc., Dalton Trans.* **1984**, 1349.
[94] K. O. Strømme, S. Hauge, P. M. Jørgensen, S. Refn, *Acta Chem. Scand.* **1959**, *13*, 2089.
[95] G. B. M. Vaughan, A. J. Mora, A. N. Fitch, P. N. Gates, A. S. Muir, *J. Chem. Soc., Dalton Trans.* **1999**, 79.
[96] M. C. Aragoni, M. Arca, F. A. Devillanova, M. B. Hursthouse, S. L. Huth, F. Isaia, V. Lippolis, A. Mancini, H. Ogilvie, *Inorg. Chem. Commun.* **2005**, *8*, 79.
[97] K. Sonnenberg, P. Pröhm, C. Müller, H. Beckers, S. Steinhauer, D. Lentz, S. Riedel, *Chem. Eur. J.* **2018**, *24*, 1072.
[98] K. M. Fromm, R. D. Bergougnant, A. Y. Robin, *Z. Anorg. Allg. Chem.* **2006**, *632*, 828.
[99] C. W. Cunningham, G. R. Burns, V. McKee, *Inorg. Chim. Acta* **1990**, *167*, 135.
[100] L. Mann, G. Senges, K. Sonnenberg, H. Haller, S. Riedel, *Eur. J. Inorg. Chem.* **2018**, 28, 3330.
[101] H. Haller, *Dissertation*, Albert-Ludwigs-Universität Freiburg, Freiburg (Breisgau), **2014**.
[102] K.-F. Tebbe, R. Buchem, *Z. Anorg. Allg. Chem.* **1998**, *624*, 671.
[103] S. Ivlev, P. Woidy, V. Sobolev, I. Gerin, R. Ostvald, F. Kraus, *Z. Anorg. Allg. Chem.* **2013**, *639*, 2846.
[104] D. Hausmann, A. Eich, C. Feldmann, *J. Mol. Struct.* **2018**, *1166*, 159.
[105] C. Walbaum, M. Richter, U. Sachs, I. Pantenburg, S. Riedel, A.-V. Mudring, G. Meyer, *Angew. Chem. Int. Ed.* **2013**, *52*, 12732.
[106] B. Schmidt, K. Sonnenberg, H. Beckers, S. Steinhauer, S. Riedel, *Angew. Chem. Int. Ed.* **2018**, *57*, 9141.
[107] a) A. G. Sharpe, *Q. Rev., Chem. Soc.* **1950**, *4*, 115; b) E. H. Wiebenga, E. E. Havinga, K. H. Boswijk, *Adv. Inorg. Chem. Radiochem.* **1961**, *3*, 133.
[108] S. Seidel, K. Seppelt, *Science* **2000**, *290*, 117.
[109] A. R. Mahjoub, A. Hoser, J. Fuchs, K. Seppelt, *Angew. Chem. Int. Ed.* **1989**, *28*, 1526.
[110] K. O. Christe, W. W. Wilson, *Inorg. Chem.* **1989**, *28*, 3275.
[111] L. S. Bartell, R. M. Gavin, Jr., H. B. Thompson, C. L. Chernick, *J. Chem. Phys.* **1965**, *43*, 2547.
[112] A. R. Mahjoub, K. Seppelt, *Angew. Chem. Int. Ed.* **1991**, *30*, 323.
[113] Y.-R. Luo, *Comprehensive Handbook of Chemical Bond Energies*, CRC Press, Boca Raton, **2007**.
[114] S. P. Borikar, T. Daniel, V. Paul, *Tetrahedron Lett.* **2009**, *50*, 1007.
[115] a) J. Salazar, R. Dorta, *Synlett.* **2004**, 1318; b) V. Kavala, S. Naik, B. K. Patel, *J. Org. Chem.* **2005**, *70*, 4267.
[116] T. M. Beck, H. Haller, J. Streuff, S. Riedel, *Synthesis* **2014**, *46*, 740.
[117] V. M. Zelikman, V. S. Tyurin, V. V. Smirnov, N. V. Zyk, *Russ Chem Bull* **1998**, *47*, 1541.

[118] T. Schlama, K. Gabriel, V. Gouverneur, C. Mioskowski, *Angew. Chem. Int. Ed.* **1997**, *36*, 2342.
[119] a) S. S. Tartakoff, C. D. Vanderwal, *Org. Lett.* **2014**, *16*, 1458; b) C. V. Vogel, H. Pietraszkiewicz, O. M. Sabry, W. H. Gerwick, F. A. Valeriote, C. D. Vanderwal, *Angew. Chem. Int. Ed.* **2014**, *53*, 12205; c) W.-J. Chung, J. S. Carlson, C. D. Vanderwal, *J. Org. Chem.* **2014**, *79*, 2226; d) Z. A. Könst, A. R. Szklarski, S. Pellegrino, S. E. Michalak, M. Meyer, C. Zanette, R. Cencic, S. Nam, V. K. Voora, D. A. Horne et al., *Nat. Chem.* **2017**, *9*, 1140.
[120] N. Huwyler, E. M. Carreira, *Angew. Chem. Int. Ed.* **2012**, *51*, 13066.
[121] N. Zhou, Q. Wang, A. J. Lough, H. Yan, *Can. J. Chem.* **2012**, *90*, 625.
[122] G. Boschloo, A. Hagfeldt, *Acc. Chem. Res.* **2009**, *42*, 1819.
[123] S.-E. Chun, B. Evanko, X. Wang, D. Vonlanthen, X. Ji, G. D. Stucky, S. W. Boettcher, *Nat. Commun.* **2015**, *6*, 7818.
[124] Z.-S. Wang, K. Sayama, H. Sugihara, *J. Phys. Chem. B* **2005**, *109*, 22449.
[125] X. Li, A. van den Bossche, T. Vander Hoogerstraete, K. Binnemans, *Chem. Comm.* **2018**, *54*, 475.
[126] A. van den Bossche, E. de Witte, W. Dehaen, K. Binnemans, *Green Chem.* **2018**, *51*, 1.

# 3. Objectives

The present dissertation has evolved as part of the project "IL-RFB" financed by the Federal Ministry of Education and Research (dt.: "Bundesministerium für Bildung und Forschung") in cooperation with the group of Prof. Dr. Ingo Krossing (Albert-Ludwigs-Universität Freiburg) and the Fraunhofer ISE (Freiburg). It is desired to obtain a redox flow battery with an energy density of at least 150 Wh $L^{-1}$ employing neat ionic liquids based on polyhalides and halometalates.
The purpose of our work within the project is the "Investigation of Ionic Liquids for the use as Active Material in New Redox-Flow Batteries: Synthesis, Characterization, and Application of Polyhalides" (dt.: "Erforschung von Ionischen Flüssigkeiten für den Einsatz als Aktivmassen in neuartigen Redox-Flow-Batterien: Synthese, Charakterisierung und Anwendung von Polyhalogeniden"). One of the proposed redox systems includes halostannates and poly(inter)halides. A feasible discharge reaction may be the oxidation of a halostannate(II) (e.g. bromostannate(II)) to the corresponding halostannate(IV) (e.g. bromostannate(IV)) while a higher polyhalide (e.g. $[Br_9]^-$) is reduced to the corresponding trihalide (e.g. $[Br_3]^-$). The formed monohalides may pass through a suitable ion selective membrane to the negative half cell where they combine with the formed tin(IV) ions.

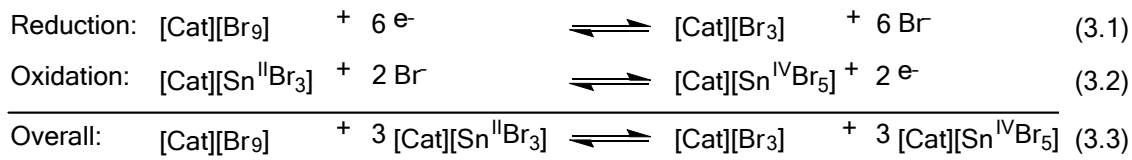


This redox system (equations (3.1)–(3.3)) is not limited to polybromides but also the use of polychlorides or polyinterhalides is possible. Consequently, one aim of this work is the synthesis of bromostannates(II, IV) and polyhalides (polybromides, polychlorides, polyinterhalides). Ideally, the compounds are to be synthesized as room temperature ionic liquids with a low melting point and viscosity as well as a high electrical conductivity and electrochemical activity. The characterization of these new compounds shall include IR- and Raman spectroscopy, supplementary mass spectrometry and NMR spectroscopy, and most crucially single crystal X-ray diffraction. The experimental findings are to be compared to high-level quantum chemical calculations. If successful, one can use cyclic voltammetry to analyze the ionic liquids electrochemically and evaluate the suitability of the compounds in battery measurements.

# 4. Synthesis and Characterization of Bromostannate and Polybromide Ionic Liquids

The first step on the long way to the desired new redox flow battery is the synthesis of room temperature ionic liquids based on bromostannates and polybromides in order to subsequently use them as electrolytes in said RFB. The reason for the consideration of bromostannates and polybromides is that both are abundantly available, cheap, and both should undergo redox reactions. This has been shown for polyhalides in solar-cells and can be expected for tin because of its stable oxidation states of +II and +IV. The successful synthesis of these anions depends on the correct choice of the cation. Therefore, this work concentrates on the synthesis of ILs, which are liquid at room temperature. Due to the cooperation with partners within our BMBF project, the electrochemical characterization and possible application in redox flow batteries was examined outside this dissertation.[1,2] Parts of the experimental work described in this chapter include results from internships of Tyler Gully and Tim Küllmey under the guidance and supervision of the author of this dissertation.

## 4.1 Bromostannates

To the best of our knowledge, only one report mentions the effort to synthesize ILs, or RT-ILs for that matter, based on bromostannates.[1] Similarly, only one publication has characterized a $[SnBr_5]^-$ species crystallographically.[3] In contrast, $[SnBr_3]^-$ is a well known anion,[4] which is a poorer σ-donor and π-acceptor than the analogous $[SnCl_3]^-$.[5]

The synthesis of [Cat][$SnBr_3$] and [Cat][$SnBr_5$] (Cat = cation) is quite simple. Stoichiometric amounts of $SnBr_2$ or $SnBr_4$, respectively, are added to a bromide salt without the use of a solvent, see equations (4.1) and (4.2). Homogenization and completion of the reaction are achieved by heating the mixture to 80 °C for one day.

$$SnBr_2 + [Cat]Br \longrightarrow [Cat][SnBr_3] \quad (4.1)$$

$$SnBr_4 + [Cat]Br \longrightarrow [Cat][SnBr_5] \quad (4.2)$$

### 4.1.1 Bromostannates(IV)

Burgenmeister has attempted to synthesize [HMIM][$SnBr_5$] (HMIM=1-hexyl-3-methylimidazolium) as a room temperature ionic liquid.[1] Unfortunately, he observed that the compound obeys the following equilibrium (4.3).

$$2\,[HMIM][SnBr_5] \rightleftharpoons [HMIM]_2[SnBr_6] + SnBr_4 \quad (4.3)$$

At room temperature $[HMIM]_2[SnBr_6]$ and $SnBr_4$ are present, and only at elevated temperatures (>70 °C) the desired $[HMIM][SnBr_5]$ is predominant. His analysis of the thermodynamic cycle showed that the driving force for this is the large lattice energy of $[HMIM]_2[SnBr_6]$.[1] Consequently, it is possible to obtain $[SnBr_5]^-$-based ionic liquids when using a suitable cation because the lattice energy will be different.

One easy approach is to change the chain length of the alkyl chain at the imidazolium cation. The lengthening of the hexyl chain should initially lower the lattice energy due to insufficient Coulomb packing while the additional lengthening should at some point lead to enhanced van der Waals forces between the alkyl chains, leading to a higher melting point.[6] Indeed, we successfully synthesized $[OMIM][SnBr_5]$ (OMIM=1-octyl-3-methylimidazolium), as a room temperature ionic liquid. $^{119}$Sn NMR spectroscopy showed a single signal at δ = –1415 ppm, which is located between that of $SnBr_4$ (δ = ca. – 40 ppm) and $[SnBr_6]^{2-}$ (δ = ca. –2070 ppm).[7] This already proves that a pentacoordinated tin(IV) species is present in the liquid phase, which speaks strongly in favor of $[OMIM][SnBr_5]$. Additionally, we were able to grow single crystals from the IL, supporting that $[SnBr_5]^-$ also exists in the solid as $[OMIM][SnBr_5]$, see Fig. 4.1. The compound crystallizes in the monoclinic space group $P2_1/c$.

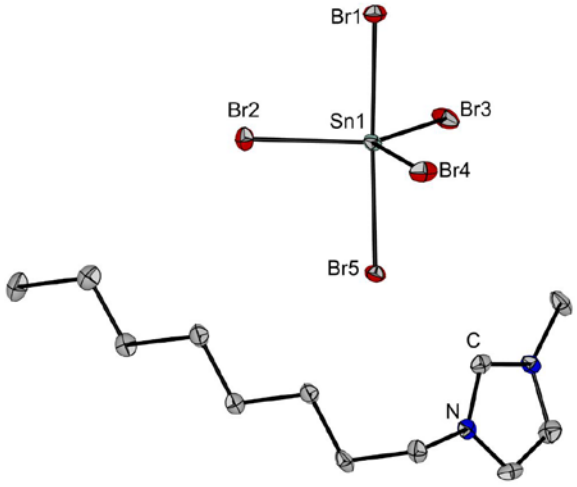


**Figure 4.1.** Structure of $[OMIM][SnBr_5]$ in the solid. Ellipsoids shown at the 50% probability level. Hydrogen atoms are ommited for clarity.

The trigonal bipyramidal anion shows typical shorter equatorial bond lengths (249.4(1) – 250.7(1) pm) and longer axial bond lengths between Sn1–Br1 (256.6(2) pm) and Sn1–Br5 (259.5(1) pm). The Raman spectrum of $[OMIM][SnBr_5]$ at 77 K (in the relevant region between 100 and 300 $cm^{-1}$) shows four bands at 248 (*E*'), 198 ($A_1$'), 158 ($A_1$'), and 103 (*E*') $cm^{-1}$, which agree very well to previous spectroscopic investigations of solid $[NEt_4][SnBr_5]$ (257, 202,

154, 109 $cm^{-1}$).[8] The compound is therefore characterized here and its electrochemical characterization can be found in the works of our BMBF partners.[9]

### 4.1.2 Bromostannates(II)

Since the $[OMIM]^+$ cation was able to stabilize $[SnBr_5]^-$ at room temperature, which was the crucial step, the same cation was used to synthesize $[SnBr_3]^-$. It needs to be noted that working stoichiometrically is important because the ratio of $SnBr_2$:$Br^-$ is essential. For $[SnBr_3]^-$ a 1:1 ratio is required, while at higher $SnBr_2$ amounts $[Sn_2Br_5]^-$[10] (ratio 2:1) is obtained. At substoichiometric amounts of $SnBr_2$, anions such as $[Sn_2Br_8]^{4-}$[11] (ratio 1:2) or $[SnBr_4]^{2-}$[12] (also ratio 1:2) are feasible and have been described in the literature. The reaction of one equivalent $SnBr_2$ with one equivalent [OMIM]Br forms a light yellow liquid. The $^{119}$Sn NMR spectrum shows only one signal at $\delta = 46$ ppm for the neat ionic liquid, and at $\delta = 71$ ppm when dissolved in acetonitrile. It has already been described that the $^{119}$Sn chemical shift of tin(II) halides is strongly dependent on the cation and the solvent at hand and typically ranges between −100 and +400 ppm.[7] In addition, the Raman spectrum of $[OMIM][SnBr_3]$ at 77 K (in the relevant region between 100 and 300 $cm^{-1}$) shows distinct bands at 195 (A'), 183 (A"), and 168 (A') $cm^{-1}$, which are again in good agreement with literature known values (202, 186, 176 $cm^{-1}$).[13]

Table 4.1 contains the physical properties ($^{119}$Sn NMR shift, density $\rho$, kinematic viscosity $\eta_{kin}$, dynamic viscosity $\eta_{dyn}$, electrical conductivity $\sigma$) at room temperature of $[OMIM][SnBr_3]$, $[OMIM][SnBr_5]$, and [OMIM]Br in comparison.

**Table 4.1**. Physical properties of $[OMIM][SnBr_3]$, $[OMIMSnBr_5]$, and [OMIM]Br at 25 °C in comparsion.

| Property | $[OMIM][SnBr_3]$ | $[OMIM][SnBr_5]$ | [OMIM]Br |
|---|---|---|---|
| $^{119}$Sn NMR [ppm] | +46 | +1415 | – |
| $\rho$ [g $cm^{-3}$] | 1.85 ± 0.10 | 2.15 ± 0.10 | 1.15 ± 0.10 |
| $\eta_{kin}$ [$mm^2$ $s^{-1}$] | 251 ± 5 | 183 ± 3 | 3470 ± 71 |
| $\eta_{dyn}$ [mPa s] | 464 ± 8 | 394 ± 10 | 3990 ± 88 |
| $\sigma$ [mS $cm^{-1}$] | 0.52 ± 0.10 | 0.48 ± 0.10 | 0.06 ± 0.10 |

$[OMIM][SnBr_3]$ and $[OMIM][SnBr_5]$ show a significantly lower kinematic viscosity of 251 and 183 $mm^2$ $s^{-1}$, respectively, in contrast to the starting material [OMIM]Br (3470 $mm^2$ $s^{-1}$), which is also a RT-IL. Another method to show the lower viscosity is the so-called "dynamic viscosity", which can easily be calculated by multiplication of the kinematic viscosity with the corresponding density of the compound. Also the dynamic viscosities of $[OMIM][SnBr_3]$ (464 mPa s) and $[OMIM][SnBr_5]$ (394 mPa s) are lower than that of [OMIM]Br by a factor of ten but the absolute values are still rather high. In conjunction with lower viscosities, the conductivity of the bromostannate compounds (ca. 0.5 mS $cm^{-1}$) is higher than that of [OMIM]Br (0.06 mS $cm^{-1}$).

## 4.2 Polybromides

Haller *et al.* reported on the room-temperature ionic liquid [HMIM][$Br_9$] including its temperature dependent conductivity.[14] We want to deepen our understanding of the electrical conductivity of polybromides in view of the RFB and synthesize RT-ILs, preferably [OMIM][$Br_3$] and [OMIM][$Br_9$] to have all parts of the charged ([Cat][$SnBr_3$] and [Cat][$Br_9$]) and discharged ([Cat][$SnBr_5$] and [Cat][$Br_3$]) electrolyte liquid at room temperature and with the same cation to prevent cross contamination through a membrane in a future battery setup.

### 4.2.1 Temperature dependent conductivity

When Haller *et al.* investigated the temperature dependence of the conductivity ($\sigma$(T)) of [HMIM][$Br_9$], they showed that the increase of conductivity with increasing temperature can be modeled using either the well-known Arrhenius equation (eq. 4.4) or the Vogel-Fulcher-Tammann (VFT) equation (see eq. 4.5).[14] Both are dependent on the variable temperature T and the fitting parameter $A_\sigma$. The Arrhenius equations also takes the activation energy $E_A$ and the universal gas constant R into account, while the VFT equation considers the fitting parameters k and the Vogel temperature $T_{VFT}$, which is typically 30 – 50 K below the glass transition temperature $T_g$ of the corresponding IL.[15] The VFT equation was initially used to describe the temperature dependent viscosity of ionic liquids but is also applicable to conductivity, and shows a better fit to experimental values than the Arrhenius equation does.[14]

$$\sigma_{Arrhenius}(T) = A_\sigma \cdot e^{\frac{-E_A}{RT}} \tag{4.4}$$

$$\sigma_{VFT}(T) = A_\sigma \cdot e^{\frac{-k}{T-T_{VFT}}} \tag{4.5}$$

The Stokes-Einstein equation (eq. 4.6) needs to be considered as well. It shows that the diffusion coefficient D depends on the paramters k (Boltzmann constant), T (temperature), c (constant), η (viscosity) and r (effective radius of the diffusing species).[15]

$$D = \frac{kT}{c\pi\eta r} \tag{4.6}$$

Since the conductivity correlates with the diffusion coefficient, the conductivity of an IL is not only a function of the temperature but also depends on the viscosity of the compound.[15]

In order to systematically analyze factors influencing the conductivity of polybromides, we investigated the influence of the specific polybromides (tribromide vs. nonabromide, Figure 4.2 a) and b)), the substitution pattern of the ammonium cations of the same molar mass (Figure 4.2 c)) and the type of cation (Figure 4.1 d)).

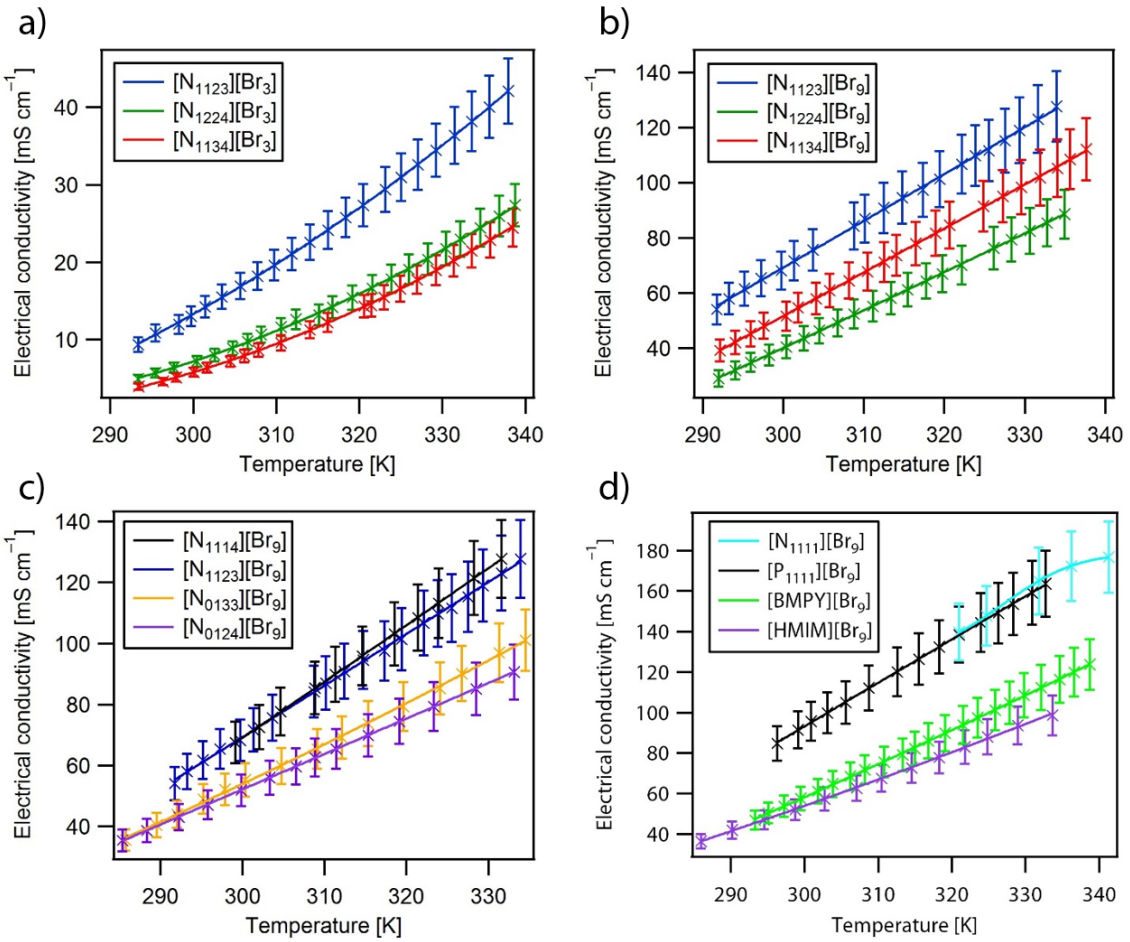


**Figure 4.2.** Temperature dependent conductivity of polybromides. a) Asymetrically substituted ammonium tribromides b) Asymetrically substituted ammonium nonabromides c) Nonabromide salts of equal molar mass d) Nonabromides stabilized by different cation classes.

In Figure 4.2 a) and b) we examined the conductivity of ammonium based tribromides and nonabromides, respectively. For the tetraalkylammonium cations we use the notation $[N_{abcd}]^+$ with a, b, c, d = number of carbon atoms in the *n*-alkyl chain. The compound with the least molar mass, here ($[N_{1123}][Br_x]$), shows the highest conductivity, both for tribromides (X = 3) and nonabromides (X = 9). The cations $[N_{1134}]^+$ and $[N_{1224}]^+$ both have the same molar mass of 144.3 g mol$^{-1}$ and show the same conductivity within the margin of error for tribromides but $[N_{1134}][Br_9]$ shows a slightly higher conductivity than $[N_{1224}][Br_9]$ does over the entire temperature range. This leads us to the conclusion that within one class of cations the conductivity increases with decreasing molar mass of the cation, which is a factor already mentioned in the literature.[16] It can also be seen that tribromides are less conductive than the corresponding nonabromides

which is a result of the lower viscosity of tribromides, see Table 4.2. The kinematic viscosity of nonabromides (4.6 – 8.9 $mm^2\ s^{-1}$) is about one tenth of the kinematic viscosity of the corresponding tribromides (32.6 – 99.7 $mm^2\ s^{-1}$). At room temperature the tribromides under investigation showed conductivities of 5 – 12 mS $cm^{-1}$ while the nonabromides were in the range of 38 –54 mS $cm^{-1}$. The melting points $T_m$ of the tribromides (280 – 291 K) are considerably above those of the corresponding nonabromides (242 – 267 K).

**Table 4.2**. Physical properties of the investigated ammonium based tri- and nonabromides 25 °C in comparsion.

| Ionic liquid | ρ [g $cm^{-3}$] | $\eta_{kin}$ [$mm^2\ s^{-1}$] | $\eta_{dyn}$ [mPa s] | $T_m$ | σ [mS $cm^{-1}$] |
|---|---|---|---|---|---|
| $[N_{1123}][Br_3]$ | 1.85 ± 0.1 | 32.6 | 60.3 | 285 ± 10 | 12.0 ± 0.8 |
| $[N_{1224}][Br_3]$ | 1.56 ± 0.1 | 99.7 | 155.5 | 291 ± 10 | 6.4 ± 0.4 |
| $[N_{1134}][Br_3]$ | 1.57 ± 0.1 | 63.0 | 98.9 | 280 ± 10 | 5.2 ± 0.4 |
| $[N_{1123}][Br_9]$ | 2.37 ± 0.1 | 4.6 | 10.8 | 258 ± 10 | 65.4 ± 4.6 |
| $[N_{1224}][Br_9]$ | 2.25 ± 0.1 | 8.9 | 20.0 | 242 ± 10 | 37.6 ± 2.6 |
| $[N_{1134}][Br_9]$ | 2.24 ± 0.1 | 6.6 | 14.9 | 267 ± 10 | 48.2 ± 3.4 |

Since the molar mass has an influence on the conductivity, we were interested in the influence of the substitution pattern of ammonium cations of equal molar mass based on the examples of $[N_{1114}]^+$, $[N_{1123}]^+$, $[N_{0133}]^+$, $[N_{0124}]^+$. The "0" stands for an alkyl chain with 0 carbon atoms in the alkyl chain, i.e. only a hydrogen atom. Unexpectedly, the conductivity of the four nonabromides differed and resulted in two sets of two equally conductive nonabromides. Both ammonium salts with four alkyl chains were more conductive than the ammonium cations with three alkyl chains and a hydrogen atom. The lower conductivity may be rationalized by the interaction of this partially positive hydrogen atom with the nonabromide.

Changing the ammonium cations to phosphonium cations ($[N_{1111}][Br_9]$ vs. $[P_{1111}][Br_9]$) does not change the conductivity but rather leads to a lower melting point of the nonabromide ($[N_{1111}][Br_9]$ is solid and $[P_{1111}][Br_9]$ is liquid at room temperature). It should be kept in mind that phosphonium salts are commercially more expensive than the corresponding ammonium salts and hence might be unsuitable for redox flow batteries under financial considerations. Therefore, we additionally looked at $[BMPY][Br_9]$ (BMPY = 1-butyl-4-methylpyridinium) and compared it to the known $[HMIM][Br_9]$[14] which both possess comparable conductivites at room temperature of about 50 mS $cm^{-1}$.

The temperature dependent conductivites of Figure 4.2 were fitted to the VFT-equation and the obtained parameters (material dependent constants $A_\sigma$ and k) are listed in Table 4.3. All polybromide ionic liquids have a Vogel temperature $T_{VFT}$ of around 200 – 220 K, which means that their glass transition temperatures are in the range of 230 – 250 K, which is typical for ILs.[15]

**Table 4.3**. Obtained paramters for the VFT equation for the examined tribromides and nonabromides.

| Ionic liquid | $A_\sigma$ [mS cm$^{-1}$] | k [K] | $T_{VFT}$ [K] |
|---|---|---|---|
| $[N_{1123}][Br_3]$ | 526 ± 42 | 307 ± 16 | 217 ± 3 |
| $[N_{1224}][Br_3]$ | 860 ± 215 | 481 ± 60 | 199 ± 7 |
| $[N_{1134}][Br_3]$ | 577 ± 65 | 387 ± 23 | 216 ± 3 |
| $[BMPY][Br_9]$ | 812 ± 57 | 254 ± 16 | 204 ± 3 |
| $[N_{1123}][Br_9]$ | 677 ± 99 | 215 ± 31 | 206 ± 8 |
| $[N_{1224}][Br_9]$ | 475 ± 25 | 183 ± 9 | 226 ± 2 |
| $[N_{1134}][Br_9]$ | 556 ± 29 | 187 ± 10 | 222 ± 2 |

So far, we have shown the factors influencing the conductivity of polybromides, however, the question of the mechanism behind it still needs to be answered. Therefore, we collaborated with the Kremer group (Universität Leipzig) who performed broadband dielectric spectroscopy, which is a method of impedance spectroscopy. This method helps understand the dielectric properties of a compound and its molecular motion.[17]

In a first step, we have to expand the temperature range of the conductivity measurement. We chose one example to illustrate this: $[N_{1123}][Br_3]$ (Fig. 4.3).

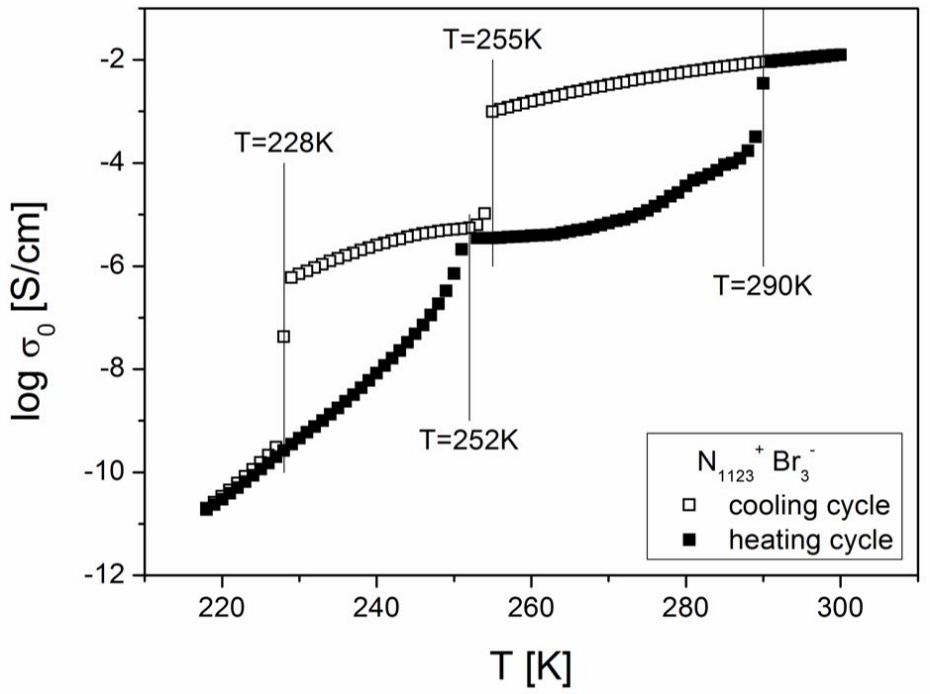


**Figure 4.3.** Temperature dependent conductivity of $[N_{1123}][Br_3]$. Figure kindly provided by Falk Frenzel (Universität Leipzig).[18]

The temperature dependent conductivity of $[N_{1123}][Br_3]$ at temperatures below room temperature (220 – 300 K) shows a strong hysteresis between the cooling and the heating cycle. When the sample is cooled down from room temperature, two steps at 255 K and 228 K are observed, while the heating cycle reveals an edge at 252 K and a step at 290 K.[18] The nature of these steps were additionally investigated by differential scanning calorimetry (DSC) and X-ray diffraction by the author of this dissertation.

The DSC experiment showed an endothermic process at 250 ± 10 K and an exothermic one at 285 ± 10 K. Moreover, a drop of $[N_{1123}][Br_3]$ in a capillary was cooled at the diffractometer with a rate of 240 K $h^{-1}$ and the sample was measured every 10 K between 260 K and 295 K for the cooling and heating cycle. The cooling rate was reduced to 10 K $h^{-1}$ and the sample was measured every 5 K between 210 and 260 K to see a sharp transition in said region. Upon cooling, no reflexes were observed until T = 225 ± 5 K. When the sample was subsequently heated, it remained crystalline until T = 290 ± 10 K.

Taking all these methods into consideration, the following explanation can be given for the processes taking place. When the liquid sample is cooled, it remains liquid until T = 255 K at which point it becomes amorphous and later on the transition from amorphous to crystalline is seen (T = 228 K). The subsequent heating of the compound does not lead to a transition from crystalline to amorphous, which could have been expected for the edge at T = 252 K. Finally, at T = 290 K $[N_{1123}][Br_3]$ melts (transition solid to liquid).

Lastly, as a result of the X-ray diffraction measurements, we were able to obtain the molecular structure of $[N_{1123}][Br_3]$ in the solid (Fig. 4.4).

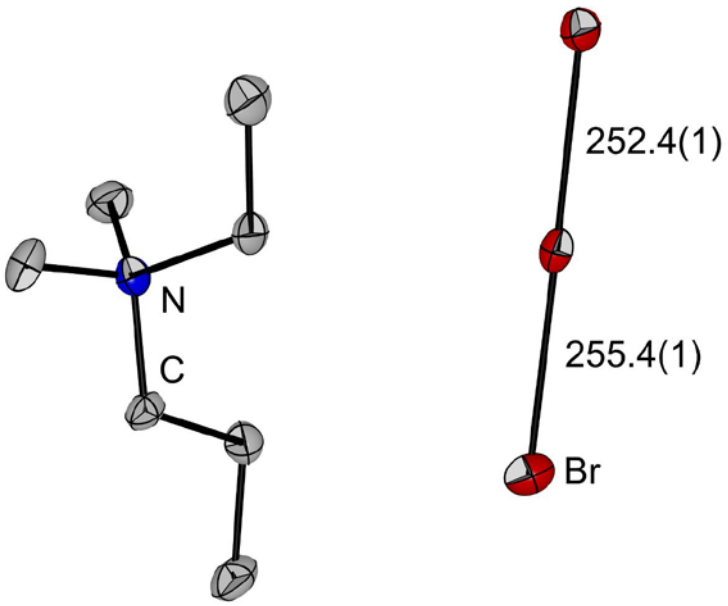


**Figure 4.4.** Structure of $[N_{1123}][Br_3]$ in the solid. Ellipsoids are shown at the 50% probability level. Hydrogens are omitted for clarity and bond lengths are given in [pm].

Our collaboration partners in the Kremer group have performed and analyzed the broadband dielectric spectroscopy experiments and found that the charge transport mechanism of the investigated ammonium tri- and nonabromides can be described as a "dynamic glass transition assisted hopping" mechanism.[18,19] We refrain from showing a more in-depth analysis here but the sophisticated experiments and detailed discussion will soon be available in the corresponding publication.[19]

### 4.2.2 [OMIM]$^+$-based Polybromides

We have seen that the bromine content of polybromides has an effect on the electrical conductivity and we observed that nonabromides are more conductive than the corresponding tribromides. Whereas the ionic liquids [HMIM]Br and [OMIM]Br have low conductivities in the range of μS cm$^{-1}$ and elemental bromine $Br_2$ is an isolator, polybromides have a high conductivity in the range of mS cm$^{-1}$. This means that the conductivity is a function of the molar fraction of $Br_2$ ($\chi(Br_2)$) and must undergo at least one maximum. We performed three experiments to gain a more detailed understanding:

1.) Starting from neat [OMIM]Br ($\chi(Br_2) = 0$), we added $Br_2$, up to $\chi(Br_2) = 0.83$
2.) Starting from neat $Br_2$ ($\chi(Br_2) = 1$), we added [OMIM]Br, up to $\chi(Br_2) = 0.91$
3.) We measured separately prepared samples with $\chi(Br_2)$ of 0.53, 0.79, 0.89, and 0.95 as a control experiment.

All experiments fit very nicely together and are shown in one graph (Fig. 4.5).

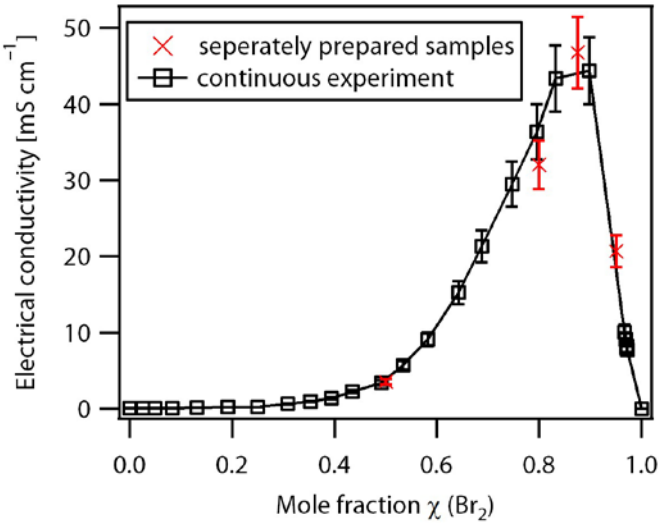


**Figure 4.5.** Electrical conductivity at 25 °C of a mixture of [OMIM]Br as a function of the mole fraction of bromine, $\chi(Br_2)$. Black dots indicate measurements from a continuous experiment and red dots stem from seperately prepared samples.

Between $\chi(Br_2) = 0$ and $\chi(Br_2) = 0.50$ the conductivity increases slowly from 36.6 μS cm$^{-1}$ to 3.4 mS cm$^{-1}$. Subsequently, the conductivity increases significantly until $\chi(Br_2) = 0.83$ at which point the slope drastically descreases as the maximum is almost reached, assuming a continuous differentiable curve. After $\chi(Br_2) = 0.91$ the conductivity decreases until $\chi(Br_2) = 1$, when a conductivity of 0 μS cm$^{-1}$ was measured. We therefore expected the maximum conductivity to lie between $\chi(Br_2) = 0.83$ (43.4 mS cm$^{-1}$) and $\chi(Br_2) = 0.91$ (44.4 mS cm$^{-1}$). Indeed, a separately prepared sample with $\chi(Br_2) = 0.89$ shows an even higher conductivity of 46.8 mS cm$^{-1}$. We

crystallized the sample with $\chi(Br_2)$ = 0.53 and obtained [OMIM][$Br_3$] which we expected, see Fig. 4.6.

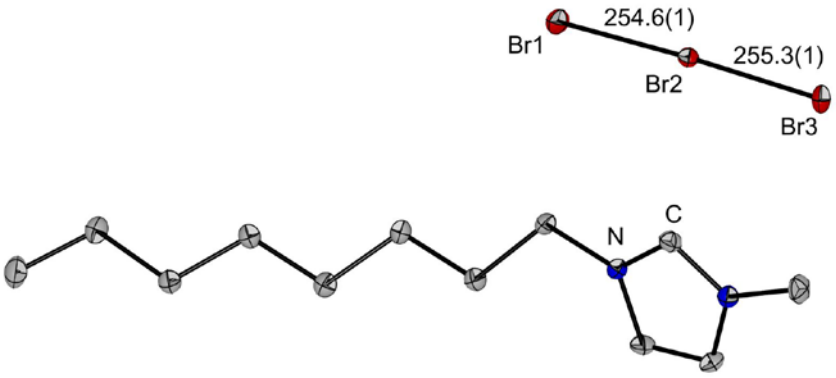


**Figure 4.6.** Structure of [OMIM][$Br_3$] in the solid. Ellipsoids shown at the 50% probability level. Hydrogen atoms are ommited for clarity.

The course of this function (Fig. 4.5) may be explained in the following manner. Initially the conductivity slowly increases because the viscosity of the system is lowered by the addition of bromine until the tribromide $[Br_3]^-$ is formed. Now the charge transport mechanism can set in and the conductivity increases drastically. At some point, obviously around $\chi(Br_2) \approx 0.90$, the concentration has reached a critical, low level and hence the conductivity decreases rapidly until almost only bromine is left.

## 4.3 Conclusion

For a new redox flow battery based on neat ionic liquids, it is essential to synthesize the electrolytes as room temperature ionic liquids. We clearly showed that both the charged ([OMIM][$Br_9$] and [OMIM][$SnBr_3$]) and discharged ([OMIM][$Br_3$] and [OMIM][$SnBr_5$]) electrolytes have been successfully prepared and well characterized. Fig. 4.7 depicts the four important electrolytes as RT-ILs, which were fortunately stabilized by the same cation, $[OMIM]^+$. The relatively high viscosities and low conductivities of the bromostannates present a problem in the subsequent application as an electrolyte in a new RFB because it will be more difficult to pump rather viscous liquids than aqueous media. A possible solution is the addition of a small portion of a solvent to drastically lower the viscosity and thereby increasing the conductivity as well. This idea has been successfully pursued by our BMBF partners. These electrolytes, with and without the addition of a solvent, were examined electrochemically by cyclic voltammetry and battery measurements. Unfortunately, it was observed that the bromostannates undergo irreversible redox reactions and that the battery has a low open circuit voltage of only <0.5 V in addition to a short lifespan.[9] As

a result, it was decided to pursue more promising alternatives within the mentioned BMBF project.

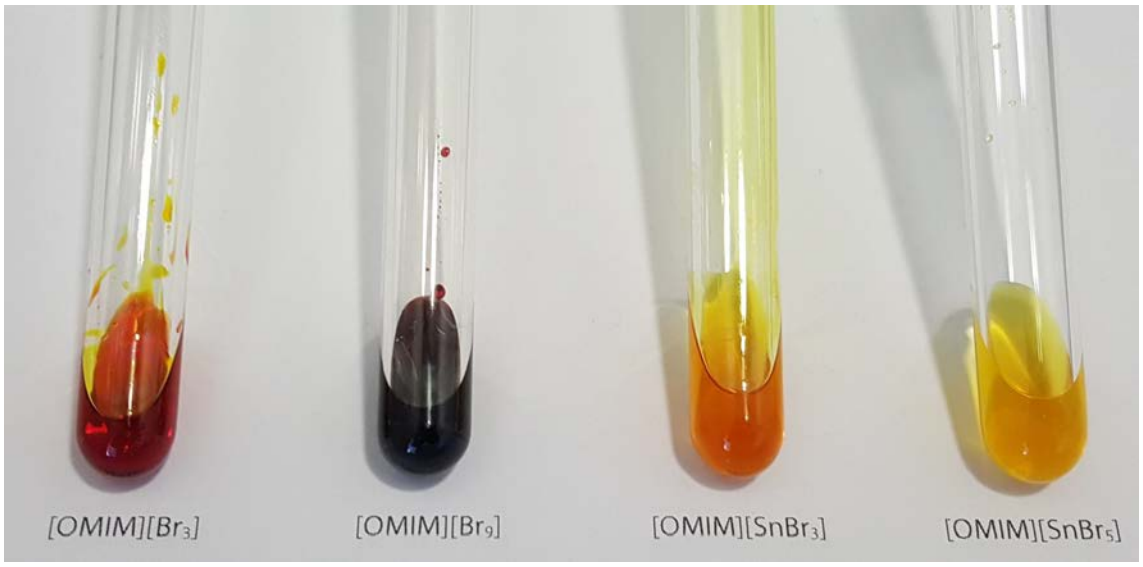


**Figure 4.7.** Physical appearance of the synthesized room temperature ionic liquids from left to right: [OMIM][$Br_3$], [OMIM][$Br_9$], [OMIM][$SnBr_3$], [OMIM][$SnBr_5$].

The conductivity of polybromides was closely investigated. On the one hand a more practical approach was pursued by investigating the factors influencing the conductivity. It was shown that the conductivity is the highest for polybromides with a cation of low molar mass and for a mole fraction of bromine of $\chi(Br_2) \approx 0.9$. On the other hand, the mechanism behind it was closely examined in collaboration with the Kremer group (Universität Leipzig) and it was shown that the charge transport can be described as a "dynamic glass transition assisted hopping" mechanism.
As a result of the efforts to find suitable polyhalide electrolytes, we greatly expanded the known structural diversity of polybromides and polychlorides which will be discussed in chapter 5, 6, and 8.

## 4.4 References

[1] B. Burgenmeister, *Dissertation*, Albert-Ludwigs-Universität Freiburg, Freiburg (Breisgau), **2017**.
[2] T. A. Gully, *Internship Report*, Freie Universität Berlin, Berlin, **2017**.
[3] C. Pettinari, M. Pellei, A. Cingolani, D. Martini, A. Drozdov, S. Troyanov, W. Panzeri, A. Mele, *Inorg. Chem.* **1999**, *38*, 5777.
[4] a) G. Thiele, B. R. Serr, *Z. Kristallog. – Cryst. Mater.* **1996**, *211*, 1; b) J. C. Avery, M. A. Hanson, R. H. Herber, K. J. Bladek, P. A. Rupar, I. Nowik, Y. Huang, K. M. Baines, *Inorg. Chem.* **2012**, *51*, 7306.
[5] J. H. Nelson, W. L. Wilson, L. W. Cary, N. W. Alcock, H. J. Clase, G. S. Jas, L. Ramsey-Tassin, J. W. Kenney, *Inorg. Chem.* **1996**, *35*, 883.

[6] F. Endres, D. MacFarlane, A. Abbott, *Electrodeposition from ionic liquids*, Wiley-VCH, Weinheim, **2008**.
[7] B. Wrackmeyer, *Annu. Rep. NMR Spectrosc.* **1999**, 203.
[8] J. A. Creighton, J. H. S. Green, *J. Chem. Soc. A* **1968**, 808.
[9] a) T. A. Gully, *Master Thesis*, Freie Universität Berlin, Berlin, **2017**; b) T. Gully, K. Sonnenberg, S. Riedel, *Electrochemical Characterization of Ionic Liquids based on Bromostannates, manuscript in preparation*
[10] M. Veith, V. Huch, R. Lisowsky, P. Hobein, *Z. Anorg. Allg. Chem.* **1989**, *569*, 43.
[11] G. S. Lorena, H. Hasegawa, Y. Takahashi, J. Harada, T. Inabe, *Chem. Lett.* **2014**, *43*, 1535.
[12] C. P. Raptopoulou, A. Terzis, G. A. Mousdis, G. C. Papavassiliou, *Z. Naturforsch., B: Chem. Sci.* **2002**, *57*, 645.
[13] U. Müller, N. Mronga, C. Schumacher, K. Dehnicke, *Z. Naturforsch., B: Chem. Sci.* **1982**, *37*, 1122.
[14] H. Haller, M. Hog, F. Scholz, H. Scherer, I. Krossing, S. Riedel, *Z. Naturforsch.* **2013**, *68b*, 1103.
[15] C. Cimmunges, R. Barhdadi, M. Laurent, M. Troupel, *J. Chem. Eng. Data* **2006**, *51*, 680.
[16] F. Fan, W. Wang, A. P. Holt, H. Feng, D. Uhrig, X. Lu, T. Hong, Y. Wang, N.-G. Kang, J. Mays, A. P. Sokolov, *Macromolecules* **2016**, *49*, 4557.
[17] F. Kremer, A. Schönhals, *Broadband Dielectric Spectroscopy*, Springer, Berlin, **2003**.
[18] F. Frenzel, F. Kremer, *personal communication.*
[19] F. Frenzel, K. Sonnenberg, F. Kremer, S. Riedel, *manuscript in preparation.*

## 4.5 Experimental section

**Conductometer**

Conductivity measurements were recorded with a Mettler Toledo SevenCompact S230 Conductivity meter and INLAB 710 Sensor.

**1-methyl-3-octylimidazolium pentabromostannate(IV)**

In a Schlenk tube [OMIM]Br (0.35 g, 1.27 mmol, 1 eq.) was weighted in. Subsequently liquid $SnBr_4$ (0.57 g, 1.32 mmol, 1 eq.) was added. The initially non miscibile mixture was stirred and heated to 65 °C for 4 hours and then cooled to room temperature. The product was a light yellow liquid.

Raman (77 K): $\tilde{\nu}$ = 2954 (w), 2930 (w), 2909 (w), 2856 (w), 1415 (vw), 1021 (vw), 248 (vw), 198 (vs), 158 (w), 103 (m) $cm^{-1}$.

$^{119}$Sn-NMR (149 MHz, pure substance): δ = –1511 (s, **Sn**$Br_5$) ppm.

**1-methyl-3-octylimidazolium pentabromostannate(II)**

In a Schlenk tube [OMIM]Br (1.25 g, 4.54 mmol, 1 eq.) was weighted in. Subsequently solid $SnBr_2$ (1.26 g, 4.52 mmol, 1 eq.) was added. The reaction mixture was vigorously stirred and heated to 65 °C over night and then cooled to room temperature. The product was a yellow/orange liquid.

Raman (77 K): $\tilde{\nu}$ = 2954 (m), 2908 (m), 2853 (m), 1450 (w), 195 (m), 183 (m), 168 (m), 149 (w) 74 (vs) $cm^{-1}$.

$^{119}$Sn-NMR (149 MHz, pure substance): δ = +46 (s, **Sn**$Br_3$) ppm.

**Ethyldimethylpropylammonium tribromide ([$N_{1123}$][$Br_3$])**

In a Schlenk tube [$N_{1123}$]Br (2.4 g, 12.5 mmol) was weighted in. Subsequently bromine (2.1 g, 13.2 mmol, 1.1 eq.) was added slowly under stirring to give rise to a red liquid. The reaction was stirred over night.

Raman (77 K): $\tilde{\nu}$ = 3029 (vw), 2977 (vw), 2952 (vw), 1450 (vw), 258 (w), 206 (w), 167 (vs) $cm^{-1}$.

$^1$H-NMR (401 MHz, pure substance): δ = 2.02 (2 H, N-C**H₂**-$CH_3$), 1.87 (2 H, N-C**H₂**-$CH_2$-$CH_3$), 1.67 (6 H, N-C**H₃**), 0.34 (2 H, $CH_2$-C**H₂**-$CH_3$), –0.06 (3 H, N-$CH_2$-C**H₃**), –0.45 (3 H, $CH_2$-$CH_2$-C**H₃**) ppm.

**Butyldiethylmethylammonium tribromide ([$N_{1224}$][$Br_3$])**

In a Schlenk tube [$N_{1224}$]Br (2.4 g, 10.9 mmol) was weighted in. Subsequently bromine (1.9 g, 12.2 mmol, 1.1 eq.) was added slowly under stirring to give rise to a red liquid. The reaction was stirred over night.

Raman (77 K): $\tilde{\nu}$ = 2991 (vw), 2943 (vw), 256 (m), 199 (m), 165 (vs) $cm^{-1}$.

$^1$H-NMR (401 MHz, pure substance): δ = 1.96 (4 H, N-C**H₂**-$CH_3$), 1.82 (2 H, N-C**H₂**-$(CH_2)_2$-$CH_3$), 1.58 (3 H, N-C**H₃**), 0.26 (2 H, $CH_2$-C**H₂**-$CH_2$-$CH_3$), –0.05 (2 H, $CH_2$-C**H₂**-$CH_3$), –0.10 (6 H, N-$CH_2$-C**H₃**), –0.48 (3 H, $CH_2$-$CH_2$-C**H₃**) ppm.

**Butyldimethylpropylammonium tribromide ([$N_{1134}$][$Br_3$])**

In a Schlenk tube [$N_{1134}$]Br (2.4 g, 10.8 mmol) was weighted in. Subsequently bromine (1.8 g, 11.4 mmol, 1.1 eq.) was added slowly under stirring to give rise to a red liquid. The reaction was stirred over night.

Raman (77 K): $\tilde{\nu}$ = 2966 (vw), 2926 (vw), 1449 (vw), 256 (w), 205 (w), 165 (vs) $cm^{-1}$.

$^1$H-NMR (401 MHz, pure substance): δ = 1.97 (4 H, N-C**H₂**-$CH_2$-$CH_3$ and N–C**H₂**-$CH_2$-$CH_2$), 1.77 (6 H, N-C**H₃**), 0.39 (4 H, N-$CH_2$-C**H₂**-$CH_3$ and $CH_2$-C**H₂**-$CH_2$-$CH_3$), 0.01 (2 H, $CH_2$–$CH_2$–C**H₂**-$CH_3$), –0.40 (6 H, N-$CH_2$-$CH_2$-C**H₃** and $CH_2$-$CH_2$-$CH_2$-C**H₃**) ppm.

**Ethyldimethylpropylammonium nonabromide ([$N_{1123}$][$Br_9$])**

In a Schlenk tube [$N_{1123}$]Br (1.9 g, 9.6 mmol) was weighted in. Subsequently bromine (6.0 g, 37.8 mmol, 3.9 eq.) was added slowly under stirring to give rise to a dark red liquid. The reaction was stirred over night.

Raman (77 K): $\tilde{\nu}$ = 289 (w), 276 (w), 256 (vs) $cm^{-1}$.

$^1$H-NMR (401 MHz, pure substance): δ = 1.52 (2 H, N-C**H₂**-$CH_3$), 1.35 (2 H, N-C**H₂**-$CH_2$-$CH_3$), 1.22 (6 H, N-C**H₃**), –0.02 (2 H, $CH_2$-C**H₂**-$CH_3$), –0.38 (3 H, N-$CH_2$-C**H₃**), 0.76 (3 H, $CH_2$-$CH_2$-C**H₃**) ppm.

**Butyldiethylmethylammonium nonabromide ($[N_{1224}][Br_9]$)**

In a Schlenk tube $[N_{1224}]Br$ (1.5 g, 6.8 mmol) was weighted in. Subsequently bromine (4.4 g, 28.0 mmol, 4.1 eq.) was added slowly under stirring to give rise to a dark red liquid. The reaction was stirred over night.

Raman (77 K): $\tilde{\nu}$ = 286 (m), 275 (s), 262 (vs) $cm^{-1}$.

$^1$H-NMR (401 MHz, pure substance): δ = 1.57 (4 H, N-C**H$_2$**-$CH_3$), 1.41 (2 H, N-C**H$_2$**-$(CH_2)_2$-$CH_3$), 1.22 (3 H, N-C**H$_3$**), –0.05 (2 H, $CH_2$-C**H$_2$**-$CH_2$-$CH_3$), –0.29 (2 H, $CH_2$-C**H$_2$**-$CH_3$), –0.36 (6 H, N-$CH_2$-C**H$_3$**), –0.73 (3 H, $CH_2$-$CH_2$-C**H$_3$**) ppm.

**Butyldimethylpropylammonium nonabromide ($[N_{1134}][Br_9]$)**

In a Schlenk tube $[N_{1134}]Br$ (1.5 g, 6.8 mmol) was weighted in. Subsequently bromine (4.9 g, 31.0 mmol, 4.5 eq.) was added slowly under stirring to give rise to a dark red liquid. The reaction was stirred over night.

Raman (77 K): $\tilde{\nu}$ = 283 (w), 266 (vs) $cm^{-1}$.

$^1$H-NMR (401 MHz, pure substance): δ = 1.47 (4 H, N-C**H$_2$**-$CH_2$-$CH_3$ and N-C**H$_2$**-$CH_2$-$CH_2$), 1.32 (6 H, N-C**H$_3$**), 0.07 (2 H, N-$CH_2$-C**H$_2$**-$CH_3$), 0.02 (2 H, $CH_2$-C**H$_2$**-$CH_2$-$CH_3$), –0.30 (2 H, $CH_2$-$CH_2$-C**H$_2$**-$CH_3$), –0.68 (3 H, N-$CH_2$-$CH_2$-C**H$_3$**), –0.74 (3 H, $CH_2$-$CH_2$-$CH_2$-C**H$_3$**) ppm.

**1-butyl-4-methylpyridinium nonabromide ([BMPY][$Br_9$])**

In a Schlenk tube [BMPY]Br (2.0 g, 8.8 mmol) was weighted in. Subsequently bromine (5.6 g, 35.3 mmol, 4.0 eq.) was added slowly under stirring to give rise to a dark red liquid. The reaction was stirred over night.

Raman (77 K): $\tilde{\nu}$ = 3087 (vw), 2937 (vw), 2918 (vw), 287 (m), 272 (w), 248 (vs) $cm^{-1}$.

$^1$H-NMR (401 MHz, pure substance): δ = 6.77 (2 H, CH-C**H**=C), 6.18 (2 H, N=C**H**-CH), 2.81 (2 H, N-C**H$_2$**-$CH_2$), 1.02 (3 H, C-C**H$_3$**), 0.32 (2 H, $CH_2$-C**H$_2$**-$CH_2$), –0.29 (2 H, $CH_3$-C**H$_2$**-$CH_2$), –0.76 (3 H, C**H$_3$**-$CH_2$) ppm.

**1-methyl-3-octylimidazolium bromide ([OMIM]Br) bromine mixture with $\chi(Br_2)$ = 0.53**

In a Schlenk tube [OMIM]Br (2.6 g, 9.5 mmol) was weighted in. Subsequently bromine (1.7 g, 10.7 mmol, 1.1 eq.) was added slowly under stirring to give rise to a red liquid. The reaction was stirred over night.

Raman (77 K): $\tilde{\nu}$ = 2951 (vw), 2887 (vw), 1414(vw), 262 (w), 213 (vw), 165 (vs) $cm^{-1}$.

**1-methyl-3-octylimidazolium bromide ([OMIM]Br) bromine mixture with $\chi(Br_2)$ = 0.79**

In a Schlenk tube [OMIM]Br (1.9 g, 6.7 mmol) was weighted in. Subsequently bromine (4.0 g, 25.3 mmol, 3.8 eq.) was added slowly under stirring to give rise to a dark red liquid. The reaction was stirred over night.

Raman (77 K): $\tilde{\nu}$ = 265 (vs) $cm^{-1}$.

**1-methyl-3-octylimidazolium bromide ([OMIM]Br) bromine mixture with $\chi(Br_2) = 0.89$**

In a Schlenk tube [OMIM]Br (1.6 g, 5.7 mmol) was weighted in. Subsequently bromine (7.0 g, 44.3 mmol, 7.7 eq.) was added slowly under stirring to give rise to a dark red liquid. The reaction was stirred over night.

Raman (77 K): $\tilde{\nu}$ = 296 (s, sh), 285 (vs, sh), 274 (vs) $cm^{-1}$.

**1-methyl-3-octylimidazolium bromide ([OMIM]Br) bromine mixture with $\chi(Br_2) = 0.95$**

In a Schlenk tube [OMIM]Br (0.8 g, 3.0 mmol) was weighted in. Subsequently bromine (9.1 g, 57.5 mmol, 19.0 eq.) was added slowly under stirring to give rise to a dark red liquid. The reaction was stirred over night.

Raman (77 K): $\tilde{\nu}$ = 298 (vs), 271 (m) $cm^{-1}$.

**[OMIM]Br/Bromine mixture with varying $\chi(Br_2)$**

We placed [OMIM]Br in a Schlenk flask and stepwise added bromine. After every step we measured the conductivity. To obtain the last data points we reversed the procedure, thus we added [OMIM]Br to provided bromine. The relevant data is summed up in the following table 4.2.

**Table 4.2.** Electrical conductivity of [OMIM]Br/bromine mixture at different $\chi(Br_2)$ at 25 °C.

| $\chi(Br_2)$ | $m(Br_2)$ [g] | $n(Br_2)$ [mmol] | m([OMIM]Br) [g] | n([OMIM]Br) [mmol] | σ [mS $cm^{-1}$] |
|---|---|---|---|---|---|
| 0.00 | 0.00 | 0.0 | 4.42 | 16.0 | 0.04 |
| 0.03 | 0.07 | 0.4 | 4.42 | 16.0 | 0.04 |
| 0.05 | 0.13 | 0.8 | 4.42 | 16.0 | 0.05 |
| 0.08 | 0.23 | 1.5 | 4.42 | 16.0 | 0.07 |
| 0.13 | 0.38 | 2.4 | 4.42 | 16.0 | 0.11 |
| 0.19 | 0.60 | 3.8 | 4.42 | 16.0 | 0.19 |
| 0.25 | 0.84 | 5.3 | 4.42 | 16.0 | 0.21 |
| 0.31 | 1.13 | 7.2 | 4.42 | 16.0 | 0.64 |
| 0.35 | 1.38 | 8.7 | 4.42 | 16.0 | 0.92 |
| 0.39 | 1.64 | 10.4 | 4.42 | 16.0 | 1.40 |
| 0.43 | 1.95 | 12.3 | 4.42 | 16.0 | 2.24 |
| 0.49 | 2.46 | 15.6 | 4.42 | 16.0 | 3.40 |
| 0.53 | 2.90 | 18.4 | 4.42 | 16.0 | 5.69 |
| 0.58 | 3.54 | 22.4 | 4.42 | 16.0 | 9.12 |
| 0.64 | 4.55 | 28.8 | 4.42 | 16.0 | 15.29 |
| 0.69 | 5.57 | 35.3 | 4.42 | 16.0 | 21.30 |
| 0.75 | 7.46 | 47.3 | 4.42 | 16.0 | 29.50 |
| 0.80 | 9.86 | 62.5 | 4.42 | 16.0 | 36.40 |
| 0.83 | 12.52 | 79.3 | 0.43 | 1.6 | 43.40 |
| 0.90 | 22.27 | 141.1 | 0.43 | 1.6 | 44.40 |
| 0.97 | 7.04 | 44.6 | 0.43 | 1.6 | 10.07 |
| 0.97 | 7.66 | 48.5 | 0.43 | 1.6 | 9.13 |
| 0.97 | 8.11 | 51.4 | 0.43 | 1.6 | 8.21 |
| 0.97 | 8.28 | 52.4 | 0.43 | 1.6 | 8.04 |
| 0.97 | 8.47 | 53.7 | 0.43 | 1.6 | 7.72 |
| 0.53 | 1.69 | 10.7 | 2.61 | 9.5 | 3.51 |
| 0.79 | 4.00 | 25.3 | 1.85 | 6.7 | 32.0 |
| 0.89 | 6.99 | 44.3 | 1.57 | 5.7 | 46.8 |
| 0.95 | 9.08 | 57.5 | 0.83 | 3.0 | 20.7 |

**Table 4.3.** Crystallographic details for all structures of bromostanntes and polybromides in chapter 4.

| | **[OMIM][$Br_3$]** | **[OMIM][$SnBr_5$]** | **[$N_{1123}$][$Br_3$]** |
|---|---|---|---|
| Empirical formula | $C_{12}H_{23}Br_3N_2$ | $C_{12}H_{23}Br_5N_2Sn$ | $C_7H_{18}Br_3N$ |
| Formula weight | 435.05 | 713.56 | 355.95 |
| Temperature/K | 100 | 99.99 | 102.59 |
| Crystal system | Triclinic | Monoclinic | Orthorhombic |
| Space group | $P\bar{1}$ | $P2_1/c$ | $P2_12_12_1$ |
| a/Å | 9.2005(6) | 16.8858(8) | 11.6037(16) |
| b/Å | 15.5783(11) | 7.3914(3) | 13.599(2) |
| c/Å | 24.9018(18) | 17.5046(7) | 7.7510(11) |
| α/° | 104.551(2) | 90 | 90 |
| β/° | 95.331(2) | 104.260(2) | 90 |
| γ/° | 102.903(2) | 90 | 90 |
| Volume/Å$^3$ | 3325.1(4) | 2117.43(16) | 1223.1(3) |
| Z | 8 | 4 | 4 |
| $\rho_{calc}$ g/cm$^3$ | 1.738 | 2.238 | 1.933 |
| μ/mm$^{-1}$ | 7.264 | 10.636 | 9.847 |
| F(000) | 1712 | 1336 | 688 |
| Crystal size/mm$^3$ | 0.33 x 0.22 x 0.09 | 0.30 x 0.17 x 0.06 | 0.32x0.09x0.07 |
| Radiation | MoKα (λ= 71.073 pm) | MoKα (λ= 71.073 pm) | MoKα (λ= 71.073 pm) |
| 2Θ range for data collection/° | 4.6 to 55.216 | 4.802 to 50.78 | 4.614 to 52.92 |
| Reflections collected | 235926 | 28115 | 61423 |
| Independent reflections | 15335 [$R_{int}$ = 0.0640, $R_{sigma}$ = 0.0263] | 3884 [$R_{int}$ = 0.0745, $R_{sigma}$ = 0.0433] | 2533 [$R_{int}$ = 0.0840, $R_{sigma}$ = 0.0259] |
| Data/restraints/parameters | 15335/0/621 | 3884/0/192 | 2533/0/105 |
| Goodness-of-fit on F$^2$ | 1.022 | 1.022 | 1.211 |
| Final R indexes [I ≥ 2σ(I)] | $R_1$ = 0.0256, $wR_2$ = 0.0474 | $R_1$ = 0.0228, $wR_2$ = 0.0424 | $R_1$ = 0.0329, $wR_2$ = 0.0599 |
| Final R indexes [all data] | $R_1$ = 0.0415, $wR_2$ = 0.0518 | $R_1$ = 0.0338, $wR_2$ = 0.0456 | $R_1$ = 0.0369, $wR_2$ = 0.0608 |
| Largest diff. peak/hole/ e Å$^{-3}$ | 0.51/-0.78 | 0.49/-0.77 | 0.81/-0.91 |

# 5. Formation and Characterization of $[BrC(NMe_2)_2][Br_3]$ and $[BrC(NMe_2)_2]_2[Br_8]$ in Ionic Liquids

This chapter is based on the publication "Karsten Sonnenberg, Patrick Pröhm, Simon Steinhauer, Anja Wiesner, Carsten Müller, Sebastian Riedel, *Formation and Characterization of $[BrC(NMe_2)_2)][Br_3]$ and $[BrC(NMe_2)_2)]_2[Br_8]$ in Ionic Liquids*, *Z. Anorg. Allg. Chem.* **2017**, *643*, 101–105." (DOI: 10.1002/zaac.201600337).



Karsten Sonnenberg designed the project, performed parts of the experiment and wrote the paper. Patrick Pröhm did some of the experiments and quantum-chemical calculations under the guidance and supervision of Karsten Sonnenberg. Carsten Müller performed the solid-state quantum-chemical calculations. Anja Wiesner performed the characterization by X-ray diffraction. Simon Steinhauer and Sebastian Riedel corrected the manuscript. Sebastian Riedel supervised the project and provided scientific guidance.

https://doi.org/10.1002/zaac.201600337

# 6. Closing the Gap: Structural Evidence for the Missing Hexabromide Dianion $[Br_6]^{2-}$

This chapter is based on the publication "Karsten Sonnenberg, Patrick Pröhm, Carsten Müller, Helmut Beckers, Simon Steinhauer, Dieter Lentz, Sebastian Riedel, *Closing the Gap: Structural Evidence for the Missing Hexabromide Dianion $[Br_6]^{2-}$, Chem. Eur. J.* **2018**, *24*, 1072–1075." (DOI: 10.1002/chem.201705912).



Karsten Sonnenberg designed the project, performed the majority of the experiments and characterization and wrote the paper. Patrick Pröhm did some of the experiments and quantum-chemical calculations under the guidance and supervision of Karsten Sonnenberg. Carsten Müller performed the solid-state quantum-chemical calculations. Dieter Lentz characterized some of the compounds by X-ray diffraction. Simon Steinhauer, Helmut Beckers and Sebastian Riedel provided scientific guidance, suggestions and corrected the manuscript.

https://doi.org/10.1002/chem.201705912

# 7. Investigation of the Basic Chemical Behavior of BrCl with $Cl^-$, $Br^-$, and $I^-$

Haller has shown that polybromides can be RT-ILs with a high electrical conductivity.[1] However, many polybromides especially the tribromides are solids and are therefore unsuitable for the use as neat electrolytes in new redox flow batteries. Bromine monochloride (BrCl) has a higher vapor pressure than bromine ($Br_2$) and therefore it is reasonable to assume that polyinterhalides based on BrCl have a lower melting point than the corresponding polybromides.

Unfortunately, while $[Br_2Cl]^-$ and $[BrCl_2]^-$ have been reported, a systematic investigation of polyinterhalides based on BrCl has not been conducted before the start of this dissertation. It shall be noted that in the meantime, Schmidt *et al.* have given an in-depth report on higher polyinterhalides based on chloride and bromine monochloride.[2] Therefore, it is the purpose of this work to lay the ground work of the chemical behavior of a halide $X^-$ (X = Cl, Br, I) with BrCl. Parts of the experimental work described in this chapter include results from an internship of Jonathan Schneider under the guidance and supervision of the author of this dissertation.

## 7.1 Reaction of BrCl with $Cl^-$

As expected, the reaction of a chloride salt (e.g. tetrabutylammonium chloride, $[NBu_4]Cl$) and one equivalent of BrCl yields $[BrCl_2]^-$, see eq. (7.1). The reaction enthalpy is calculated to be exothermic with –172 kJ $mol^{-1}$ (D3-B3LYP/def2-TZVPP).

$$Cl^- + BrCl \longrightarrow [BrCl_2]^- \qquad (7.1)$$

We obtained a Raman spectrum of the reaction mixture which clearly shows a band at 273 $cm^{-1}$ corresponding to the symmetric stretch of the $[BrCl_2]^-$ ion.[3] Additionally, we grew single crystals which were measured by X-ray diffraction, see Fig. 7.1. $[NBu_4][BrCl_2]$ crystallizes in the monoclinic space group *C*2/*c*. It is without a doubt that the compound has been synthesized. However, the crystal quality was quite poor and is only sufficient as supporting material but not for publication. Nevertheless, the crystallographic analysis is in agreement with the Raman spectrum of one symmetric $[BrCl_2]^-$ with a bond length of 246.6(3) pm. As no side reactions occurred, it is worth aiming at synthesizing larger polyinterhalides based on BrCl and $Cl^-$, which has since been done successfully.[2]

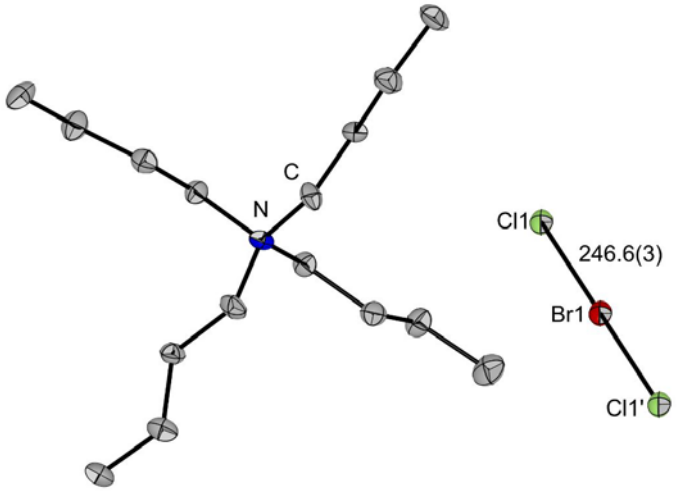


**Figure 7.1.** Structure of $[NBu_4][BrCl_2]$ in the solid. Ellipsoids shown at the 50% probability level. Hydrogens are omitted for clarity. Bond lengths given in [pm].

## 7.2 Reaction of BrCl with $Br^-$

In a similar fashion, we evaluated the reaction of $[NBu_4]Br$ with one equivalent of BrCl. We anticipate the formation of $[Br_2Cl]^-$ which is again calculated to be exothermic by –151 kJ $mol^{-1}$ (D3-B3LYP/def2-TZVPP), see eq. (7.2). However, the Raman spectrum was not as conclusive as reaction 7.1.

$$Br^- + BrCl \longrightarrow [Br_2Cl]^- \qquad (7.2)$$

$$2\,[Br_2Cl]^- \longrightarrow [BrCl_2]^- + [Br_3]^- \qquad (7.3)$$

The Raman spectrum of the reaction mixture shows four bands (276, 225, 193, and 168 $cm^{-1}$) in the region of interest between 100 and 300 $cm^{-1}$. Only the bands at 225 and 193 $cm^{-1}$ can be

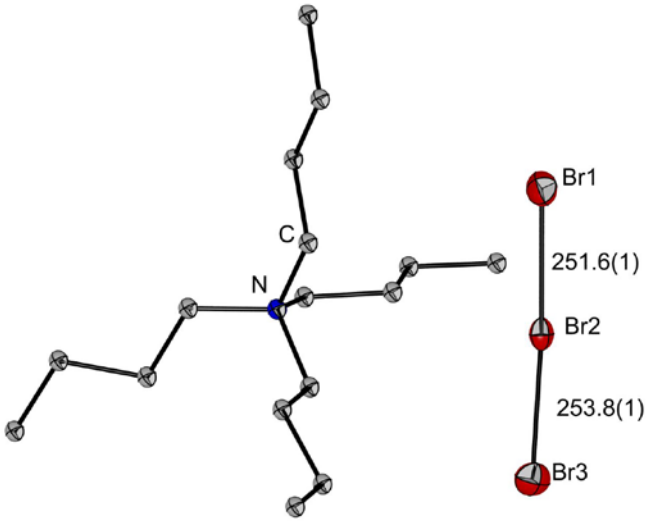


**Figure 7.2.** Structure of $[NBu_4][Br_3]$ in the solid. Ellipsoids shown at the 50% probability level. Hydrogens are omitted for clarity. Bond lengths given in [pm].

assigned to $[Br_2Cl]^-$.[4] Upon crystallization of the reaction mixture, two sort of crystals of orange and yellow color were visible. Fortunately, we were able to measure both kind of crystals by means of X-ray diffraction. The yellow ones were $[NBu_4][BrCl_2]$, which we discussed in the previous chapter. The orange crystals were $[NBu_4][Br_3]$, crystallizing in the triclinic space group $P\bar{1}$, and whose molecular structure in the solid is already known, see Fig. 7.2. This explains the Raman spectrum because the band at 276 $cm^{-1}$ can be assigned to the symmetric $[BrCl_2]^-$ while the Raman band at 168 $cm^{-1}$ corresponds to the tribromide $[Br_3]^-$.[5]

Quantum-chemical calulcations support the experimental findings. The disproportionation of $[Br_2Cl]^-$ into $[BrCl_2]^-$ and $[Br_3]^-$ (eq. (7.3)) is slightly exothermic by –1 kJ $mol^{-1}$ (D3-B3LYP/def2-TZVPP) which means that there is a balanced equilibrium and all three species are present under ambient conditions. This is in agreement with Evans *et al.* who made the same observation when adding $Br_2$ to $Cl^-$, also expecting $[Br_2Cl]^-$ but receiving a mixture of $[Br_3]^-$, $[BrCl_2]^-$, and $[Br_2Cl]^-$.[4]

## 7.3 Reaction of BrCl with $I^-$

In order to complete our studies, we also investigated the reaction of an iodide salt with bromine monochloride. To our surprise, the following two reaction were found to occur.

$$I^- + 2\,BrCl \longrightarrow [ICl_2]^- + Br_2 \qquad (7.4)$$

$$I^- + 4\,BrCl \longrightarrow [ICl_4]^- + 2\,Br_2 \qquad (7.5)$$

A coordination of BrCl to a central $I^-$ was not observed, but rather redox reactions yielding $[ICl_2]^-$ and $[ICl_4]^-$, depending on the amount of BrCl used, see equations (7.4) and (7.5). Both reactions are calculated (D3-B3LYP/def2-TZVPP) to be exothermic with $\Delta H_f$ = –193 kJ $mol^{-1}$ (eq. 7.4) and $\Delta H_f$ = –271 kJ $mol^{-1}$ (eq. 7.5), which is in agreement with the experimental observations. The reaction of $[NBu_4]I$ with two equivalents of BrCl yielded $[NBu_4][ICl_2]$, crystallizing in the

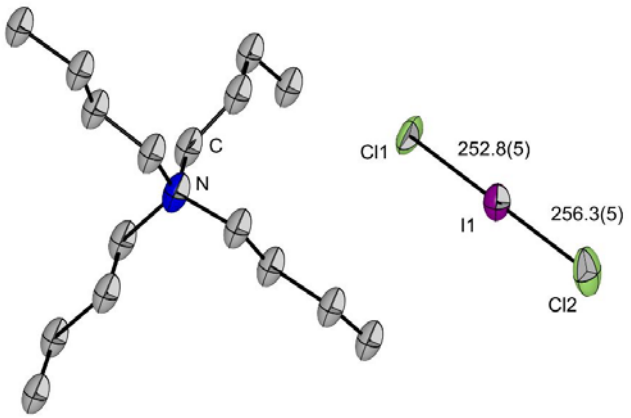


**Figure 7.3.** Structure of $[NBu_4][ICl_2]$ in the solid. Ellipsoids shown at the 50% probability level. Hydrogens are omitted for clarity. Bond lengths given in [pm].

monoclinic space group $P2_1/n$. Again, the crystal data is not suitable for publication but undeniably gives viable information on the reaction product.

Since tetrabutylammonium $[NBu_4]^+$ is not ideal for crystallization in comparison to tetraalkyklammonium cations with shorter chain lengths, we switched to the tetramethylammonium $[NMe_4]^+$ cation. The reaction of $[NMe_4]I$ with five equivalents of BrCl results in $[NMe_4][ICl_4] \cdot Br_2$, see Fig. 7.4. The anionic structure is interesting as it once again underlines the concept of halogen-halogen bonding.

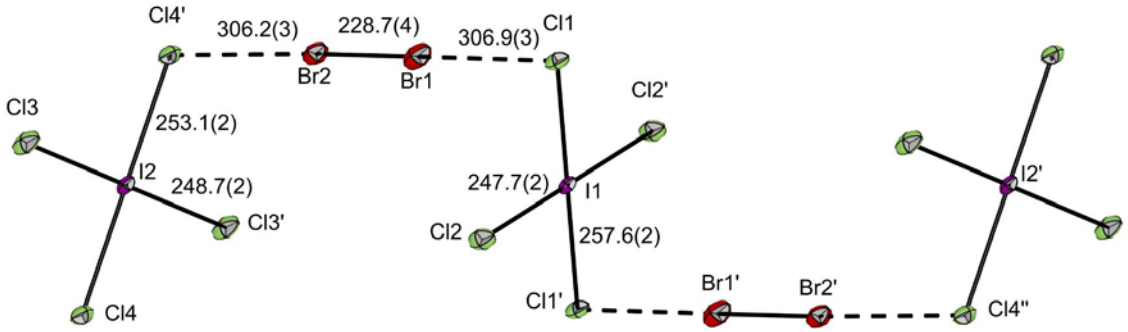


**Figure 7.4.** Anionic structure of $[ICl_4]^- \cdot Br_2$ in $[NMe_4][ICl_4] \cdot Br_2$ in the solid. Ellipsoids shown at the 50% probability level. Cations are omitted for clarity. Bond lengths given in [pm].

While the cation $[NMe_4]^+$ does not influence the motif of the anionic chain by any interaction, the latter would not be possible with much larger cations. The small cations are situated in the voids of the chain and larger cations like $[NBu_4]^+$ would be too big for said voids. The anionic chain consists of $[ICl_4]^-$ units interconnected by $Br_2$ moieties.

This fits precisely to the spectroscopic observation with three significant Raman bands at 296 ($\nu(Br_2)$),[6] 280 ($\nu_s([ICl_4]^-)$) and 257 ($\nu_{as}([ICl_4]^-)$) $cm^{-1}$.[7]

The bond length of this embedded $Br_2$ molecule (228.7(4) pm) is not elongated in comparison to elemental bromine (229.4(2) pm[8]) within the margin of error. However, the $[ICl_4]^-$ anions deviate from their ideal symmetry of $D_{4h}$ because two I–Cl bond lengths are present in each $[ICl_4]^-$ anion, reducing their symmetry to $D_{2h}$, see Figure 7.4. Both crystallographically independent $[ICl_4]^-$ anions show a similar behavior. The elongation of the I1–Cl1 and I2-Cl4 bonds (257.6(2) and 253.1(2) pm, respectively) is due to the interaction to the $Br_2$ molecules, while the chlorine atoms Cl2 and Cl3 of the shorter I–Cl bonds (247.7(2) and 248.7(2) pm, respectively) show no interaction to neighboring chains or cations within the sum of the van der Waals radii. The crystal data set was solved as a non-merohedral twin and showed that the compound $[NMe_4][ICl_4] \cdot Br_2$ crystallizes in the triclinic space group $P\bar{1}$.

## 7.4 Conclusion

We have explored the reaction of BrCl with halides $X^-$ (X = Cl, Br, I). It became clear that large polyinterhalides of the form $[X(BrCl)_n]^-$ are only possible for X = Cl. In the case of X = Br a mixture of various triinterhalides is obtained. The reaction of BrCl with $I^-$ yielded $[ICl_2]^-$ and $[ICl_4]^-$ showing that redox reactions occurred. Based on this ground laying work, large polyinterhalides with BrCl and $Cl^-$ have since been prepared.[2]

## 7.5 References

[1] H. Haller, M. Hog, F. Scholz, H. Scherer, I. Krossing, S. Riedel, *Z. Naturforsch.* **2013**, *68b*, 1103.
[2] B. Schmidt, K. Sonnenberg, H. Beckers, S. Steinhauer, S. Riedel, *Angew. Chem. Int. Ed.* **2018**, *57*, 9141.
[3] W. Gabes, H. Gerding, *J. Mol. Struct.* **1972**, *14*, 267.
[4] J. C. Evans, G. Y.-S. Lo, *J. Chem. Phys.* **1966**, *45*, 1069.
[5] X. Chen, M. A. Rickard, J. W. Hull, C. Zheng, A. Leugers, P. Simoncic, *Inorg. Chem.* **2010**, *49*, 8684.
[6] H. Stammreich, R. Forneris, *J. Chem. Phys.* **1954**, *22*, 1624.
[7] B. Burgenmeister, K. Sonnenberg, S. Riedel, I. Krossing, *Chem. Eur. J.* **2017**, *23*, 11312.
[8] B. M. Powell, K. M. Heal, B. H. Torrie, *Mol. Phys.* **1984**, *53*, 929.

## 7.6 Experimental Details

**Tetrabutylammonium dichlorobromate $[NBu_4][BrCl_2]$**

Bromine monochloride (0.14 g, 1.21 mmol, 1 eq) was condensed onto tetrabutylammonium chloride (0.34 g, 1.21 mmol, 1 eq). The reaction mixture turned bright orange. Raman spectra were obtained from this reaction mixture. Crystallization occurred upon cooling to 5 °C over night.

Raman (298 K): $\tilde{\nu}$ = 2960 (m), 2932 (vs), 2874 (s), 2751 (vw), 1459 (w), 902 (vw), 882 (vw), 273 (vs) $cm^{-1}$.

**Tetrabutylammonium tribromide $[NBu_4][Br_3]$**

Bromine monochloride (0.18 g, 1.52 mmol, 1 eq) was condensed onto tetrabutylammonium bromide (0.49 g, 1.51 mmol, 1 eq). The reaction mixture turned red. Raman spectra were obtained from this reaction mixture. Upon crystallization two kind of crystals were obtained, orange and yellow. The orange crystals were $[NBu_4][Br_3]$. The yellow crystals were the previously obtained $[NBu_4][BrCl_2]$.

Raman (298 K): $\tilde{\nu}$ = 2965 (m), 2934 (m) 2913 (m), 2874 (m), 1449 (w) 1057 (vw), 903 (vw), 880 (vw), 276 (w), 225 (w), 193 (m), 168 (vs) $cm^{-1}$.

**Tetrabutylammonium dichloroiodate $[NBu_4][ICl_2]$**

Bromine monochloride (0.14 g, 1.21 mmol, 1 eq) was condensed onto tetrabutylammonium chloride (0.34 g, 1.21 mmol, 1eq). The reaction mixture turned bright orange. Raman spectra were obtained from this reaction mixture. Crystallization occurred upon cooling to 5 °C over night.

Raman (298 K): $\tilde{\nu}$ = 2973 (w), 2930 (w), 2868 (w), 733 (vw), 318 (vw), 284 (vs), $cm^{-1}$.

**Tetramethylammonium tetrachloroiodate bromine solvate $[NMe_4][ICl_4]\cdot Br_2$**

Bromine monochloride (1.17 g, 10.13 mmol, 5 eq) was condensed onto tetramethylammonium iodide (0.41 g, 2.04 mmol, 1eq). The reaction mixture turned red. Raman spectra were obtained from this reaction mixture. Crystallization occurred after solvation in dichloromethane (0.1 mL) and subsequent cooling to 5 °C over night.

Raman (298 K): $\tilde{\nu}$ = 3030 (vw), 2975 (vw), 2920 (vw), 2815 (vw), 1445 (vw), 950 (vw), 754 (vw), 420 (w, sh), 403 (w), 296 (s), 280 (vs), 257 (m), 137 (w) $cm^{-1}$.

**Table 7.1.** Crystallographic details for all structures obtained by reaction of BrCl with $Cl^-$, $Br^-$, and $I^-$.

| | **$[NBu_4][BrCl_2]$** | **$[NBu_4][Br_3]$** | **$[NBu_4][ICl_2]$** | **$[NMe_4][ICl_4]\cdot Br_2$** |
|---|---|---|---|---|
| Empirical formula | $C_{16}H_{36}BrCl_2N$ | $C_{16}H_{36}Br_3N$ | $C_{16}H_{35.6}Cl_2IN$ | $C_4H_{12}Br_2Cl_4IN$ |
| Formula weight | 393.27 | 482.19 | 439.85 | 502.67 |
| Temperature/K | 100.13 | 99.94 | 99.99 | 100.03 |
| Crystal system | Monoclinic | Triclinic | Monoclinic | Triclinic |
| Space group | C2/c | $P\bar{1}$ | $P2_1/n$ | $P\bar{1}$ |
| a/Å | 13.0013(7) | 9.0209(10) | 13.6645(10) | 8.4234(17) |
| b/Å | 9.9810(5) | 9.9357(12) | 8.9838(6) | 8.9823(18) |
| c/Å | 15.9400(9) | 12.5680(14) | 18.1784(15) | 10.769(2) |
| α/° | 90 | 109.603(7) | 90 | 79.91(3) |
| β/° | 94.531(3) | 90.454(7) | 105.921(4) | 73.57(3) |
| γ/° | 90 | 97.837(7) | 90 | 63.83(3) |
| Volume/$Å^3$ | 2062.01(19) | 1049.5(2) | 2146.0(3) | 700.2(3) |
| Z | 4 | 2 | 4 | 2 |
| $\rho_{calc}$ g/$cm^3$ | 1.267 | 1.526 | 1.361 | 2.384 |
| μ/$mm^{-1}$ | 2.247 | 7.058 | 13.945 | 8.717 |
| F(000) | 832 | 488 | 902 | 468 |
| Crystal size/$mm^3$ | 0.24x0.19x0.13 | 0.04x0x04x0.005 | 0.34x0x12x0.02 | 0.46x0.13x0.13 |
| Radiation | MoKα (λ= 71.073 pm) | CuKα (λ= 154.178 pm) | CuKα (λ= 154.178 pm) | MoKα (λ= 71.073 pm) |
| 2Θ range for data collection/° | 5.128 to 55.248 | 7.478 to 120.546 | 7.222 to 122.012 | 5.062 to 54.464 |
| Reflections collected | 23580 | 12555 | 10912 | 2591 |
| Independent reflections | 2389 [$R_{int}$ = 0.0826, $R_{sigma}$ = 0.0349] | 2640 [$R_{int}$ = 0.0780, $R_{sigma}$ = 0.2292] | 2061 [$R_{int}$ = 0.0744, $R_{sigma}$ = 0.1287] | 2591 [$R_{int}$ = 0.0887, $R_{sigma}$ = 0.0326] |
| Data/restraints/parameters | 2389/0/95 | 2640/0/89 | 2061/0/93 | 2591/0/116 |
| Goodness-of-fit on $F^2$ | 1.052 | 1.07 | 1.04 | 1.167 |
| Final R indexes [I ≥ 2σ(I)] | $R_1$ = 0.0905, $wR_2$ = 0.2828 | $R_1$ = 0.0836, $wR_2$ = 0.1033 | $R_1$ = 0.1094, $wR_2$ = 0.2610 | $R_1$ = 0.0516, $wR_2$ = 0.1412 |
| Final R indexes [all data] | $R_1$ = 0.1058, $wR_2$ = 0.2968 | $R_1$ = 0.2144, $wR_2$ = 0.1300 | $R_1$ = 0.1856, $wR_2$ = 0.3038 | $R_1$ = 0.0593, $wR_2$ = 0.1485 |
| Largest diff. peak/hole/ e $Å^{-3}$ | 3.83/-2.02 | 0.94/-0.98 | 1.60/-1.07 | 1.93/-1.95 |

# 8. Investigation of Large Polychloride Anions: $[Cl_{11}]^-$, $[Cl_{12}]^{2-}$, and $[Cl_{13}]^-$

This chapter is based on the publication "Karsten Sonnenberg, Patrick Pröhm, Nico Schwarze, Helmut Beckers, Sebastian Riedel, *Investigation of Large Polychloride Anions: $[Cl_{11}]^-$, $[Cl_{12}]^{2-}$, and $[Cl_{13}]^-$, Angew. Chem. Int. Ed.* **2018**, *57*, 9136–90140." (DOI: 10.1002/anie.201803486).



Karsten Sonnenberg designed the project, performed parts of the experiment and wrote the paper. Patrick Pröhm did some of the experiments and quantum-chemical calculations. Carsten Müller performed the solid-state quantum-chemical calculations. Nico Schwarze did some of the experiments. Patrick Pröhm, Nico Schwarze, Helmut Beckers and Sebastian Riedel corrected the manuscript and provided scientific guidance.

https://doi.org/10.1002/anie.201803486

# 9. Summary

In the framework of the global energy transition, this dissertation unequivocally broadened the spectrum of poly(inter)halides and supported a deeper understanding of the conductivity of polybromides. Together with bromostannates, the latter were considered as redox active species in a new redox flow battery based on neat ionic liquids containing said anions. The charged electrolyte would comprise $[SnBr_3]^-$ on the one hand and $[Br_9]^-$ on the other. The discharged electrolytes in return would include $[SnBr_5]^-$ and $[Br_3]^-$, respectively. In order to achieve this, the synthesis of a bromostannate(IV) ($[SnBr_5]^-$) ionic liquid was of prime concern, since tin(IV) usually prefers an octahedral coordination, e.g. $[SnBr_6]^{2-}$. To date, there is only one crystallographic report on $[SnBr_5]^-$ and other works show that, for example, the split of $[HMIM][SnBr_5]$ into $[HMIM]_2[SnBr_6]$ and $SnBr_4$ is due to the relatively large lattice energy of $[HMIM]_2[SnBr_6]$.

In the present work, it was demonstrated, how this can be overcome by employing the $[OMIM]^+$ cation, giving rise to the hitherto only room temperature ionic liquid of a tin(IV) species, namely $[OMIM][SnBr_5]$. The compound was unambiguously characterized by $^{119}Sn$ NMR and Raman spectroscopy as well as single crystal X-ray diffraction. To prevent cross contamination, the other electrolytes should contain the same cation. Indeed, the synthesis of $[OMIM][SnBr_3]$, $[OMIM][Br_3]$, and $[OMIM][Br_9]$ was successful and the compounds were obtained as room temperature ionic liquids. They were characterized by NMR and Raman spectroscopy, and $[OMIM][Br_3]$ was additionally identified by X-ray diffraction.

The conductivity of polybromides was closely investigated. While [OMIM]Br and $Br_2$ possess a neglible electrical conductivity, polybromides are highly conductive in comparison. Therefore, the electrical conductivity was examined as a function of the mole fraction of bromine ($\chi(Br_2)$). It was shown that the conductivity very slowly increases from $\chi(Br_2) = 0$ to $\chi(Br_2) = 0.5$, which corresponds to the lowering of the viscosity and the formation of a tribromide $[Br_3]^-$, at which point it drastically increases until approximately $\chi(Br_2) = 0.9$. This can be explained by a dynamic glass transition assisted hopping mechanism. After $\chi(Br_2) = 0.9$ the conductivity decisively decreases until $\chi(Br_2) = 1$ because of a low ion concentration. The charge transport mechanism of polybromides was established because of broadband dielectric spectroscopic investigations in collaboration with the Kremer group of the Universität Leipzig. Moreover, it was demonstrated that, apart from the mole fraction, the molecular mass of the cation has an influence. As expected, the general rule applies that the smaller the molecular mass, the higher the conductivity ($\sigma([N_{1123}][Br_x] > \sigma([N_{1134}][Br_x])$).

Apart from their electrochemical characterization, polybromides were also investigated with respect to their structural diversity. The hexabromide dianion $[Br_6]^{2-}$ was successfully synthesized and its existence closes the last remaining gap between the tribromide $[Br_3]^-$ and the undecabromide $[Br_{11}]^-$. This dianion consists of two interacting tribromides in an L-shape fashion, even though quatum-chemical calculations on the RI-MP2/aug-cc-pVTZ level of theory predict the theoretical T-shaped $[Br_6]^{2-}$ to be the global minimum. However, the observed dianion deviates from this geometry because of favorable halogen–halogen interactions between the anion and cation. The latter also sterically prevents the T-structure. This highly interesting compound was thoroughly characterized by X-ray diffraction, IR- and Raman spectroscopy, and quantum-chemical calculations as well as supplementary mass spectrometry and NMR spectroscopy.

The influence of the solvent on the synthesis and crystallization of polybromides was evaluated. Especially the preparation of an octabromide dianion $[Br_8]^{2-}$ in an eutectic mixture of two ionic liquids, [BMP]Br and [BMP][OTf], was reported and compared to the lighter homologous $[Cl_8]^{2-}$ which was prepared in the same fashion, resulting in the same structural parameters and motif of a planar Z-like structure.

Since the number of isolated polychlorides is very little ($[Cl_3]^-$, $[Cl_5]^-$, and $[Cl_8]^{2-}$), we were eager to transfer our knowlegde of polybromides to polychlorides. Fortunately, we were able to synthesize a variety of new polychlorides, expanding the set of known polychlorides by the high-order polychloride monoanions $[Cl_{11}]^-$ and $[Cl_{13}]^-$. The undecachloride $[Cl_{11}]^-$ and tridecachloride $[Cl_{13}]^-$ were stabilized by bulky, weakly coordinating cations. The former was obtained in two motifs. In $[AsPh_4][Cl_{11}]$ and $[PPh_4][Cl_{11}]$ the anions form infinite one dimensional chains, while the undecachloride in $[PNP][Cl_{11}] \cdot Cl_2$ is isolated with a distorted $C_{4v}$ symmetry and an embedded chlorine molecule which is not part of the anion. The largest polyhalide monoanion ever reported was synthesized in the framework of this dissertation. The first and hithero only isotridecahalide $[Cl_{13}]^-$ in $[PNP][Cl_{13}]$ shows a distorted octahedral geometry and represents the anion with the highest chlorine content, together with the aforementioned $[Cl_{11}]^- \cdot Cl_2$. On top of that, we were also able to isolate the hitherto largest polychloride dianion $[Cl_{12}]^{2-}$, which exists in the salt $[NMe_3Ph]_2[Cl_{12}]$. All polychloride compounds were characterized by $^1H$ and $^{13}C$ NMR, and Raman spectroscopy as well as X-ray diffraction. The experimental findings were compared to, and supporeted by, high-level quantum-chemical calculations.

Having synthesized a large number of new polyhalides in a variety of synthetic approaches, we broadened the spectrum of polyhalides and enhanced the understanding of the bonding situation in very interesting compounds. The physical properties of the synthesized polybromides and bromostannates were tuned to obtain room temperature ionic liquids which can be analyzed regarding their performance in new redox flow batteries.

# 10. Publications and Conference Contributions

## 10.1 Publications

**Publications as part of this thesis:**

[1] K. Sonnenberg, P. Pröhm, S. Steinhauer, A. Wiesner, C. Müller, S. Riedel, *Z. Anorg. Allg. Chem.* **2017**, *643*, 101–105.
[2] K. Sonnenberg, P. Pröhm, C. Müller, H. Beckers, S. Steinhauer, D. Lentz, S. Riedel, *Chem. Eur. J.* **2018**, *24*, 1072–1075. (HOT PAPER)
[3] K. Sonnenberg, P. Pröhm, N. Schwarze, C. Müller, H. Beckers, S. Riedel, *Angew. Chem. Int. Ed.* **2018**, *57*, 9136–9140.
[4] K. Sonnenberg, L. Mann, F. Redeker, B. Schmidt, S. Riedel, *manuscript in preparation*

**Additional publications:**

[5] B. Burgenmeister, K. Sonnenberg, S. Riedel, I. Krossing, *Chem. Eur. J.* **2017**, *23*, 11312–11322.

[6] B. Schmidt, K. Sonnenberg, H. Beckers, S. Steinhauer, S. Riedel, *Angew. Chem. Int. Ed.* **2018,** *57*, 9141–9145.
[7] L. Mann, G. Senges, K. Sonnenberg, H. Haller, S. Riedel, *Eur. J. Inorg. Chem.* **2018**, *28*, 3330–3337.

[8] K. Sonnenberg, S. Riedel, *Aktuelle Wochenschau der Gesellschaft Deutscher Chemiker (GDCh)*, https://www.aktuelle-wochenschau.de/main-navi/archiv/chemie-der-elemente-2016/kw41-brom.html (05.10.2018).

## 10.2 Conference Contributions

**Posters:**

07/15 3. Tag der Anorganischen Chemie, Freie Universität Berlin, Germany

12/15 3rd International Conference on Ionic Liquid-based Materials (ILMAT III), Berlin, Germany

09/16 18. Wöhler Tagung, Berlin, Germany

07/17 5. Tag der Anorganischen Chemie, Freie Universität Berlin, Germany

09/17 8th International Meeting on Halogen Chemistry (HALCHEM VIII), Inuyama, Japan

09/18 19. Wöhler Tagung, Regensburg, Germany

10/18 6. Tag der Anorganischen Chemie, Freie Universität Berlin, Germany

**Talks:**

07/16 4. Tag der Anorganische Chemie, Freie Universität Berlin, Germany

# 11. Curriculum vitae

The curriculum vitae is not included for reasons of data protection.